PARAMETRIC ANALYSIS OF ARCHIMEDES SCREW TURBINE FOR

MICRO HYDROPOWER GENERATION USING CFD

BY

CHIDA SIMON PHAREZ

A THESIS SUBMITTED TO THE SCHOOL OF ENGINEERING,

DEPARTMENT OF MECHANICAL AND PRODUCTION ENGINEERING IN

PARTIAL FULFILMENT OF THE REQUIREMENT FOR THE AWARD OF

MASTER OF SCIENCE IN ENERGY STUDIES

MOI UNIVERSITY

2023

DECLARATION

Declaration by candidate

I hereby declare that this thesis is my original work and in no part or whole was it copied from any other work. Any quotations were duly acknowledged. Likewise, this work should not in part or wholly appear in any other work without the consent of the author and/or Moi University.

Signature…………………………………………………Date………………………..…

Chida Simon Pharez

TEC/PGMP/09/18

Declaration by Supervisors

This thesis has been submitted for examination with our approval as University Supervisors.

Signature………………………………………………..Date…………….…..…………

Prof. Zachary Siagi

Moi University, Department of Mechanical and Production Engineering.

Signature………………………………………….…..Date…………..…..…………

Dr. Jerry Ochola

Moi University, Department of Manufacturing and Textile Engineering.

DEDICATION

I dedicate this thesis to my family and friends for the encouragement they generously

offered throughout the project period.

ACKNOWLEDGEMENT

ABSTRACT

Archimedes Screw Turbine (AST) is a growing technology in micro-hydropower generation, specifically suited for sites having very low hydraulic heads of less than 5m. However, mechanical efficiencies of installed ASTs are limited to a range of 60% to 80%. The main objective of this research was to numerically investigate how both the mechanical power and mechanical efficiency of the AST are impacted by varying related parameters: angle of inclination/screw length (β/L) and number of blades/pitch (N/S). Specific objectives were: to develop a 3D CAD model of an AST using typical parameters and dimensions and hence simulate flow through the machine; to determine the combined effect of each of the two sets of related parameters (β/L and N/S) on torque, mechanical power and efficiency of an AST and finally to establish optimal values of AST's parameters based on the results obtained from the second objective. 3D geometry of a reference AST of dimensions N=4, β=24.5°, L=617 mm, external diameter (D_o)=381 mm, internal diameter (D_i)=168 mm and pitch (S)=381 mm was developed using two CAD software packages: Solidworks and Design modeler. Tetrahedral and hex dominant mesh types were applied for the rotating and stationary parts respectively. CFX 2019 R1, which is an ANSYS-based CFD (Computational Fluid Dynamics) code, was used to numerically analyze the flow in order to determine pressure field and generated torque from which both mechanical power and efficiency of the turbine were computed. The flow was modeled as transient, multiphase (water and air) and turbulent, hence K-ϵ turbulence method was used to solve Reynolds averaged Navier-Stokes equations. Pressure was found to increase radially outwards to a maximum value (1447 Pa for reference screw) at the tip of blade. Torque oscillated about mean value (4.04 Nm for reference screw) with an amplitude that decreased with decreasing rotational speed. Decrease in inclination angle (β) and corresponding increase in screw length (L) led to increase in torque, mechanical power and mechanical efficiency. Highest values of both average and peak efficiencies were 83.4% and 89.4% respectively, produced by the screw inclined at 10°. Increase in number of blades (N) and corresponding increase in pitch (S) did not show a clear pattern on efficiency, but the screw geometry having 4 blades produced the highest average efficiency of 71.9% at a bucket width ratio (Wbr) of 0.17. Thus, optimal parameters were N = 4, W_{br} = 0.17, smallest tested value of β (10°) and n in the range of 30 rpm to 40 rpm. Numerical results were validated using data from experimental study of AST by Simmons et al. (2019). Peak efficiency from the numerical results closely estimated that from experimental data, especially for rotational speed not exceeding 45 rpm. In conclusion: slower rotational speeds reduce the amplitude of torque fluctuations; designs based on related parameters (β/L and N/S) were found to improve both the mechanical power and efficiency of the AST (for example, the highest average mechanical efficiency improved by 15.7% from 67.7% for designs based on β to 83.4% for designs based on β/L); further, AST designs based on β/L had more impact on AST's efficiency than those based on N/S which had an improvement on average mechanical efficiency of 4.2% from 67.7% for designs based on N to 71.9% for designs based on N/S. The following areas were recommended for further research: tests on related parameters at different values of diameter ratio, D_r (this study used D_r = 0.44); effect of torsional yielding and sagging on maximum screw length; and lastly, since scaling for AST has not been established, tests on the related parameters using full-size prototype ASTs should be conducted.

KEY WORDS

Micro-hydropower, Archimedes screw turbine, Computational fluid dynamics, Related

parameters, Constant hydraulic head, Bucket width ratio, Transient analysis.

TABLE OF CONTENTS

LIST OF TABL

LIST OF FIGUR

NOMENCLATURE

β Inclination angle [degree]. The angle between the global horizontal and the centerline of the turbine.

D_i internal diameter [m].

D_o external diameter [m].

D_r Diameter ratio ($D_r = D_o/D_i$)

f   Fill factor/Fill level. Ratio of bucket fill to optimal bucket fill without overflow.

g   gravitational acceleration at the surface of the earth (≈ 9.81 m/s^2)

G_w gap width [m]. It is the clearance between blade tip and the trough.

H   Hydraulic head across the ends of an AST. It is used for calculating input power.

H_s Maximum hydraulic head at a micro-hydropower site. It is used for calculating available power.

L   Screw length [m]. The Flighted length of the AST.

L_r Length ratio. Ratio of screw length (L) to external diameter (D_o).

$\dot{m}$ Mass flow rate [kg/s],

n   Rotational speed [rev/min]. Number of rotations of the screw per minute.

n_b Number of buckets.

N   Number of blades

Pa   Pascal. SI unit for pressure.

P_{avail} Available power [W]. It is the power available at a site, calculated using maximum hydraulic head available at a specific hydropower site.

P_{in} Input power [W]; calculated using head drop across the screw ends.

$P_{mech.}$ Mechanical power [W]. Power output produced at the turbine shaft.

Q   Flow rate [m^3/s].

S   Pitch [m].

S_r Pitch ratio. The ratio of pitch (S) to external diameter (D_o).

T   Torque [Nm]

ρ Density [kg/m^3].

ω Angular velocity [rad/s].

W_{br} Bucket width ratio. Ratio of bucket width (W_b) to external diameter (D_o).

ACRONYMS AND ABBREVIATIONS

ASG   Archimedes Screw Generator. Refers to an assembly of AST, constant speed

gearbox and a generator.

ASP   Archimedes Screw Pump

AST   Archimedes Screw Turbine

ASTs Archimedes Screw Turbines.

CAD Computer Aided Design.

CFD Computational Fluid Dynamics

OPERATIONAL DEFINATION OF TERMS

Bucket: Space between two adjacent blades of Archimedes screw.

Bucket width   shortest distance from tip of a blade to the next blade tip, whether of the same blade or not.

Efficiency   mechanical efficiency of an AST

Outputs parameters of AST   Torque, mechanical power and efficiency of an AST.

Pitch   shortest distance from tip of a blade to the next blade tip of the same blade.

Power   mechanical power of an AST

Related parameters   Two parameters that are proportional to one another, hence they can be related by an equation such that a change in the value of one parameter automatically leads to a definite change in the value of the other.

Rotational speed   Angular velocity in revolutions per minute (rpm).

CHAPTER ONE: INTRODUCTION

1.0 Background of the Study

Electrical energy deficiency is one of the main causes of underdevelopment in rural and remote areas of developing countries (Fulford et al., 2000). Renewable energy, especially micro-hydroelectric power (power <100 kW), has been fronted as a promising option for meeting the energy demand by the rural populations (Laghari et al., 2013). However, micro-hydro sites are characterized by low hydraulic head (head<10 m); hence their development is curtailed by techno-economic challenges, particularly the trade-in between cost and mechanical efficiency of hydro-turbines for the sites (Nuramal et al, 2017).

The search for appropriate machines for the micro-hydro sites is currently concentrated around improving the efficiency of the Archimedes Screw Turbine (AST) which is a growing hydro-technology known for its cost-effectiveness, robustness, simplicity, and ability to operate at very low hydraulic heads of less than 5 m (Lashofer et al., 2012). However, the mechanical efficiency of installed AST's is limited to the range of 60% to 80% (YoosefDoost & Lubitz, 2020). Thus, AST's efficiency is much lower than that of high head reaction and impulse turbines that are recorded, in terms of the weighted average mechanical efficiency, as 95 % and 92 % respectively (Paish, 2002).

1.1 Brief Introduction to Hydro Turbines

Hydro-turbines are machines that convert energy in water into mechanical energy required to drive an electrical generator. They are classified either in terms of how torque is generated (impulse or reaction turbines) or the size of hydraulic head at which they best operate.

Impulse turbines are designed on the principle of impulsive force created when high-speed jet of water strikes rotor blade (Kozyn, 2016). Available potential energy is initially converted to kinetic energy of water jet at the nozzle (Kothandaraman, 2017). Figure 1.1 shows the working principle of impulse turbine.
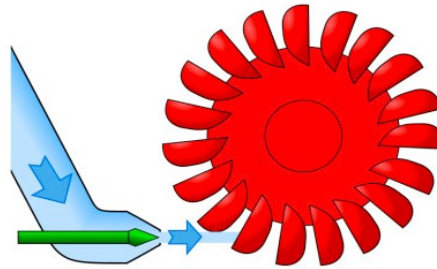
Figure1. 1: Working Principle of Impulse Turbine (Breeze, 2018)

Conversely, reaction turbines are designed on the principle of reaction force. Motion of water between the runner blades create pressure differences hence a lift force that in turn causes rotation of the turbine (Kothandaraman, 2017). Figure 1.2 shows parts and working principle of a reaction turbine.
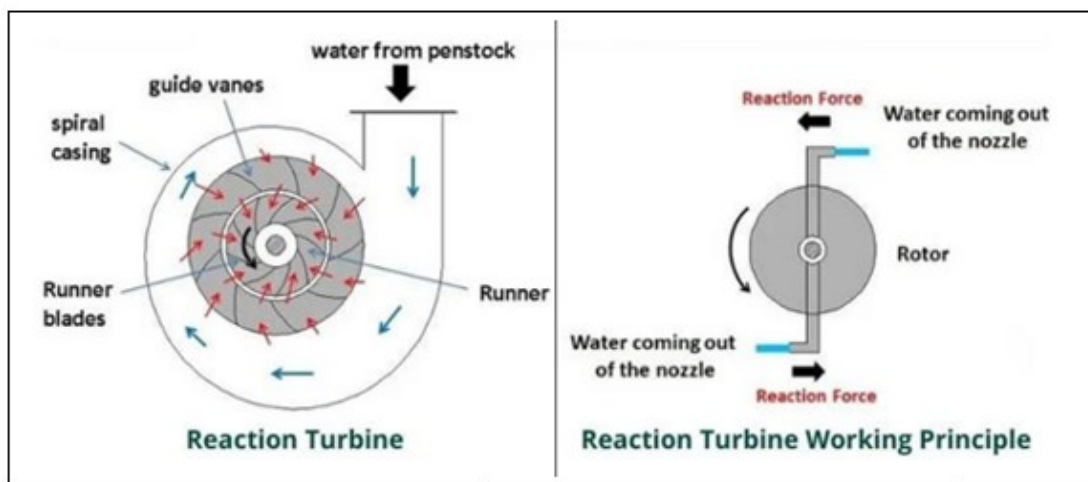
Figure1. 2: Parts and Working Principle of Reaction Turbine (Mechanicaljungle, n.d)

Based on hydraulic head, hydro turbines can be classified as high head (head>50 m), medium head (head: 10 – 50 m) or low head (head<10 m) machines (Kothandaraman, 2017). Table 1.1 shows a list of hydro turbines and the ranges of head at which they best operate. Kaplan and crossflow turbines are the traditional machines for low head micro- hydro sites, the former being first-choice (El Najjar, 2017).

Table 1. 1: Operational Hydraulic Heads for Hydro-turbines (Adapted from Celikdemir, 2017)

Turbines	Head>100 m	20<Head<100 m	5<Head<20 m	Head<5 m
Impulse	Pelton Turgo	Crossflow Turgo Multi-Jet Pelton	Crossflow Multi-Jet Pelton	Water-wheel
Reaction		Francis	Propeller Kaplan	Propeller Kaplan

The main differences between the turbines is in their geometries. Figure 1.3 shows drawings of some of the machines.
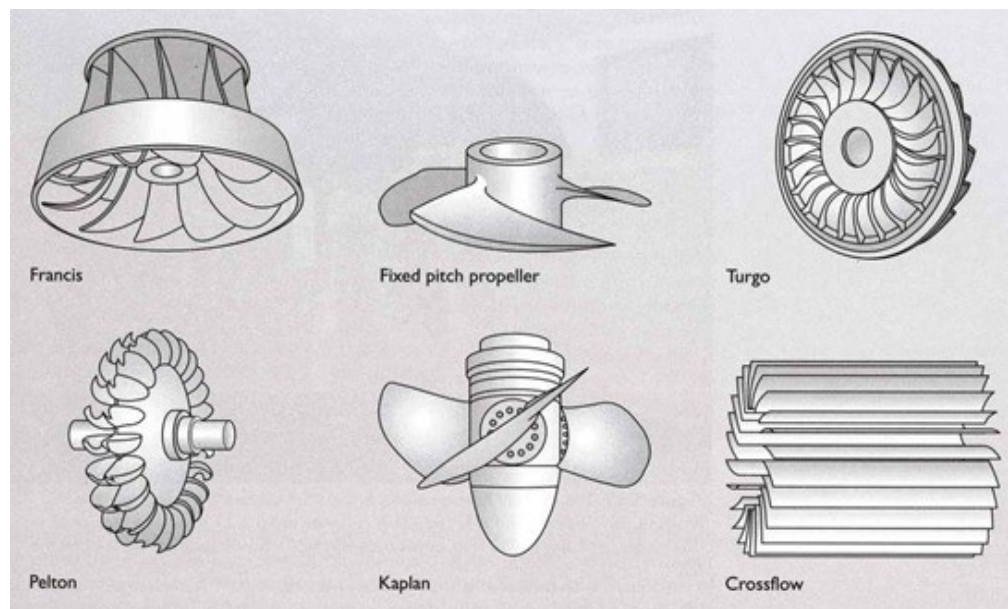
Figure1. 3: Images of Different Types of Hydro-Turbines (Hatata et al., 2019)

1.2 Turbines for Low Head Applications

1.2.1 Kaplan Turbine

Kaplan is a propeller turbine that has been fitted with adjustable pitch vanes in order to increase its mechanical efficiency. The machine can be designed to achieve high mechanical efficiency values, but at the expense of high initial and maintenance costs (Kotronis, 2016). Figure 1.4 shows main components of Kaplan turbine.
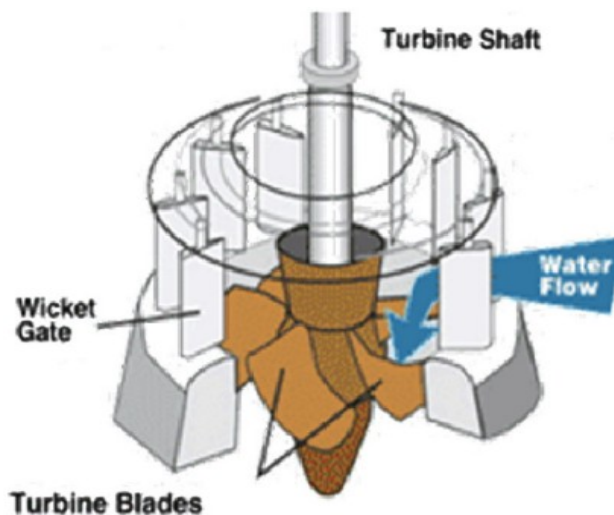
Figure 1. 4: Kaplan Turbine, Main Components (Okot, 2013)

1.2.2 Crossflow Turbine

This is an impulse turbine that consists of lengthy curved blades that are welded circumferentially around two parallel end-disks as shown in Figure 1.5. Water transversely passes through the turbine hence it interacts twice with the blades before exiting; thus, most of the kinetic energy is transmitted to the rotor (Doven et al., 2020). However, the machine has lower mechanical efficiency than Kaplan turbine and is not suitable for sites having less than 10 m of hydraulic head (Kotronis, 2016).

Cross Flow Turbine   Transverse flow
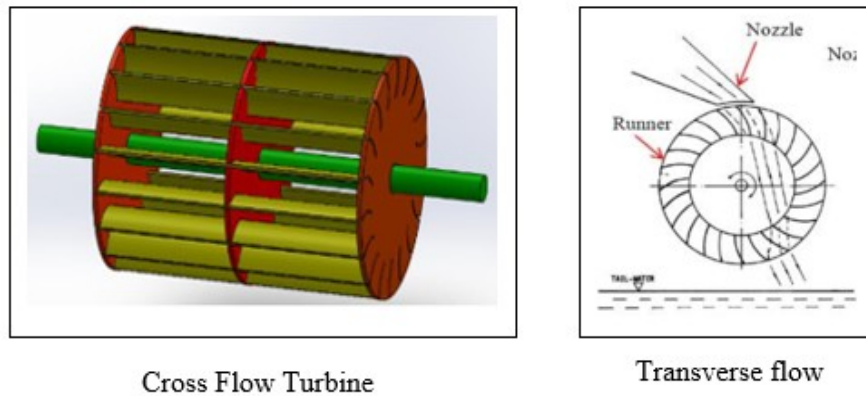
Figure1. 5: Cross Flow Turbine (Hidayat et al., 2020)

1.3 Archimedes Screw Turbine (AST)

The Archimedes screw is an old technology accredited to Archimedes (Kotronis, 2016). Over centuries the machine was famous for its application as a water pump particularly for moving water from low to higher grounds for the purposes of irrigation (Rorres, 2000). Figure 1.6 shows the application of Archimedes screw as a pump (ASP).
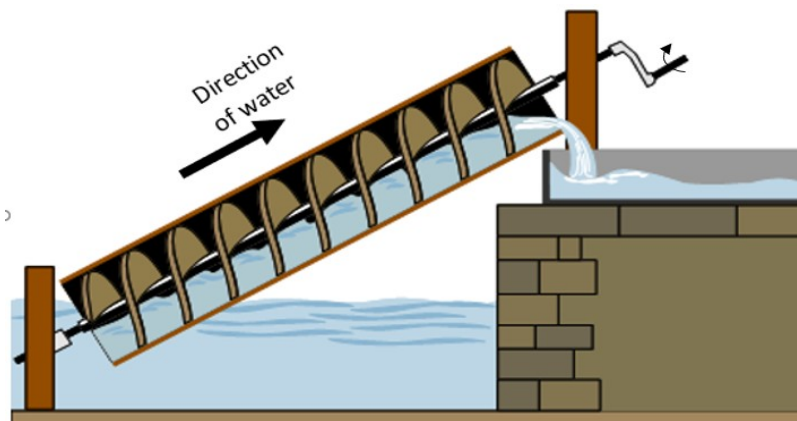
Figure1. 6: Archimedes Screw Pump (Mechstuff, 2021)

A recent development in the application of Archimedes screw came at the end of the 20th century whereby the machine acquired a new function as a hydro turbine (Lyons, 2014). Figure 1.7 shows Archimedes Screw generator (ASG) which is an assembly of AST and electrical generator via a gearbox.
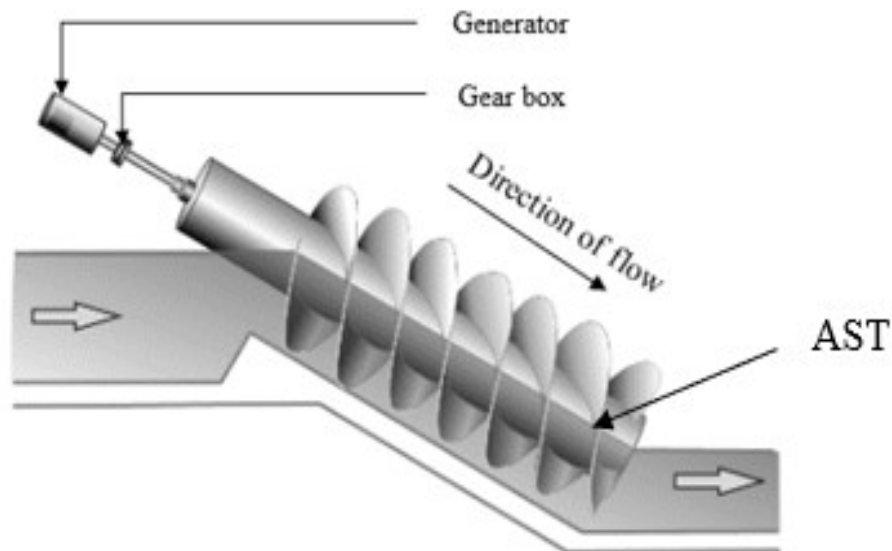
Figure1. 7: Archimedes Screw Generator (Adapted from Yulianto, 2019)

1.4 Parameters and Working Principle of Archimedes Screw Turbine (AST)

The AST comprises a shaft mounted on two bearings (one at each end) and a helical blade or helical blades welded along the length of the shaft. It is operated based on the principle of conservation of energy. Water at the inlet possess potential energy that is converted into mechanical energy of a rotating shaft. The process begins by water filling the spaces between adjacent blades hence exerting pressure on the blades. The pressure generates torque which causes the screw to rotate. An AST can be coupled to a generator via a gearbox in order to convert the mechanical energy to electrical energy. The AST-Generator system is known as Archimedes screw generator (ASG).

The mechanical efficiency of an AST is dependent on several geometric parameters some of which their optimal values have not been established (Kotronis, 2016). The parameters include pitch (S), number of blade (N), internal diameter (D_i), gap width (G_w), rotational speed (n), head (H) across the AST, fill factor (f), external diameter (D_o), screw length (L), flow rate (Q), and inclination angle (β) (Waters, 2015). Further,

a novel internal parameter, bucket width (W_b), has been introduced. Figure 1.8 shows geometric parameters of an AST having 2 blades.
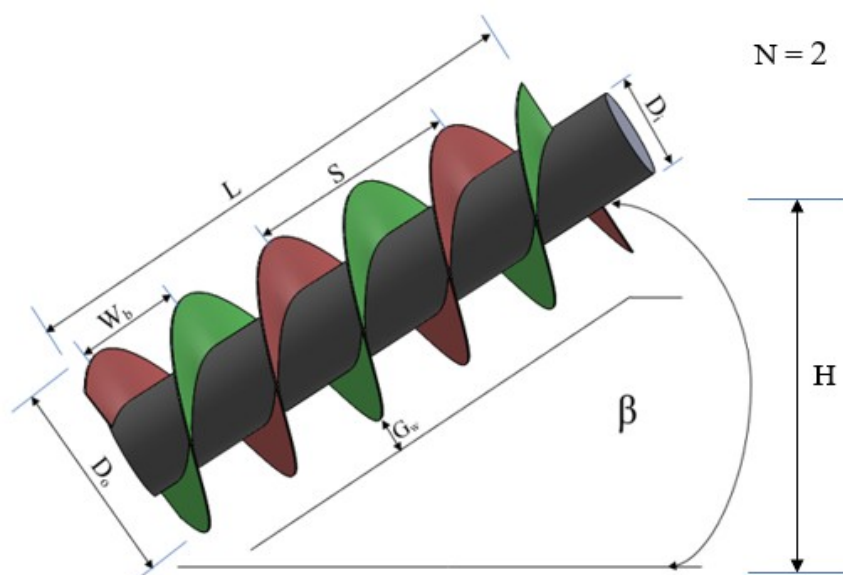
Figure 1. 8: Geometric Parameters of an AST having 2 Blades

1.5 Parametric studies on Archimedes Screw Turbine (AST)

Studies on AST have predominantly concentrated on individual effect of each AST parameter on the efficiency of the machine (Warjito et al., 2017). Results from the studies have established the following trends and optimal levels for some of the parameters of the machine: mechanical efficiency decreases with increase in gap-width (Lyons, 2014); increase in rotational speed leads to increase in both the mechanical power and efficiency of the machine up to a point beyond which further increase in the rotational speed leads to reduction in the two output parameters (Waters, 2015); lastly, both torque and mechanical efficiency of an AST increases with increase in flow rate, provided optimal fill level is not exceeded (Salam et al., 2018; Lyons, 2014).

Conversely, results from studies on the effects of some parameters such as inclination angle (β) and number of blades (N) on the mechanical efficiency of the turbine are both

inconsistent and non-conclusive. For example, Salam et al. (2018) from their experimental study of AST suggested that the mechanical efficiency of an AST increases with decreasing magnitude of β while Lyon (2014) suggested the opposite, that mechanical efficiency increases with increasing magnitude of β. Similarly, the optimal size of β has also not been established as attested to by results from different studies: 22° (Nuramal et al., 2017), 35° (Dellinger et al., 2016) and 46° (Lyons, 2014). Studies have also differed on optimal number of blades with Salam et al. (2018), Rosly et al. (2016) and Lyons (2014) suggesting 4, 3 and 2 blades respectively.

A research gap that need to be filled is the determination of the effects of related AST such as the inclination angle (β) and screw length (L) on both mechanical power and mechanical efficiency of the machine. According to Waters (2015) and Lyons (2014), studies on β should be diversified to include the combined effect of β and L under the constraint of constant size of the hydraulic head. They argued that a smaller angle with increased length may give higher values of mechanical power and efficiency. Figure

1.9 illustrates variations of β and L.
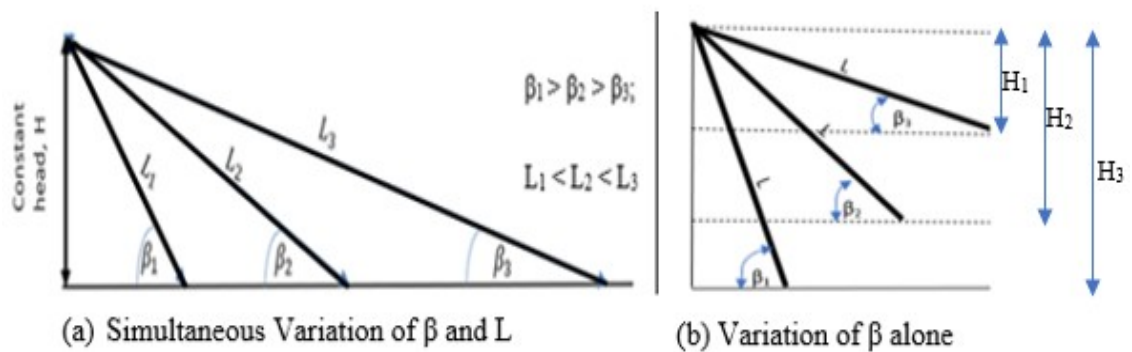
Figure 1. 9: Variations of β and L

From Figure 1.9 (a), the parametric relationship between β and L is given by equation 1.1.

$$\sin\beta=\frac{Head}{Length}\quad \textbf{Equation1.1}$$

The constant head ensured that a constant input power (P_{in}), given by $P_{in} = \rho gQH$, was applied in all the tests. In contrast, Figure 1.9 (b), shows variation of β at constant screw length for which the increase in β corresponded to decrease in head (H) and reduction in input power (P_{in}). The implied under-utilization of the available head corresponds to lower output power.

Another set of related parameters that need to be researched on is the effect of number of blades (N) and pitch (S) on the mechanical efficiency of an AST. This study is necessary in order that changes in number of buckets (n_b) do not confound the effect of

N on AST's mechanical efficiency. To maintain n_b at a constant value, a parameter named bucket width (W_b) was introduced and defined by equation 1.2.

$$W_b = \frac{S}{N}$$ **Equation 1.2**

Where $\mathbf{W_b}$ is the bucket width, **S** is pitch and **N** is the number of blades.

If the size of W_b is maintained at a constant value then modification of N leads to automatic modification of S, but number of buckets (n_b) remain constant. Figure 1.10 shows three screw geometries each having 6 buckets but different values of N and S.
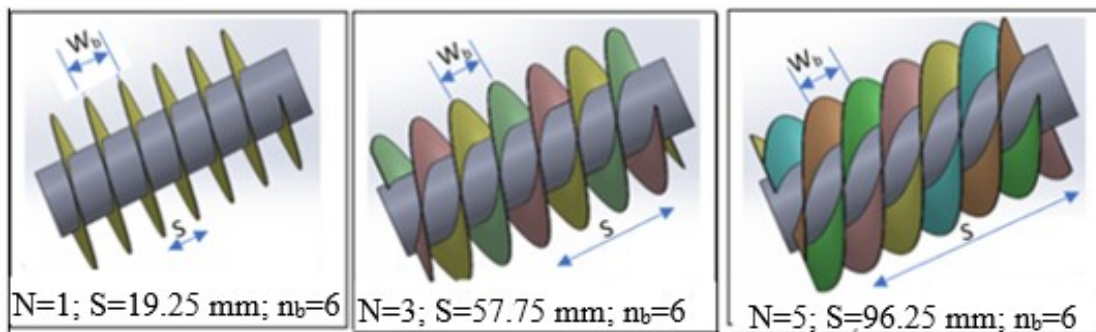
Figure 1. 10: Screws with Different Values for N and S, but Constant $\mathbf{W_b}$

1.6 Problem Statement

Archimedes Screw Turbine (AST) is a technology that is gaining popularity as a suitable machine for application at low head micro-hydropower sites. However, the mechanical efficiency of installed Archimedes screw turbines (ASTs) is limited to the range of 60 % to 80 %. Studies aimed at improving the performance of the machine have concentrated on determining the effects of individual parameters such as β and N on its mechanical power and mechanical efficiency. This approach excludes the effects of related parameters on AST's performance. Therefore, there is need to determine the combined effect of related parameters such as inclination angle/screw length (β/L) and

number of blades/pitch (N/S) on both the mechanical power and mechanical efficiency of ASTs.

1.7 Objectives of the Study

1.7.1 Main Objective

The main objective of this research was to investigate, using numerical analysis, how both the mechanical power and mechanical efficiency of the AST are impacted by varying related parameters: angle of inclination/screw length (β/L) and number of blades/pitch (N/S).

1.7.2   Specific Objectives

(i) To develop a 3D CAD model of an AST using typical parameters and dimensions and hence simulate flow through the machine.

(ii) To determine the combined effect of each of the two sets of related parameters (β/L and N/S) on torque, mechanical power and efficiency of an AST.

(iii)   To establish AST's optimal parametric values based on results obtained in (ii).

1.8 Justification and Significance of the Study

1.8.1 Justification

Kenya has enormous micro hydro potential hence the need to develop an efficient micro-hydro turbine with the aim to supply cheap and reliable electricity to villages and remote areas in the country. The potential of small rivers and streams in Kenya is estimated at 3000MW, but only 30MW has been exploited (Kiplagat et al., 2011). Further, AST technology is an industry that can be easily localized from design, fabrication and maintenance stages thus contributing to the industrialization process of the country. Lastly, the outcomes of the study will add to the knowledge base on ASTs.

1.8.2 Significance

Determination of the combined effects of related parameters will contribute towards the design of more efficient ASTs, hence make the development of micro-hydro sites more attractive to investors.

1.9 Scope and Limitations

1.9.1 Scope

The study encompassed transient simulation of flow through ASTs for ultra-low head (head < 3 m) sites. Solidworks and Design modeler CAD software programs were used for geometry creation. ANSYS-CFX, which is an Ansys-based CFD code, was used to analyze the flow.

1.9.2 Limitations

Numerical algorithms have characteristic error patterns which were not analyzed in this work.

1.10 Assumptions

Since the study is CFD based, several assumptions were made at pre-processor stage in order to operationalize the computer simulations of the flow through the turbine. The assumptions were:

(i) The maximum hydropower available for conversion to mechanical power by the turbine is solely from potential energy possessed by the fluid at the inlet.

(ii) Hydrostatic pressure of the water in screw buckets is the source of force that generates torque.

(iii) The maximum head that can be designed for an AST is determined by site conditions.

CHAPTER TWO: LITERATURE REVIEW

1

2.1 3D Archimedes Screw Turbine Model and Simulation of Flow through it

Fluid flow is numerically analyzed using Computational Fluid Dynamics (CFD) method which is defined as the analysis of systems involving fluid flow, heat transfer and associated phenomena such as chemical reactions by means of computer-based simulation (Versteeg, 2007). Geometries for numerical analysis are created using Computer Aided Design (CAD) software packages such as Solidworks and Design-modeler (Schleicher, 2012). For the case of flow through Archimedes screw turbine, outputs of interest may include pressure field and torque (Dellinger et al., 2016).

CFD codes are structured around numerical algorithms that are used to solve governing equations that describe the behavior of a fluid (Versteeg, 2007). The governing equations are basically conservation equations for mass, momentum and energy. According to Potter et al. (2016), if body forces emanate from gravity alone, the equations for transient regimes take the following forms:

- Conservation of mass

   Continuity equation;

$$\frac{\partial \rho}{\partial t} + \frac{\partial (\rho u)}{\partial x} + \frac{\partial (\rho v)}{\partial y} + \frac{\partial (\rho w)}{\partial z} = 0 \qquad \textbf{Equation 2.1}$$

- Conservation of momentum

   x-component of momentum equation;

Equation 2.2

$$\rho \frac{Du}{Dt} = -\frac{\partial p}{\partial x} + \rho g_x + \mu \nabla^2 u$$

y-component of momentum equation;

$$\rho \frac{Dv}{Dt} = -\frac{\partial p}{\partial y} + \rho g_y + \mu \nabla^2 v \qquad \textbf{Equation 2.3}$$

z-component of momentum equation;

$$\rho \frac{Dw}{Dt} = -\frac{\partial p}{\partial z} + \rho g_z + \mu \nabla^2 w \qquad \textbf{Equation 2.4}$$

where $\quad \dfrac{D}{Dt} = \dfrac{\partial}{\partial t} + u\dfrac{\partial}{\partial x} + v\dfrac{\partial}{\partial y} + w\dfrac{\partial}{\partial z}$

and $\quad \nabla^2 = \dfrac{\partial^2}{\partial x^2} + \dfrac{\partial^2}{\partial y^2} + \dfrac{\partial^2}{\partial z^2}$

- Conservation of energy (Newton's First Law of Thermodynamics)

$$
\begin{aligned}
\frac{\partial}{\partial t}&\left[\rho\left(e + \frac{V^2}{2}\right)\right] + \nabla \cdot \left[\rho\left(e + \frac{V^2}{2}\vec{V}\right)\right] \\
&= \rho\dot{q} + \frac{\partial}{\partial x}\left(k\frac{\partial T}{\partial x}\right) + \frac{\partial}{\partial y}\left(k\frac{\partial T}{\partial y}\right) \\
&\quad + \frac{\partial}{\partial z}\left(k\frac{\partial T}{\partial z}\right) - \frac{\partial(up)}{\partial x} - \frac{\partial(vp)}{\partial y} - \frac{\partial(wp)}{\partial z} + \frac{\partial(u\tau_{xx})}{\partial x} \\
&\quad + \frac{\partial(u\tau_{yx})}{\partial y} + \frac{\partial(u\tau_{zx})}{\partial z} + \frac{\partial(v\tau_{xy})}{\partial x} + \frac{\partial(v\tau_{yy})}{\partial y} \\
&\quad + \frac{\partial(v\tau_{zy})}{\partial z} + \frac{\partial(w\tau_{xz})}{\partial x} + \frac{\partial(w\tau_{yz})}{\partial y} + \frac{\partial(w\tau_{zz})}{\partial z} + \rho\vec{f}\cdot\vec{V}
\end{aligned}
$$

$\textbf{Equation 2.5}$

According to Tu et al. (2018), a CFD code consist of three main components: pre-processor, solver (processor) and post-processor. Figure 2.1 presents a framework that illustrates the interconnectivity of the three components within the CFD analysis.
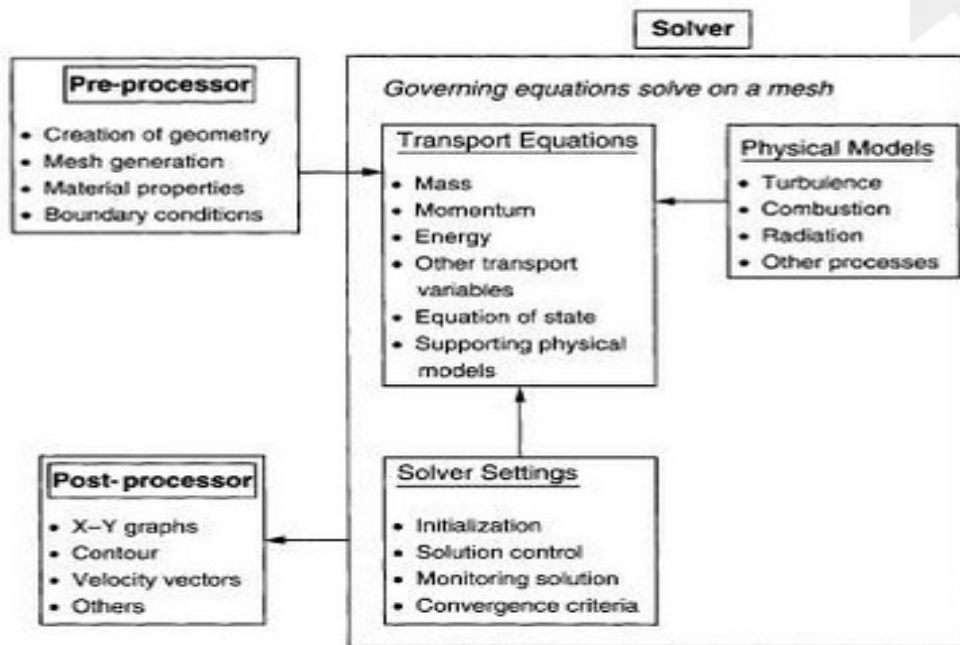
Figure 2. 1: Inter-Connectivity of Pre-Processor, Solver and Post-Processor within a CFD Framework (Tu et al., 2018)

2.1.1 Pre-Processor

Pre-processor component facilitates inputting of the following information into a CFD code: geometry, mesh, physical/material properties and boundary conditions (Tu et al., 2018).

2.1.1.1 Creation of Geometry

In order to perform numerical analysis of flow through an AST, four geometric parts (Archimedes screw, cylindrical enclosure, inlet section and outlet section) should be created and assembled in a CAD software (Dellinger et al., 2016). In order to complete the geometry for the computational domain, Boolean operation should be performed in order to subtract the screw (Dellinger et al., 2016). The imprint of the screw, which remains after performing the Boolean operation, is used as a representation of the screw during the performance of numerical computations (Waters, 2015). Dimensions of

screw models are either chosen arbitrarily or adopted from specific laboratory size screws (CA, 2018; Kozyn, 2016).

2.1.1.2 Mesh Generation

Meshing is the process of partitioning a computational domain into smaller discrete geometric and topological elements (Tu et al., 2018). Each of the elements in a mesh act as a tiny control volume in which discretized versions of the conservation equations are solved (Versteeg, 2007). The choice of mesh-type and assurance of mesh quality are key in the generation of appropriate mesh (Waters, 2015).

2.1.1.2.1 Types of Meshes

Meshes or grids are broadly categorized as either structured (mapped) or unstructured (free). A structured mesh is regular in pattern while unstructured one is irregular (Tu et al., 2018). Thus, unstructured mesh has no restrictions in terms of element shape and has no specified pattern applied to it while a structured mesh is restricted in terms of the element shape and pattern of the mesh (ANSYS, 2004). Figure 2.2 shows examples of the two types of meshes.
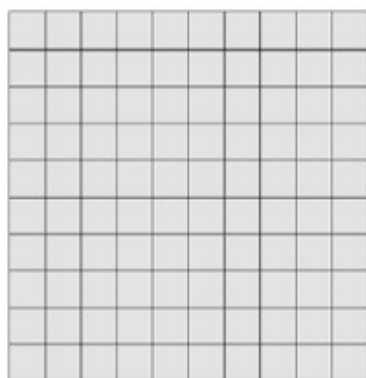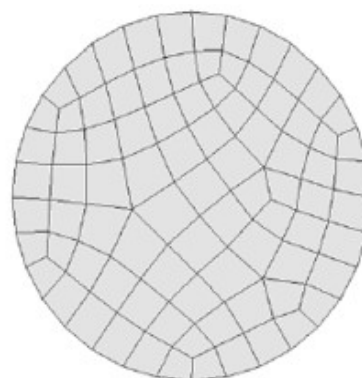
Structured Mesh   Unstructured Mesh

Figure 2. 2: Two-Dimensional (2D) Structured and Unstructured Meshes (Woodbury, 2008)

According to ANSYS (2004), a 2D structure mesh contains either purely quadrilateral or triangular elements while a structured 3D mesh contains only hexahedron elements. In addition, the regular pattern of structured mesh implies that it is best suited for fairly regularly shaped geometries (ANSYS, 2004). On the other hand, 2D and 3D unstructured meshes commonly contain triangular and tetrahedron elements respectively (Waters, 2015). Another type of element that can be used for 3D unstructured mesh is polyhedron, but its applicability is currently available only in Fluent Meshing software. Shedage (2014) describes a third category of meshes, semi-structured mesh, that is applied at regions such as boundary layer where both structured and unstructured elements do not fit well. The elements for this category of meshes include triangular prism and pyramid; the former is good for resolving boundary layer while the latter is effectively used as transition element between square and triangular faced elements and in hybrid meshes. Figure 2.3 shows sketches of common 2D and 3D the elements.
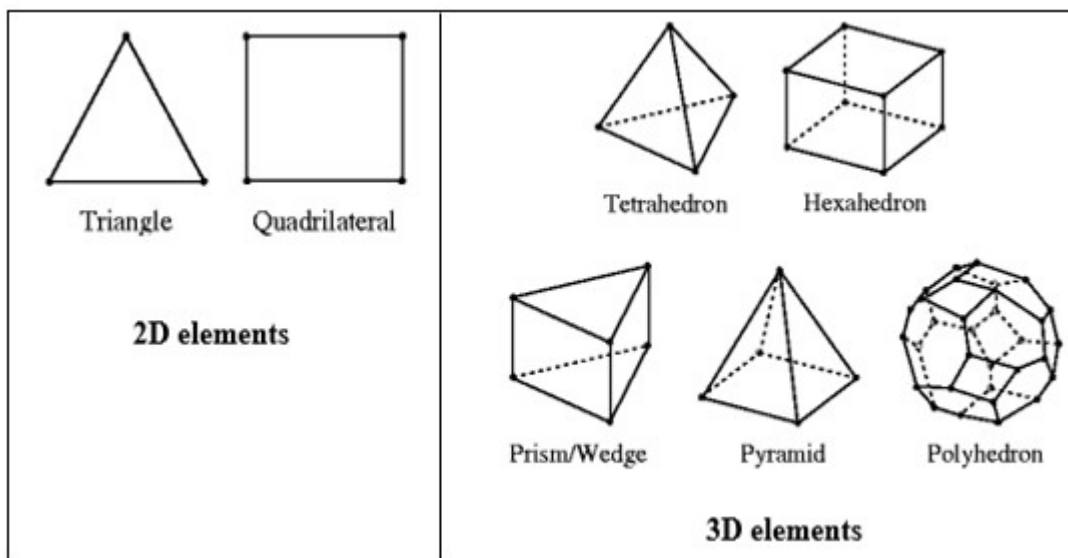
Figure 2. 3: Types of Elements (ANSYS, 2009)

The choice of element type depends on the complexity of geometry. As a general guide, Dana (2020) proposes three-point criteria for choosing type of element as follows: quadrilateral/hexahedral meshes are for simple geometries, triangular/ tetrahedral meshes with wedge elements in the boundary layers are for relatively complex geometries and lastly pure triangular/tetrahedral meshes are for complex geometries. Sometimes a fluid domain can be decomposed into multiple portions for hybrid meshing such that parts of the geometry that are regular can have structured grids and those that are complex can have unstructured grids (ANSYS, 2013). In such cases, the grids can be non-conformal which means that grid nodes do not match at block boundaries (ANSYS, 2013).

In numerical studies on AST the rotating domain has been treated as a complex geometry, hence unstructured mesh has been predominantly applied. For example, Waters (2015) meshed the domain using patch conforming tetrahedral mesh in order to properly capture the geometry of the spiral-shaped blade walls. Other works that applied the same meshing structure include CA (2018) and Espinosa (2019). Further, mesh adjacent to the walls should be fine enough to resolve the boundary layer flow (Shedage, 2014). This has been achieved mainly through increasing mesh density at areas of interest, especially within the boundary layer for the screw blades and parts of enclosure wall adjacent to the tips of blades (Waters, 2015).

2.1.1.2.2 Mesh Quality

When meshing irregular or complex geometric models the ideal shapes of mesh elements get distorted, thereby affecting mesh quality (ANSYS, 2013). There are

several parameters that can be used to measure mesh quality. These include aspect ratio, skewness, orthogonality and smoothness (ANSYS, 2013).

Skewness is a primary measure of mesh distortion/quality as it directly shows how close the mesh element is to its ideal shape (ANSYS, 2013). Figure 2.4 shows non-skewed and skewed elements.
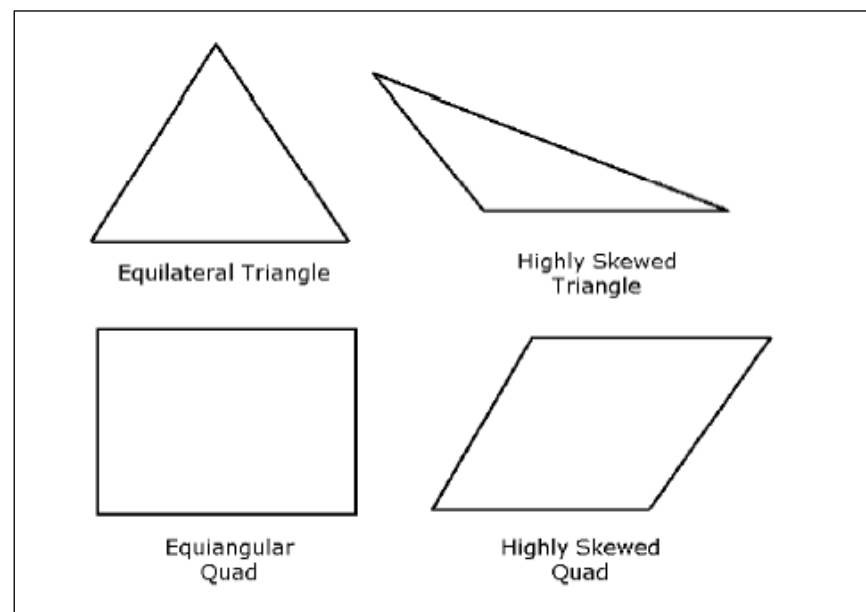
Figure 2. 4: Ideal and Skewed Triangles and Quadrilateral Elements (ANSYS, 2013)

Skewness can be measured in terms of fractional distortion of cell size. Thus:

$$Skewness = optimal\, cell\, ¿¿¿ optimal\, cell\, ¿¿¿¿$$

Equation 2.6

A non-skewed element has a skewness value of zero while the value for a highly skewed element is close to 1 (ANSYS, 2013). Thus, the smaller the skewness the

greater the element quality. Table 2.1 provides a general guide to the relationship between cell skewness and quality.

Table 2. 1: Skewness Ranges and Cell Quality (ANSYS, 2013)

Value of Skewness	Cell Quality
1	degenerate
0.9 - 1	bad (sliver)
0.75 – 0.9	poor
0.5 – 0.75	fair
0.25 – 0.5	good
0 – 0.25	excellent
0	equivalent

As a general rule, cell skewness for 2D and 3D geometries should be at worst 0.25 (excellent quality) and 0.5 (good quality) respectively (ANSYS, 2013).

Aspect ratio (distortion of length) is the ratio between the largest and smallest dimension of an element; hence its optimal value is 1 for an equilateral element such as an equilateral triangle or a square and greater than 1 for less regularly-shaped elements (ANSYS, 2013). Higher aspect ratios lead to both poorer estimates of derivatives and poorer convergence (ANSYS, 2013). Figure 2.5 illustrates optimal and large aspect ratios.
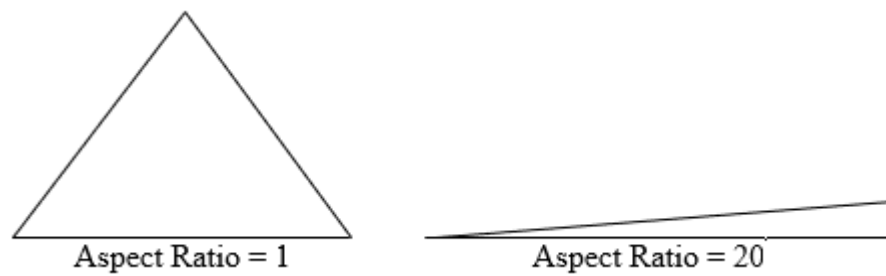
Figure 2. 5: Aspect Ratios for Triangles (ANSYS, 2013)

Orthogonality, as illustrated in Figure 2.6, is another important mesh quality parameter. Non-orthogonality refers to the angle between the vector joining two adjacent cell centers and the face normal of the common face (SIMSCALE, 2022). Angle of zero means perfect orthogonality.
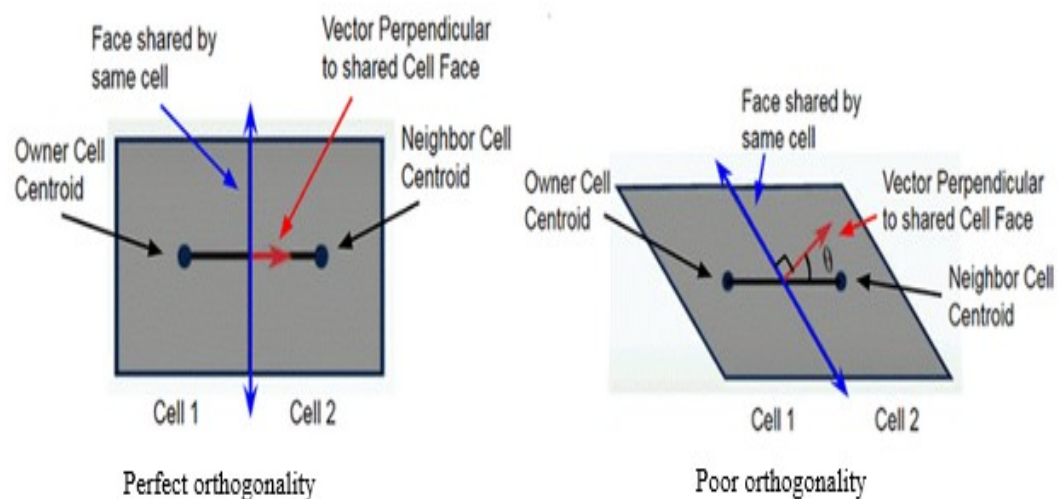
Figure 2. 6: Orthogonality (SIMSCALE, 2022)

According to SIMSCALE (2021), meshes for complex models are rarely orthogonal; thus, non-orthogonality corrections are made for stability and accuracy of computations.

Mesh quality is also affected by another parameter known as smoothness which refers to change in elemental size from one element to the next; the change should be gradual

(smooth) in order not to affect computations (Shedage, 2014). Figure 2.7 illustrates smoothness.
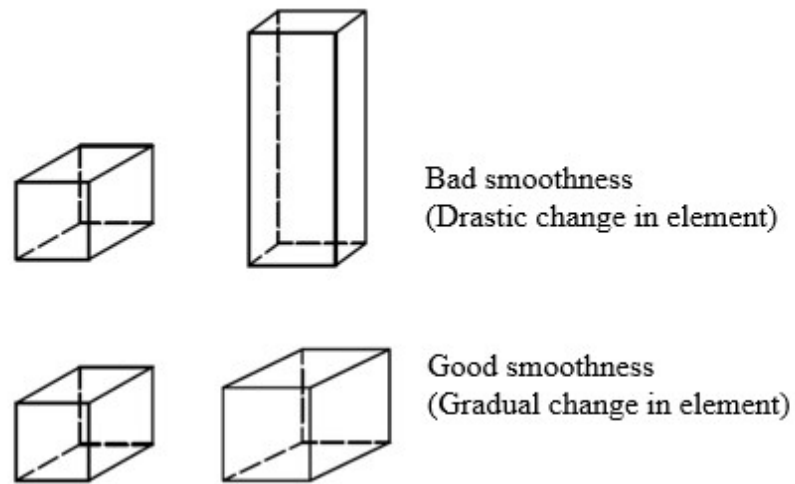
Figure 2. 7: Smoothness (Shadage, 2014)

2.1.1.3 Physical/Material Modeling

Industrial CFD flow problems have unique flow complexities, hence a CFD user should carefully implement flow physics that are unique to the particular fluid flow system (Tu et al., 2018). Figure 2.8 is a flow chart showing the various flow physics in CFD.
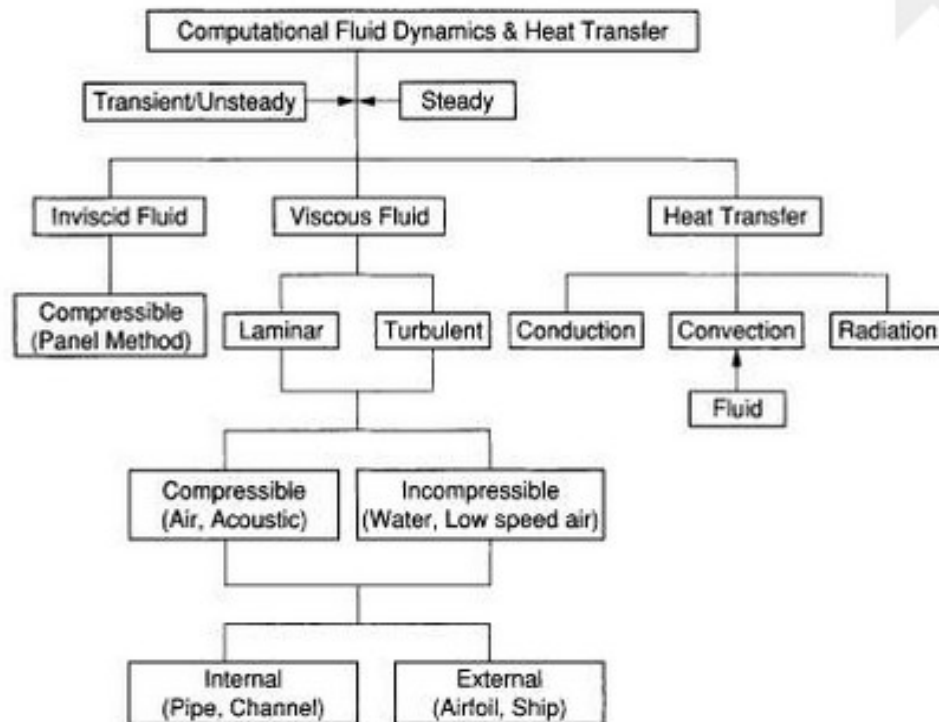
Figure 2. 8: Flow Chart Showing the Various Physics in CFD (Tu et al.,2018)

Initially, as shown in Figure 2.8, a CFD user has to decide on whether to implement transient (unsteady) or steady solution. This is followed by defining the class to which each fluid in the analysis belong; whether inviscid or viscous. Viscous fluids are further classified as either laminar or turbulent and compressible or incompressible. Another factors to consider is heat exchange **(**Tu et al., 2018**)**.

According to Lyons (2014), flow through an AST is transient, multiphase, viscous, turbulent and does not involve heat exchange.

2.1.1.3.1 Transient Flow Versus Steady Flow

Unlike for steady flow, transient (unsteady) flow is one in which flow parameters such as pressure and velocity at a point vary with time (Dellinger et al., 2016). According to Schleicher (2012), rotation of the screw makes the flow in the region close to it transient in nature. However, in most works such as Dellinger et al. (2016), Waters

(2015) and Lyons (2014), flow through the AST has been assumed to be steady in order to save on both storage space and computational time. However, it should be noted that the assumption compromises the accuracy of the simulation results (Schleicher, 2012).

2.1.1.3.2 Multiphase versus Single phase

Multiphase can either be separated such that the two fluids occupy two distinct sections of the flow domain as is the case with free surface flow or dispersed such that the phases are mixed at microscopic level as is the case of air bubbles in water (Ansys Inc., 2013). Multiphase flow in an AST is a separated type with distinct interface between water and air (Dellinger et al., 2016). Such separated systems can be modelled using Volume of Fluid (VOF) technique which is a powerful method for determining the evolution of free surface for two non-miscible phases such as water and air (Dellinger et al., 2016). The method uses cell filling (Volume fraction) to determine time evolution for boundary cells (Dellinger et al., 2016).

Literature review on AST revealed that in some studies the flow was modeled as multiphase (Lyons, 2014) while in some it was treated as single-phase comprising of water only (CA, 2018). According to Lyons (2014), modeling the flow as single-phase is not practically sound since the screw is not fully immersed in water.

2.1.1.3.3. Turbulent versus Lamina Flow

According to Lyons (2014), rotation of the screw makes the flow through an AST to be turbulent. The Navier-Stokes equations describe both laminar and turbulent flows without the need for additional information, but turbulent flow generally involve length scales that are much smaller than the smallest possible finite volume mesh (ANSYS, 2011). Thus, to account for turbulence, the original unsteady Navier-Stokes equations

are modified to include both averaged and fluctuating quantities thus creating Reynolds Averaged Navier-Stokes (RANS) equations. However, the RANS method introduces further terms with unknown parameters; the equations used to solve the unknowns define the type of turbulence method used (ANSYS, 2011).

Common turbulence models are two-equation models such as k-epsilon (k-ε) and k-omega (k-ω) in which both the velocity and length scale are solved using separate transport equations (ANSYS, 2011). Taking the k-ε model, which is good for resolving wall functions, the two additional equations are presented as follows (ANSYS, 2011):

The continuity equation becomes:

$$\frac{\partial \rho}{\partial t} + \frac{\partial}{\partial x_j}\left(\rho U_j\right) = 0$$

Equation 2.7

Momentum equation becomes:

$$\frac{\partial \rho U_i}{\partial t} + \frac{\partial}{\partial x_j}\left(\rho U_i U_j\right) = -\frac{\partial p'}{\partial x_i} + \frac{\partial}{\partial x_j}\left[\mu_{eff}\left(\frac{\partial U_i}{\partial x_j} + \frac{\partial U_j}{\partial x_i}\right)\right] + S_M$$

Equation 2.8

where S_M is the sum of body forces, μ_{eff} is the effective viscosity accounting for turbulence, and p' is modified pressure.

The effective viscosity, $\mu_{eff} = \mu + \mu_t$,

Equation 2.9

where μ_t is the turbulence viscosity which have both k (turbulent kinetic energy) and ε (turbulence dissipation rate) as its parameters. Thus:

$$\mu_t = C_\mu \rho \frac{K^2}{\varepsilon}$$

Equation 2.10

According to Schleicher (2012), K and ε are further defined in terms of turbulence intensity (I) and hydraulic diameter (D_H).

$$K = \frac{3}{2}\left(u_{avg}I\right)^2 \qquad\qquad \textbf{Equation 2.11}$$

Where u_{avg} is the average velocity and I is the turbulence intensity.

$$\varepsilon = C_\mu^{\frac{3}{4}} \frac{K^{\frac{3}{2}}}{l} \qquad\qquad \textbf{Equation 2.12}$$

Where C_μ is a constant set at 0.09, K is the turbulent kinetic energy and l is characteristic length scale given by

$$l = 0.07\, D_H \qquad\qquad \textbf{Equation 2.13}$$

Where the hydraulic diameter D_H, in this case, is the diameter of the trough.

2.1.1.3.4 Rotation

Rotation of the screw can be depicted in two ways: modeling a moving/rotating mesh with a stationary frame of reference or modeling a stationary mesh with rotating frame of reference (Schleicher, 2012).

2.1.1.3.5 Buoyancy

According to Lyons (2014), flow through an AST is influenced by gravitational pull (g) hence should be modelled as buoyant. However, it should be noted that for every inclination angle the resultant gravitational force, which is parallel to the slope, should be applied.

2.1.1.4 Specification of Boundary Conditions

Boundary types for an AST include inlet, outlet, interface, walls and openings (Dellinger et al., 2016). According to ANSYS (2012) velocity/mass flow at an inlet and static pressure at an outlet is the most robust set of boundary conditions for the machine. Further, in cases where flow is allowed both into and out of the boundary, the outlet can be modeled as an opening type boundary condition (ANSYS, 2012).

2.1.2 Processor (Solver)

CFD-Solver component numerically solves governing equations on a mesh. Basically, the process involves finding solutions for the transport (conservation) equations for mass, momentum and energy with the support of physical models for turbulence, combustion and radiation (Tu et al., 2018). The transport equations are presented in Equation 2.1 up to equation 2.5 while equations for turbulence are presented in equation 2.7 up to equation 2.13. Further, computations by the solver are guided by solver settings such as initialization, solution control, convergence criteria and monitoring of the solution.

There are three main types of numerical solution techniques: Finite Difference Method (FDM), Finite Element Method (FEM) and Spectral Method (Versteeg, 2007). CFD codes use a special type of finite difference known as Finite Volume Method (FVM) whose numerical algorithm consists of three steps: integration of the governing equations of fluid flow over all the control volumes of the domain, conversion of the resulting integral equations into a system of algebraic equations (discretization) and lastly solving the algebraic equations by an iterative method (Versteeg, 2007).

The Graphical user interface (GUI) procedure for implementing the solver algorithm is illustrated in Figure 2.9.
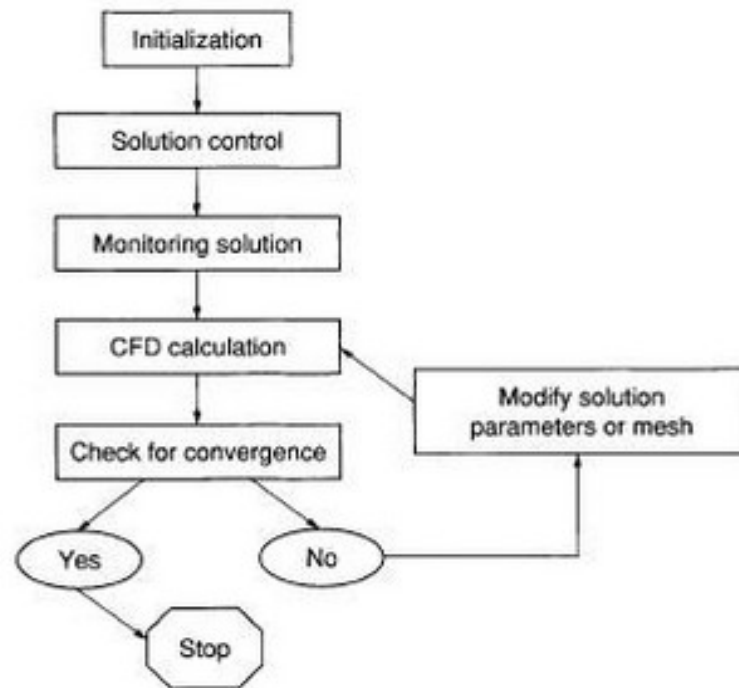
Figure 2. 9: An Overview of the Solution Procedure (Tu et al., 2018)

2.1.3 Post-Processor

Post-processor component of a CFD code facilitates visualization of results which include display of vector plots, contour plots, 2D and 3D surface plots, Particle tracking and view manipulations among others (Versteeg, 2007). According to Waters (2015), results that need to be visualized from numerical studies on AST include pressure distribution, free surface, generated torque, overflow and gap leakages.

2.2 Combined Effects of Related Parameters: Inclination Angle/ Screw Length (B/ L) and Number of Blades/Pitch (N/S)

According to Kotronis (2016), testing of the combined effect of inclination angle (β) and screw length (L) requires that head should be maintained at a constant value in

order not to affect the input power. Therefore, it is imperative to include necessary constraints when conducting tests on related parameters of an AST.

2.2.1 Inclination Angle (β) and Screw Length (L)

Studies on AST have concentrated on the effect of β, instead of the combined effect β and L, on the mechanical efficiency of the machine (Kotronis, 2016). This approach does not consider the losses in both head and input power, associated with reduction of inclination angle for an AST with a constant screw length (Waters, 2015). A good example is the experimental study by Nuramal et al. (2017) in which the head almost doubled as the angle β was increased from 22° to 40°; hence the effects observed on generated mechanical power cannot be attributed to increase in inclination angle alone, but also to increase in input power. This certainly opens a new perspective to the study of ASTs since for low head sites, increasing the head is not practical beyond the maximum head that is fixed by the geographical conditions of the site (Waters, 2015).

It is also important to note that previous tests on the effect of inclination angle (β) did not produce consistent results. Results of the works of Nuramal et al. (2017), Muller and Senior (2018) and Dellinger et al. (2016) suggested that the mechanical efficiency of the machine increases with decrease in β. In contrast, results of studies by Lyons (2014) and Salam et al. (2018) suggested the opposite -that the efficiency of an AST decreases with decrease in β. The difference could be occasioned by the fact that input power is not maintained at constant magnitude in both studies.

On his suggestion on the need to treat β and L as related parameters, Waters (2015) noted that a change in inclination angle (β) automatically triggers change in length (L). He suggested that a smaller β with longer L may give better performance.

Lyons (2014) conducted a numerical study of AST in which he simultaneously varied the inclination angle, β, and the length ratio (L_r) of the reference AST so as to keep a constant head drop across the AST. The results showed that as β increased, peak mechanical power increased towards a constant value at $β = 28^o$. However, it should be noted that maintaining a constant length ratio (L/D_o) led to modification of external diameter, hence confounding the combined effect of the related parameters, β and L.

A closure attempt at testing the combined effect of β and L was found in the experimental study by Simmons et al. (2019) in which three screws with identical parameters, except for screw length (L), were used. The head was maintained at a constant size, hence each of the screw lengths produced a different angle of inclination. The results showed that decrease in the inclination angle (β) led to increase in torque, mechanical power and efficiency of the machine. However, it should be noted that due to lack of more identical screws, only three angles were tested. Thus, there is need for more research on the combined effect of β and L on AST's efficiency.

2.2.2 Number of Blades (N) and Pitch (S)

Studies have been conducted to determine the effect of N and S as independent parameters, but not as related parameters (Songin, 2017). Further, results from the studies are conflicting. For example, Rosly et al. (2016) carried out both numerical and experimental study on AST whose results indicated that number of blades (N) have no appreciable effect on mechanical efficiency. The results showed that the efficiency marginally increases with increase in number of blades. He concluded that the marginal differences in the mechanical efficiency were not due to changes in number of blades, but instead were as a result of assumption of static blade instead of rotating blade simulation (Rosly, 2016). Waters (2015), on the other hand, conducted a numerical

study on the AST whose results showed that increase in number of blades lead to reduction in mechanical efficiency. He concluded that though the increase in number of blades increased the area under hydrostatic forces, the mechanical efficiency of the machine reduced because more blades occupy more space hence reduction in space taken by water. Results from research by Dellinger et al. (2016) showed that increasing the number of blades (N) leads to reduction in torque fluctuation. The result is important for design cases for which torque fluctuation need to be limited within a specified range of values.

Tests on the effect of pitch (S) on mechanical efficiency of AST have also yielded conflicting results. For example, Rosly et al. (2016) conducted numerical and practical tests on AST and the results indicated that the lower the number of turns (greater pitch) the higher the mechanical efficiency. This outcome implies that making the pitch infinitely small would give the highest mechanical efficiency, which is contestable on grounds having an infinitely small pitch is impractical. However, results from a study by Lyons (2014) showed that mechanical efficiency increases with increase in pitch up to a critical value of pitch ratio beyond which the efficiency drops with extra increase in pitch. He explained that beyond the optimal pitch ratio of 0.67 the rate of loss of torque due to loss of buckets become greater than the gain due to increases water volume in the buckets (Lyons, 2014).

2.3 Optimal values of AST Parameters

It is a common practice, in most studies on parametric analysis of AST, to define optimal parameter values as those that give highest mechanical efficiency (Lyons, 2014; Nuramal et al. 2017).

2.3.1 Fill Factor (f)

Tests on fill factor have shown that maximum mechanical efficiency of an AST is attained when the water level in the trough coincides with the central line of the shaft, hence the occupied bucket space is assigned a fill factor of 1 (Dellinger et al., 2016). If filled beyond this level, the fill factor becomes greater than 1 and some water overflows into a lower bucket without contributing to torque generation thus leading to overflow losses. Conversely, underfilling refers to fill levels lower than the optimal; that is $f <$ 1(Dellinger et al., 2016). Figure 2.10 illustrates optimal fill factor ($f = 1$) of buckets.
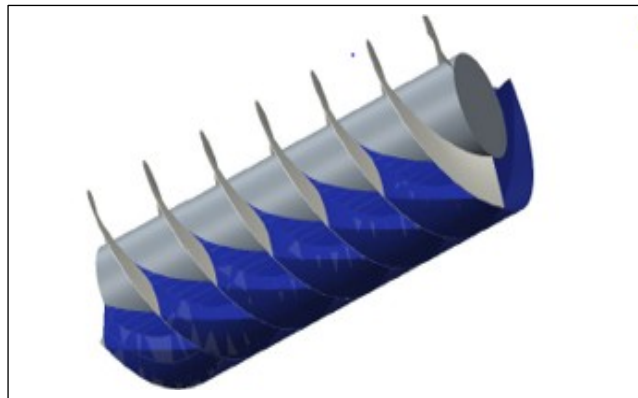
Figure 2. 10: Optimal-Fill Factor; f = 1 (Dellinger et al., 2016)

2.3.2 Inner Diameter (D_i)

The greater the inner diameter (D_i) the higher the mechanical efficiency, provided optimal diameter ratio (D_r) of 0.67 is not exceeded (Waters, 2015). Further increase in D_i beyond this point produces rapid decrease in mechanical efficiency (Waters, 2015). For comparison purposes, Rorres (2000) stated that the established optimal D_r value for Archimedes screw pump (ASP) is 0.54. According to Simmons et al. (2019), AST and ASP have different optimization goals hence their corresponding parameters may have different optimal values.

2.3.3 Gap Width (G_w)

It has been established that the smaller the gap width (G_w) the higher the values of both torque and mechanical power of AST (Kotronis, 2016). The explanation is explicit: a larger gap permits more gap leakage hence greater energy losses. Further, under-filling makes gap leakage and frictional losses to be predominant (Dellinger et al., 2016). However, it should be noted that the size of the clearance gap cannot be reduced infinitely. Limiting factors such as deflection of the shaft and the need for reasonable clearance should be considered. The greater the deflection of the shaft, the larger the size of gap width required.

According to Kotronis (2016), the maximum acceptable gap width for AST has not been established, but that of ASP can be estimated by equation 13.

$$G_{sp} = 0.0045\sqrt{D_0} \qquad\qquad \textbf{Equation 2.14}$$

Where G_{sp} is the maximum gap width for Screw Pump and D_0 is the external diameter.

It should be noted that the maximum gap width (G_w) is measures near the bearings where the deflection is minimum (Kotronis, 2016).

2.3.4. Rotational Speed (n)

According to Lyons (2014), ASTs can be designed either as fixed speed or variable speed machines, but the latter is less popular since the introduction of variable speed drive to the design significantly increases system cost. For a fixed speed AST, optimal speed is usually close to stall rotation speed (Lyons, 2014). This is expected because at slow rotation speed values buckets experience more fill, hence greater torque. Kotronis (2016), while quoting Lashofer et al. (2012), indicated that most European screw manufacturers use equation 14 to set maximum rotational speed.

$$n_{max.} = \frac{50}{D_0^{2/3}}$$

Equation 2.15

Where $n_{max.}$ is maximum rotation speed [rpm] and D_o is the external diameter [m].

2.3.5 Outer Diameter (Do)

For a given available power, an oversized AST is less efficient (Lyon, 2014). Initially it was assumed that a larger outer diameter (D_o) would result in higher power production, but results of tests that were conducted by Lyons (2014) showed the opposite. From the results torque increased with increase in D_o, but power decreased. He attributed the decrease in power to reduction in rotational speed. Since the flow rate remained constant, a larger AST would rotate at a slower pace which could be less than the optimal speed. The result can also be explained by the fact that an increase in D_o leads to decrease in three non-dimensional parameters: diameter ratio (D_r), pitch ratio (S_r) and length ratio (L_r).

2.3.6 Flow Rate (Q)

Tests conducted on flow rate have shown that the mechanical efficiency of an AST increases with increase in flow rate up to a maximum flow above which the efficiency decreases owing to overflow losses (Dellinger et al., 2016). Thus, optimal flow rate corresponds to optimal fill level.

CHAPTER THREE: METHODOLOGY

3.1 Creating a 3D AST Model and Simulating Flow through it

Ansys-CFX, which is a commercial CFD code, was used to numerically analyze fluid flow through a reference AST model. The software, due to its robustness, speed and versatility, has been predominantly used to perform simulations and analysis of turbines compared to other CFD software (Mrope et al., 2021). The analysis was done in Ansys2019R1 workbench. Pre-processing, solver (processing) and Post-processing stages of the flow analysis were done using a total of five modules as encompassed in

the CFX Project Schematic: Creation of geometry, meshing, physical set-up, computation of solution and visualization of results (Post-processing).

3.1.1 Pre-Processing

The first three modules: geometry creation, meshing and physical set-up constitutes the pre-processing stage in CFD implementation.

3.1.1.1 Creation of AST Geometry

A reference 3D Archimedes screw turbine (AST) model was created using Solidworks2018 which is a CAD software. Initially the cylindrical shaft and a helical blade were separately created. The shaft was generated using circle sketch and extrude-boss tools while the blade was created using helix sketch and sweep tools. The two parts were then joined using the 'mate' tool to form an Archimedes screw. To replicate the number of blades to four, the 'circular patterns' design tool was used. The diameter of the shaft and the inner diameter of the helical blades were assigned the same magnitudes in order to create a gap-free assembly.

The dimensions of the screw model were adopted from one of the 16 unique laboratory-size ASTs found in the Archimedes Screw Laboratory at Guelph University in Canada. The screw geometry was chosen because it has an inclination angle of 24.5° which is close to the inclination angle of 25° that is common with majority of "real-world" AST installations. Other researchers who have used the screw as a reference geometry (from which other geometries were chosen) include Simmons et al. (2019) and Songin (2017). Table 3.1 shows the dimensions of the screw.

Table 3. 1: Dimensions of Reference Screw (Simmons et al., 2019)

Parameter	Symbol	Size
Number of blades	N	4
Inner Diameter [mm]	D_i	168
Outer Diameter [mm]	D_o	381
Pitch [mm]	S	381
Flighted Length [mm]	L	617
Inclination angle [deg]	β	24.5

Image of the reference screw model is shown in Figure 3.1.
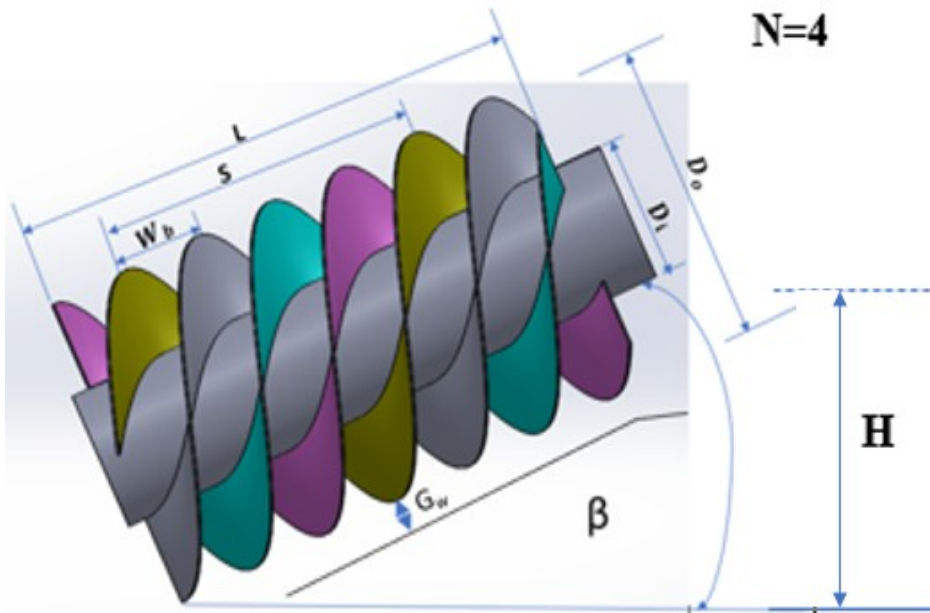
Figure 3. 1: Reference Screw Model

The screw length (L), the pitch (S), the number of blades (N) and the inclination angle (β) of the screw model were parameterized in order to make it easy to modifying the model, as would be necessary, to create different screw geometries.

Apart from the screw, some complementary geometries were also created in Solidworks. They included a cylindrical enclosure (trough), an inlet part and an outlet section. The trough was created using circle sketch and extrude-boss tools while both

inlet and outlet sections were created using sketching tolls for line and angle and boss-extrude tool. The diameter and length of the cylindrical enclosure were set to 383 mm and 625 mm respectively. This created a clearance, known as gap width (G_w), of 1 mm between the trough and the tips of the blades. Figure 3.2 shows the geometry of the trough.
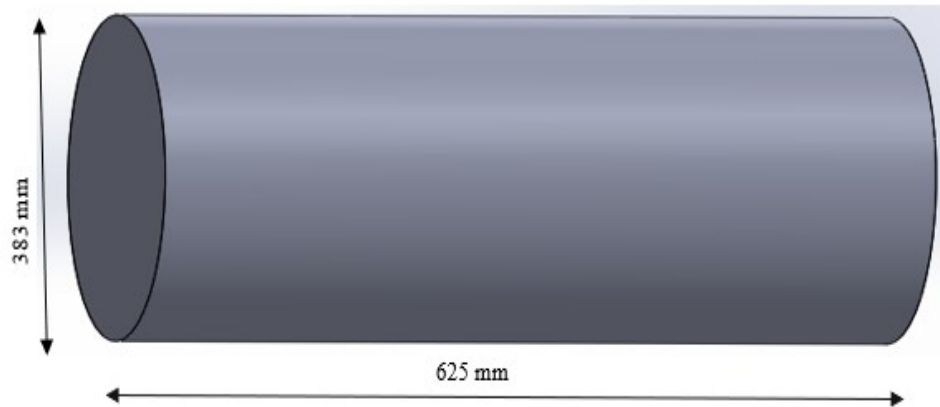
Figure 3. 2: Geometry of the Trough model

The inlet and outlet were necessary for the purposes of facilitating smooth transfer of fluids in and out of the AST. The computational geometry, as shown in Figure 3.3, was put together using the 'assembly' tool.
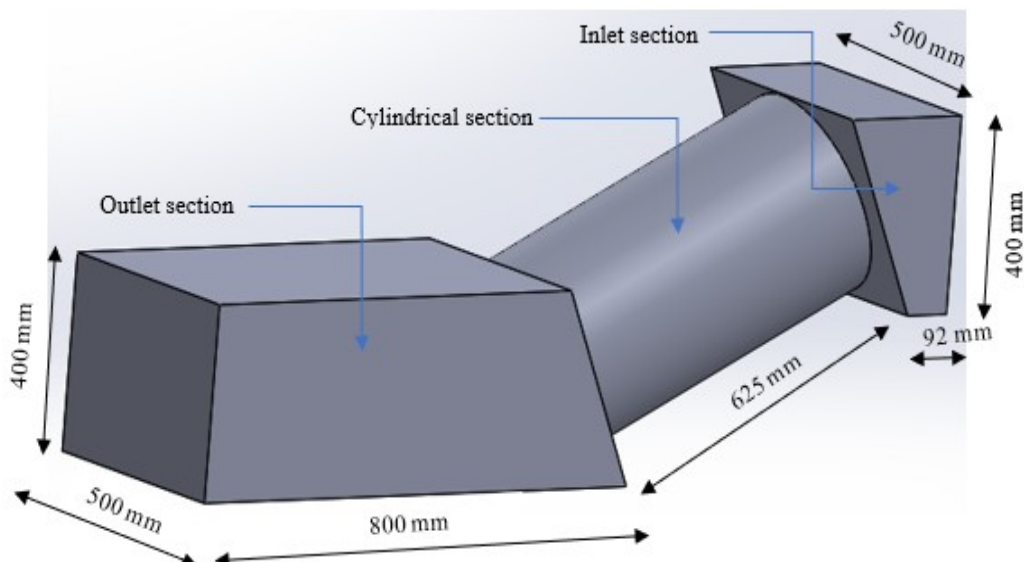
Figure 3. 3: Computational Geometry for AST Model

The orientation of the AST was achieved by choosing a local coordinate system (**Coord 1**) that was defined such that its z-axis was parallel to the centerline of the screw. This was necessary since an AST is installed at an inclination angle (β), hence both its rotational axis and the direction of water flowing through it are not aligned to any of the three axes of the global coordinate system (**Coord 0**). Figure 3.4 shows the relative directions of the z-axes for the two coordinate systems.
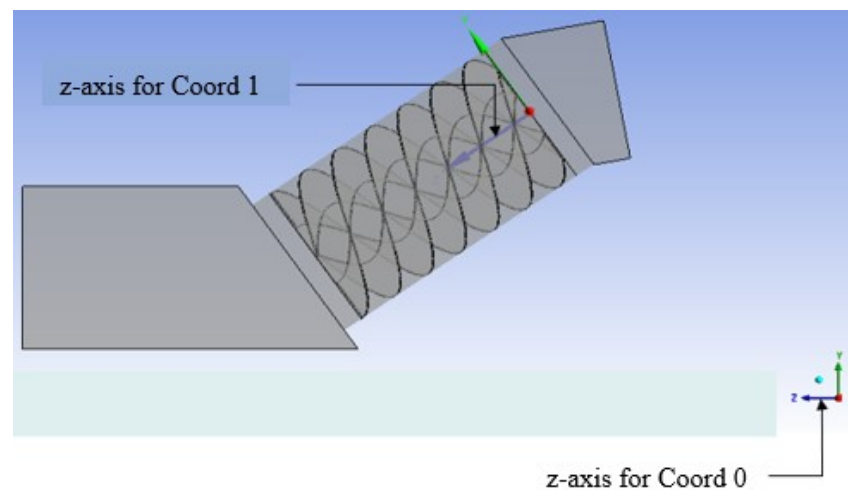
Figure 3. 4: Relative Directions of the Z-axes for Coord 0 and Coord 1

Lastly, the model shown in Figure 3.3 was imported into Ansys-based Design modeler CAD software where a user-defined enclosure was created using the enclosure tool. Boolean operation was then performed to subtract the screw from the assembly in order to form computational domain for the AST as shown in Figure 3.5.
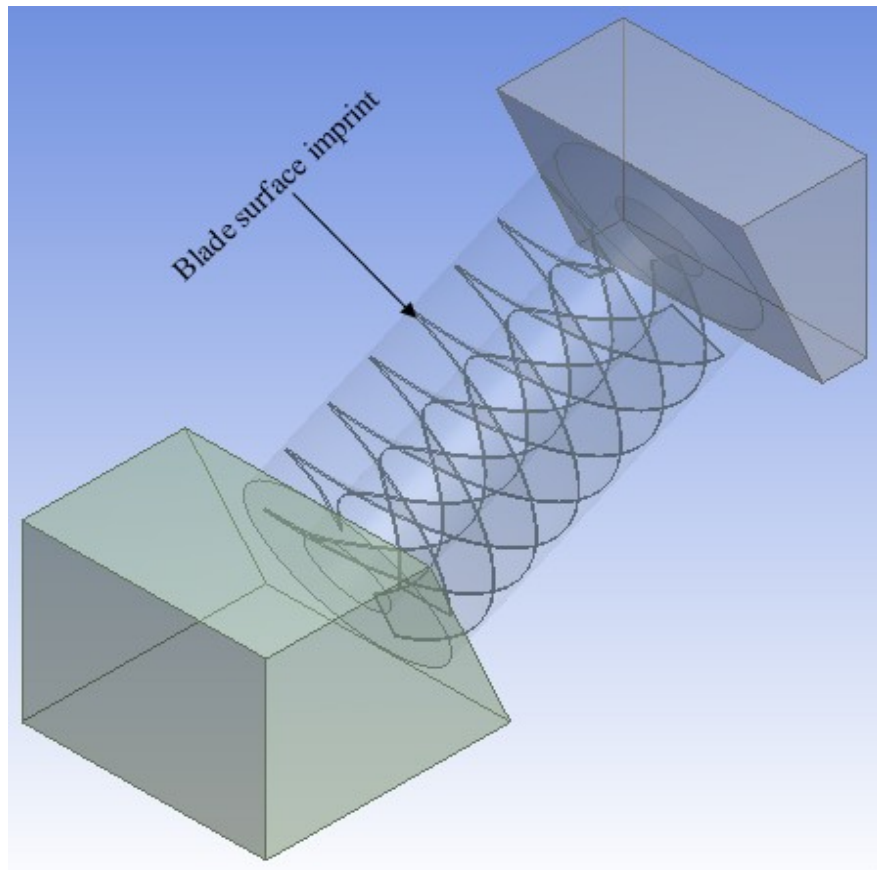
Figure 3. 5: Computational Domain for the AST Model

The imprint of the screw, labeled in Figure 3.5, was used to represent turbine-wall boundary.

3.1.1.2 Meshing

The computational domain was meshed in Ansys Meshing software. Tetrahedral mesh was chosen for the cylindrical section that hosted the imprint of the screw while hex dominant grid was applied at the inlet and outlet sections as shown in Figure 3.6.
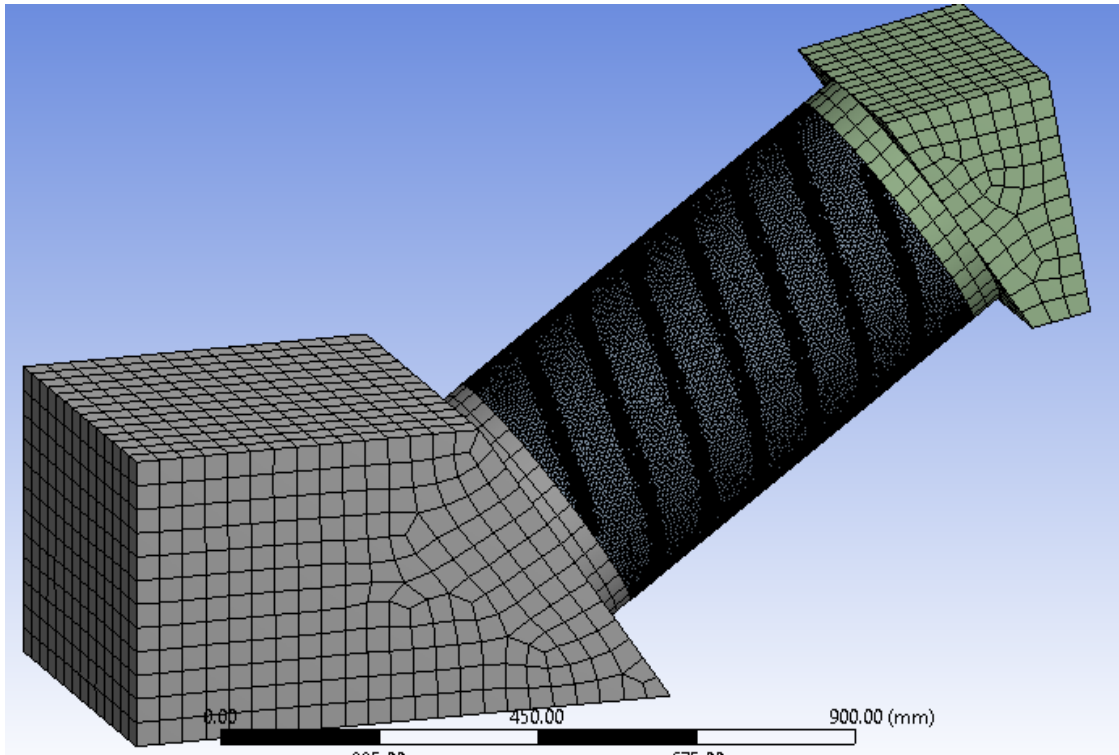
Figure 3. 6: Complete Mesh for the Computational Geometry

The use of an unstructured mesh such as tetrahedral is proven to work well with complex geometries such as that of Archimedean screw blades while a structured mesh such as hex dominant is appropriate for regular parts such as the inlet and outlet sections.

In order to effectively capture flow at the boundary layer, mesh refinement was done at wall boundaries of interest such as the screw wall and sections of the enclosure wall that are close to the blade tips. The mesh refinement tool was set to level 1 to generate mesh regions of higher element density as shown in Figure 3.7, Figure 3.8 and Figure 3.9.
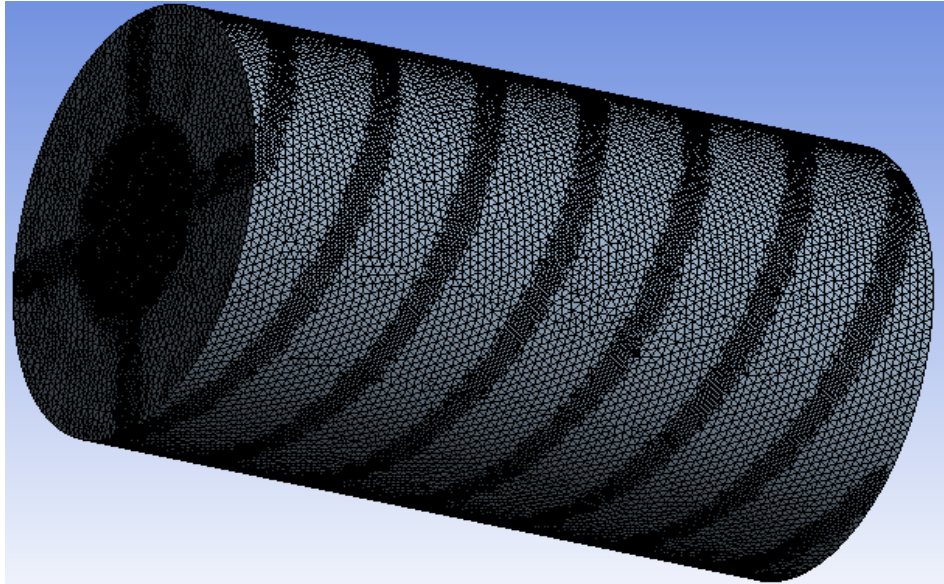
Figure 3. 7: Exterior View showing Mesh Refinement at Enclosure Wall
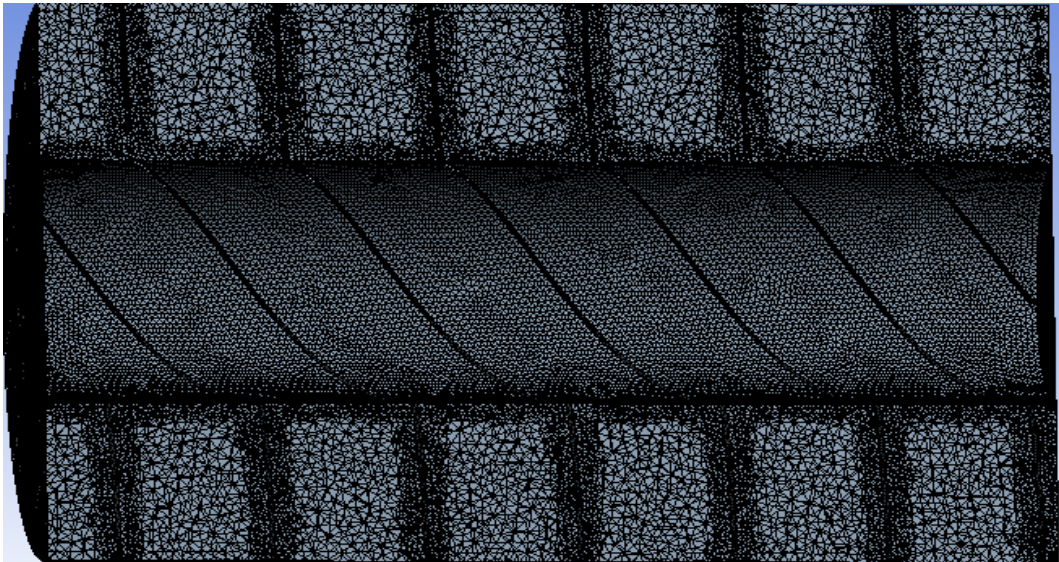
Figure 3. 8: Longitudinal View showing Mesh Refinement at Screw Wall
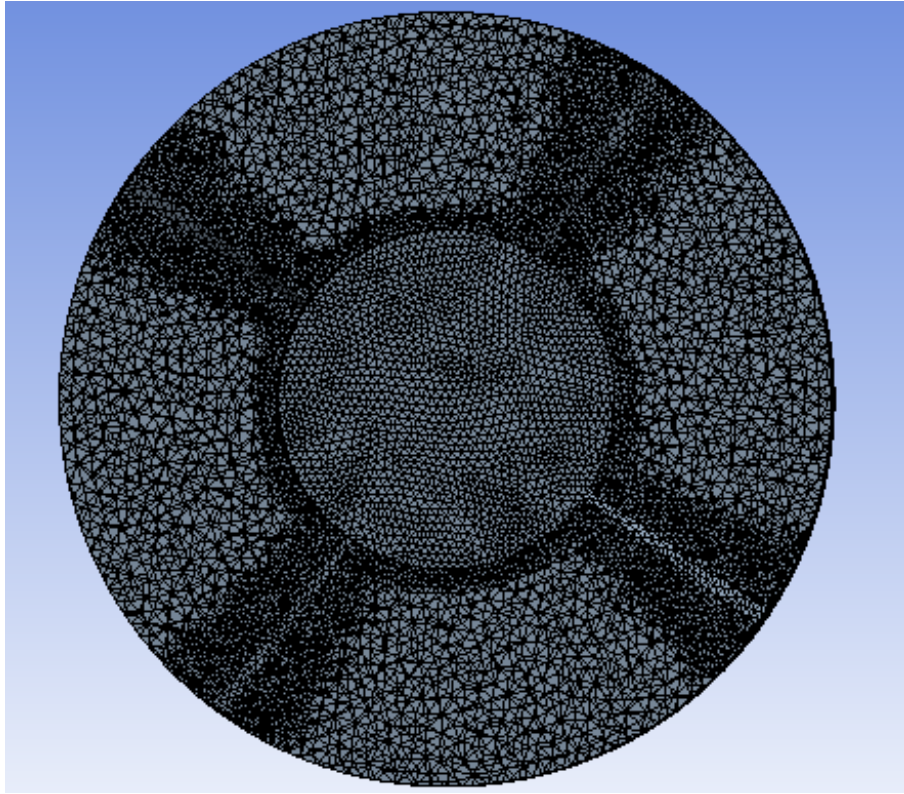
Figure 3. 9: Cross Sectional View showing Mesh Refinement at Blade Walls

Sizes of the mesh elements were as follows: tetrahedron- element size of 8 mm; hex dominant element sizes of 20 mm for inlet section and 30 mm for outlet section. The total number of elements for reference geometry was 3, 184,126.

3.1.1.3 Physical Set-up

3.1.1.3.1 Transient Analysis

The flow through the AST was modeled as transient with a total time of 12 seconds and 0.1 seconds per timestep. Thus, a total of 120 timesteps were created.

3.1.1.3.2 Multiphase

Materials for the multiphase flow were defined as water and air, both at a temperature of 25 ºC. To track the free surface between the water and air layers, the multiphase tool was set to 'homogenous with standard free surface'. The surface tension at the free

surface was modeled as a 'Continuum Surface Force' of 0.072 N/m. Both the liquids were modeled as 'continuum' as this is the common practice for handling free surface.

3.1.1.3.3 Turbulence Model

The standard k-ε turbulence model for closure was applied with wall function set to 'scalable'. The k- ε model is commonly used in CFD applications since it is accurate, simple and economical to run. Scalable wall function prompts the velocity field to flow around the immersed boundary in order to avoid the problem of streamlines penetrating an immersed solid.

3.1.1.3.4 Buoyancy

Buoyancy reference density was set at 1.185 kg/m^3, which is the density of air at 25° while primary liquid was set to water (the denser liquid) in order for the hydrostatic head to appear in its pressure field.

Further, the screw was set to rotate about the z-axis of Coord 1. Thus, the component of gravitational acceleration parallel to the axis ($g_{coord\,1}$), is given by equation 3.1.

$$g_{coord\,1} = g \cdot sin\beta \qquad\qquad \textbf{Equation 3.1}$$

Figure 3.10 illustrates the relative directions of the geodetic gravitational acceleration (g) and g.sinβ, the component of g parallel to z-axis of Coord 1.
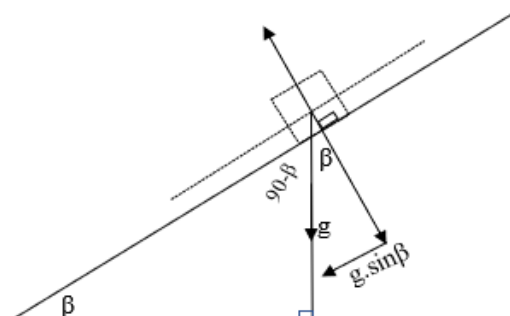
Figure 3. 10: Component of g Parallel to Z-axis of Coord 1

Unlike in steady state analysis where the magnitude of g.sinβ must be provided for every inclination angle, the process is automated in transient analysis. Thus, the buoyancy quantity was stated in the global coordinate system as **-g** [m/s^2] parallel to the y-axis.

3.1.1.3.5 Rotation of the Screw

Rotating mesh was used to depict the rotation of the screw. The mesh in the region of the reference screw was set to rotate at an angular speed of 3.14 rad/s (30 rpm) while the enclosure wall was set to 'counter rotating' in order to act as a stationary reference frame with respect to the rotating domain. 'Counter rotating' status acts to nullify the rotation speed hence computationally treats the enclosure wall as stationary. In order to make the screw wall to rotate at the same rate as that of the mesh, its angular velocity was set to 0 rad/s.

3.1.1.4 Boundary Conditions

3.1.1.4.1 Inlet

The boundary was modeled as a mass flow rate inlet. Turbulence was set to 5% which is medium intensity. The volume fraction (VF) of water was initialized as 1 while that of air as 0. The flow direction was set to "normal to boundary condition" and the flow regime was set to subsonic.

3.1.1.4.2 Outlet

The boundary was modelled as an 'opening' type boundary condition at a relative pressure of zero. The volume fraction (VF) of water was initialized as 1 while that of air as 0.

3.1.1.4.3 Openings

Boundary conditions for 'opening' type boundaries were set to ambient conditions at opening pressure and direction. The relative pressure at each opening was set to zero and the direction was set to 'normal to boundary condition'.

3.1.1.4.4 Walls

All the walls for the stationary domains were set to smooth wall with no slip and no wall adhesion.

3.1.1.4.5 Interfaces

The two circular-shaped interfaces between the rotating and the stationary domains were modelled as 'fluid-fluid' interface types. Frame change model was set to 'frozen rotor' for both the interfaces. The frozen rotor frame change model treats the rotor (turbine) as stationary; the numerical calculations are then done in such a way as if the fluid materials (water and air) are rotating at the expected practical speed of the rotor. Lastly, mesh connection was set to general grid interface (GGI).

3.1.2 Solver (processing)

CFX-Solver controls were used to apply appropriate solver settings. Equation class settings were applied for continuity, momentum, turbulence eddy dissipation, turbulence kinetic energy and volume fraction. Advection scheme was set to 'high

resolution' for both continuity and momentum while for both turbulence eddy dissipation and turbulence kinetic energy it was set to 'upwind'. Convergence criteria was based on Root Mean Square (RMS) and the 'Residual Target' was set to 10^{-4}. Torque output was monitored by setting a monitor point defined by the expression: **Tq = torque_z_Coord1@Turbine**. The solver was then run.

3.1.3 Post-Processing

CFX-Post software was used to visualize instantaneous outputs of interest such as pressure distribution on the blades, free surface, overflow, gap leakage and instantaneous torque. Pressure distribution was visualized using the 'contour' tool. Free surface, overflow and gap leakage were viewed using the 'Isosurface' tool. Magnitude of torque at an instant was viewed either from the torque monitor or by inserting a torque output expression **Tq = torque_z_Coordinate Frame 1() @Turbine** in CFX-Post and selecting the timestep of interest using the 'Timestep Selector' tool. Animation tool was used to generate timestep animation of the flow. In order to determine the average and peak values of torque for a simulation run, outputs of torque monitor points were imported into an excel sheet from where the excel expression for finding average value was applied.

3.1.4 Grid Independence

Errors due to coarseness of grid were eliminated by performing grid independence study. This is a procedure of successive refinement of an initially coarse grid until certain key results (outputs) do not change. A mesh having larger elements give inaccurate results while that having sub-optimal element is costly in terms of computational time and storage space.

To decide on the optimal element size for the computational domain, flow simulation through the reference AST model was conducted using element size as the only variable. Flow rate of 10 kg/s and rotational speed of 30 rpm were applied. Initially, element sizes for the inlet section and rotating/cylindrical part were set to 6 mm while that of the outlet was set to 30 mm. A larger elemental size was chosen for outlet part because the flow through it has lesser effect on the screw than the flow at the inlet and through the AST. Torque was monitored and the results were imported into an excel sheet for determination of average and peak values of torque. The element size for the rotating part was then changed to 7 mm and another simulation run was conducted. Further simulation runs were conducted using element sizes of 8 mm, 9 mm, 10 mm, 15 mm and 20 mm. Results of the study were presented in both tabular and graphical forms. Finally, the element size below which no appreciable change in torque could be noticed was taken as the most appropriate for this project.

3.2 Testing Effects of Related Parameters on Torque, Mechanical Power and Efficiency of AST

Two sets of related parameters, β/L and N/S, were tested to determine the effect of each set on mechanical power and mechanical efficiency of an AST.

3.2.1 Testing the Combined Effect of Inclination Angle (β) and Screw Length (L)

In this test, two related parameters (β and L) were simultaneously varied in order to create five different geometries. Assuming a micro- hydropower site having a maximum hydraulic head of equal magnitude to that of the reference screw, a head (H) of 0.256 m was used as a constraint for all the five screw geometries. Consequently, every screw length had a corresponding size of inclination angle according to the

relation $\sin \beta = \dfrac{Head}{Length}$.

All the other parameters were maintained at constant magnitudes equal to those of the reference screw. That is N= 4, β = 24.5°, L = 617 mm, D_o = 381 mm, D_i = 168 mm and S = 381 mm. Thus, five screw models of different lengths and inclination angles were created in Solidworks. The geometries were named S1, S2, S3, S4 and S5. Flow rate was maintained at a constant value of 10 kg/s. The flow rate was chosen because it was found, by Simmons et al. (2019), to be optimal under the same parameters as for this study. Table 3.2 shows corresponding values of β and L for the test.

Table 3. 2: Corresponding Values of β and L

Parameter	Symbol	S1	S2	S3	S4	S5
Inclination angle [deg]	β	10	20	24.5	30	40
Flighted Length [mm]	L	1474	748	617	512	398

Starting with the S5 screw geometry, which was inclined at 40°, transient simulation runs were conducted at seven different rotational speeds of 20 rpm, 30 rpm, 40 rpm, 50 rpm, 60 rpm, 70 rpm, and 80 rpm. For each run, torque was monitored and results were imported into an excel sheet from where both average and peak values of torque were determined. The average torque values were plotted (in excel) against rotational speed for the screw. The process was repeated for the other geometries: S4, S3, S2 and S1 in that order. All the five graphs were plotted on the same axes and analyzed. Similarly,

For each rotational speed, values of average and peak torques were used to compute the corresponding average and peak values of mechanical power and mechanical efficiency using equation 3.2 to equation 3.5.

$$Aver\,P_{mech.} = Aver\,T * \omega \qquad\qquad\qquad \textbf{Equation 3.2}$$

Where Aver $P_{mech.}$ is average mechanical power [W], Aver T is average torque [Nm] and ω is angular velocity [rad/s].

$$Peak\, P_{mech.} = Peak\, T * \omega \qquad\qquad \textbf{Equation 3.3}$$

Where Peak $P_{mech.}$ is peak mechanical power [W] and Peak T is peak torque [Nm].

$$Average\, Efficiency = \frac{Average\, mechanical\, power}{Available\, power} x\, 100\% \qquad \textbf{Equation 3.3}$$

$$Peak\, Efficiency = \frac{Peak\, mechanical\, power}{Available\, power} x\, 100\% \qquad \textbf{Equation 3.4}$$

Available power was calculated using equation 3.5.

$$P_{avail} = \dot{m}g\, H_s = \quad gQ\, H_s \qquad\qquad \textbf{Equation 3.5}$$

Where $P_{avail.}$ is available power [W], $\dot{m}$ is mass flow rate [kg/s], Q is the volume flow rare [m³/s], g is gravitational acceleration [m/s²] and H_s is the maximum available head [m].

For this study, H_s value of 0.256 m and a mass flow rate of 10 kg/s (volume flow rate of 0.0100 m³/s to 4.d.p.) was used in the simulations. Thus, available power, which was maintained at a constant value of 25 W, was calculated as:

$P_{avail} = \quad gQ\, H_s = 997\, x\, 9.81\, x\, 0.01\, x\, 0.256 = 25 W$ For further analysis of the results, other output graphs that were plotted and analyzed included average power versus rotational speed, peak power versus rotational speed, average mechanical efficiency versus rotational speed and lastly, peak mechanical efficiency versus rotational speed. The graphs were plotted in excel.

3.2.2 Testing the Combined Effect of Number of Blades (N) and Pitch (S)

In this section transient simulations were run on five different geometries to determine the combined effect number of blades (N) and pitch (S) on torque, mechanical power and efficiency of ASTs. In order to maintain a constant number of buckets for all the five geometries used in the test, a novel parameter named bucket width (W_b) and defined as $W_b = \dfrac{S}{N}$, was introduced and used as a constraint. The reference screw model was used as the baseline geometry, hence a bucket with (W_b) of 95.25 mm was applied. This translated to 6 buckets in the entire screw length of 617 mm. Other parameters included N = 4, S = 381 mm, D_i = 168 mm; D_o = 381 mm; β = 24.5°, and Q = 10 kg/s. Table 3.3 shows the corresponding values of N and S for the five geometries (S6, S7, S8, S9 and S10) which were used in the test.

Table 3. 3: Corresponding Values of Related Parameters, N and S

Parameter	Symbol	S6	S7	S8	S9	S10
Number of blades	N	2	3	4	5	6
Pitch (mm)	S	190.5	285.75	381	476.25	571.5

Initially, transient flow simulation was run for the screw geometry having 2 blades (S6) at a rotational speed of 20 rpm. Torque was monitored for the run. The transient torque results were imported into excel sheet from where average and peak torque values were determined. The procedure was repeated for different rotational speed values of 30 rpm, 40 rpm, 50 rpm, 60 rpm, 70 rpm and 80 rpm. A graph of average torque versus rotational speed was then plotted in excel. A second graph of peak torque versus rotational speed was also plotted. The entire process was repeated for the other four

screw geometries that were having 3 blades, 4 blades, 5 blades and 6 blades respectively. All the five graphs for average torque versus speed of rotation were plotted on the same axes. The same process was applied in plotting the five graphs for peak torque versus speed of rotation.

Average and peak values of torque for the runs were used to calculate average and peak values of mechanical power. Average power versus rotational speed, for each of the five geometries, were plotted; all appearing on the same axes. The same was done for peak power versus rotational speed. Lastly, values of average and peak power for the runs were used to calculate the magnitudes of average and peak mechanical efficiency. Graphs of average mechanical efficiency versus rotational speed and peak efficiency versus rotational speed were also plotted. Interpretation of the graphs was done to determine both the geometry which performed best at the bucket width (W_b) of 95.25 mm and the optimal rotational speed. Using the geometry as a baseline AST model, tests were conducted to optimize the bucket width (W_b). The value of W_b was varied between 30 mm and 127 mm and transient flow simulations carried out for nine different screw models (S11, S12, S13, S14, S15, S16, S17, S18 and S19) with different sizes of W_b. Table 3.4 shows the magnitudes of W_b for the different geometries.

Table 3. 4: Sizes of Bucket Width (W_b) for Different Geometries

Screw Geometry	S11	S12	S13	S14	S15	S16	S17	S18	S19
W_b [mm]	30	40	50	65	17.5	80	95	110	127

Torque outputs were monitored and the results were imported into excel software from where average torque for each of the nine geometries was determined. Values of

average torque were used in calculating corresponding values of average mechanical power and consequently average mechanical efficiency values. Lastly, graphs of average mechanical power versus bucket width (W_b) and average mechanical efficiency versus bucket width ratio (W_{br}) were plotted and interpreted. W_{br} is a non-dimensional parameter defined as the ratio of bucket width to external diameter (W_b/D_o).

3.3 Testing Effects of individual Parameters on Torque, Mechanical Power and Efficiency of AST

For comparison purposes, tests were conducted on individual AST parameters of interest to this study. Results from the test were used as baseline data from which the results from the combined effects of related parameters were interpreted.

3.3.1 Testing the Individual Effect of Inclination Angle (β)

In this test a single screw (the reference screw) model was used to test the effect of inclination angle (β) on torque, mechanical power and mechanical efficiency of AST. The parameters for the screw geometry were the same as those the geometries that were used in testing the combined effect of inclination angle/screw length (β/L), except that for this case the screw length (L) was kept constant at 617 mm. Parameters whose magnitudes were maintained at constant magnitudes were: $N = 4$, $D_i = 168$ mm, $D_o = 381$ mm, $S = 381$ mm, and $Q = 10$ kg/s.

Since maximum head that can be actually utilized is dictated by site properties, the tests were conducted at a maximum head of 0.256 m. Hence, the maximum angle of inclination that could be achieved was 24.5^0. Magnitudes of inclination angle (β) that

were used in the test are shown in Table 3.5. Figure 3.11 illustrates the different inclinations of the screw.

Table 3. 5: Variation of Inclination Angle (β)

Screw Geometry	S20	S21	S22
β [º]	24.5	20	10
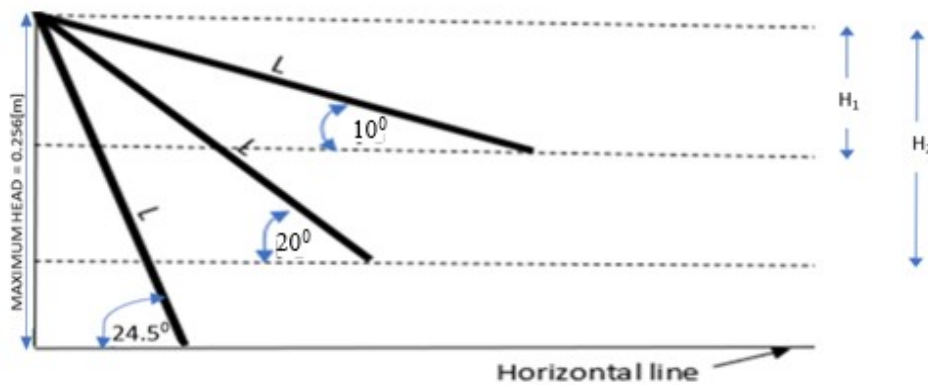
Figure 3. 11: Diagram Illustrating Maximum Angle of 24.5º

As indicated in Table 3.5, three screw geometries (S20, S21 and S22) were used in the test. Initially, flow analysis through the first geometry (S20) that had an inclination angle of 24.5º was done at a rotational speed of 20 rpm. Torque was monitored and transient torque output results were imported into excel sheet where both average and peak torque values were determined. The same procedure was repeated at 30 rpm, 40

rpm, 50 rpm, 60 rpm, 70 rpm and 80 rpm. Finally, the whole process was repeated for S21 and S22 geometries which had inclination angles of 20° and 10° respectively. Each of the following graphs were then plotted against rotational speed: average torque, peak torque, average mechanical power, peak mechanical power, average mechanical efficiency and peak mechanical efficiency. The efficiencies were calculated based on available power of 25 W. Finally, the highest output values for average and peak efficiencies were used as baseline information necessary for interpreting the results of combined effects of β and L on AST's mechanical efficiency.

3.3.2 Testing Effect of Number of Blades (N)

Except for number of blades (N) which was varied, pitch (S) and all the other parameters of the reference screw were maintained at constant magnitudes. The constant parameters were: pitch (S) = 381 mm, inclination angle (β) = 24.5°, screw length (L) = 617 mm, external dimeter (D_o) = 381 mm, internal dimeter (D_i) = 168 mm and flow rate (Q) = 10 kg/s. The number of blades (N) was progressively varied from 2 to 6, hence five different geometries (S23, S24, S25, S26, S27) were created. Table 3.6 shows the values of N for the different geometries.

Table 3. 6: Screw Geometries with Same Pitch but Different Number of Screw Blades

Screw Geometry	S23	S24	S25	S26	S27
Number of blades (N)	2	3	4	5	6

Initially, analysis of flow through the screw having 2 blades (S23) was done for different rotational speed values ranging from 20 rpm to 80 rpm. Torque was monitored

for each of the five runs. The procedure was repeated for other geometries (S24, S25, S26 and S27) whose values of N are shown in Table 3.6. As was the case with other tests, average and peak values of output parameters (torque, mechanical power and efficiency) were plotted in excel. Lastly, the highest mechanical efficiency values were used as baseline data for interpreting the combined effect of N and S on AST's efficiency.

3.4 Procedures for Determining Optimal Values of Related Parameters

3.4.1 Determining Optimal Inclination Angle/ Screw Length (B/L)

Determination of optimal value for β and corresponding value of L was based on graphs of both average and peak efficiencies versus β/L. The procedure for generating the graphs was described in section 3.2.1. A combination of β/L that gave highest mechanical efficiency was taken to be optimal. 3D surface charts were also used to supplement visualization of the results.

3.4.2 Determining Optimal Number of Blades/Pitch (N/S)

Optimization of N/S was also based on both average and peak efficiencies. Based on graphs plotted for both average and peak efficiencies versus N/S, parameter values that gave maximum mechanical efficiency were taken to be optimal. The process of generating the graphs is explained in section 3.2.2

3.4.3 Determining Optimal Value of Bucket Width (W_b)

The optimal W_b value was determined from the graph of average mechanical efficiency versus W_b. The size of W_b that gave highest mechanical efficiency was taken to be optimal.

3.5 Procedure for Validation of Results

Numerical results were validated using results of experimental data from the work of Simmons et al. (2019). The reason for the choice lies in the coincidence that the reference geometries for the two research studies are similar in size and all other parameters. The experimental procedure is briefly discussed in section 3.5.1

3.5.1 Experimental Procedure

In the experimental study of the AST, Simmons et al. (2019) used a set of three screws found in the University of Guelph's Archimedes Screw laboratory. The three screws have identical parameters except their screw length – allowing them to be set at varying inclination angles that correspond to the same flow and head conditions at the screw's inlet and outlet.

Geometric parameters for the three screws are shown in Table 3.7. The screws will be referred to as short screw, reference screw and long screw in ascending order of length.

Parameter	Symbol	Short screw	Reference screw	Long screw
Number of blades	N	4	4	4
Inner Diameter (mm)	D_i	168	168	168
Outer diameter (mm)	D_o	381	381	381
Pitch (mm)	S	381	381	381
Screw length (mm)	L	478	617	952
Inclination angle (deg.)	β	38.8	24.5	15.6

Table 3. 7 Parameters for Experimental ASTs

The reference screw was the first to be tested. The screw was installed in the Archimedes screw test rig at the University of Guelph's Archimedes Screw Laboratory. The system has settings for adjusting the rotational speed and the flow rate of water through the screw. It also has sensors that measure the flow rate, torque, rotational speed, bucket fill height, and upper and lower basin water levels.

The screw and recirculation pump were set to a specified rotational speed and flow rate, respectively. The system was then given a minute to reach an equilibrium condition before taking the torque reading. The process was then repeated at new settings: a range of five different flow rates (9, 9.5, 10, 10.5, and 11 L/s), and, at each of these flow rates, more than ten different rotational speeds ranging from 15 rpm to 60 rpm, but focusing on more 30 to 39 rpm range. A flow rate that generated highest power was taken to be the optimal flow. Torque values were recorded for each rotational speed. Tests on the short and long screws were thereafter conducted at the optimal flow rate, but at the same rotational speeds as for the reference screw. Graphs for efficiency against rotational speed were plotted for each of the screw geometries.

3.5.2 Comparison of Numerical and Experimental Results.

To verify if the numerical analysis actually approximates the performance of the AST, two graphs for mechanical efficiency against rotational speed were plotted on the same axes; one for numerical analysis and another one for experimental data.

CHAPTER FOUR: RESULTS AND DISCUSION

4.1 Creation of a Reference AST CAD Model and Simulation of Flow

A 3D reference screw model, whose image is shown in Figure 4.1, was successfully created in Solidworks CAD software. Parameters for the screw were: $N = 4$, $\beta = 24.5^{\circ}$,

L = 617 mm, D_o = 381 mm, D_i = 168 mm and S = 381 mm (Refer to Table 3.1 and Figure 3.1)
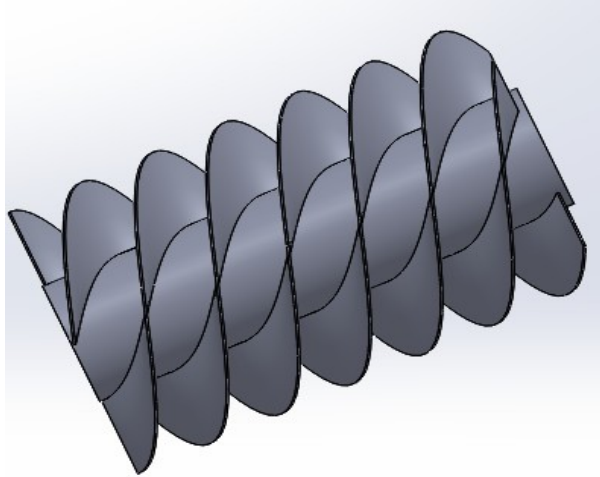
Figure 4. 1: Reference Screw Model

A flow rate of 10 kg/s (0.0100 m^3/s) and a rotational speed of 30 rpm were applied in simulating transient flow through the AST. Results of the flow analysis captured important features such as pressure distribution on the blades, free surface, overflow, gap leakage, magnitude of torque and torque-fluctuations. Figure 4.2 shows the pressure distribution on the blades.
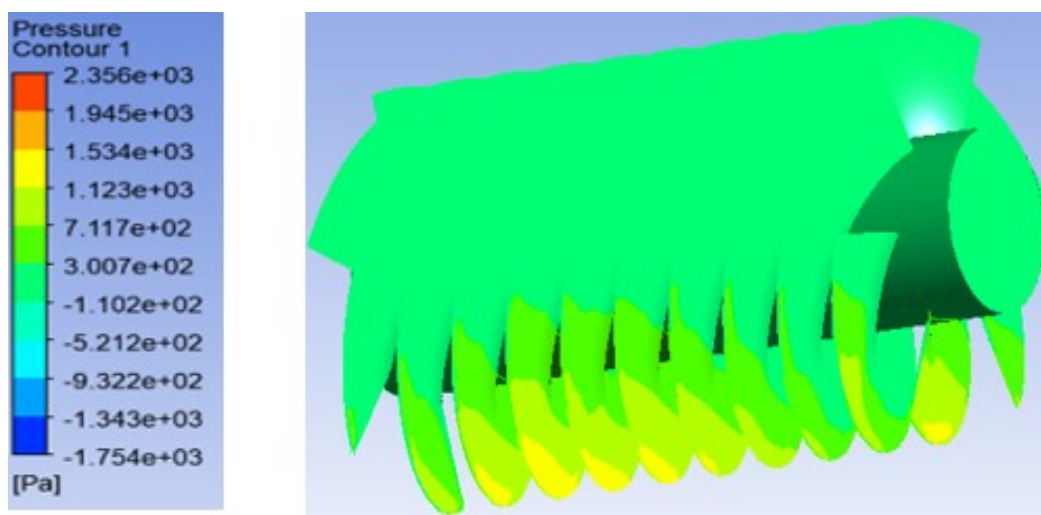
Figure 4. 2: Pressure Distribution on the Reference Screw Model

Based on the results shown in Figure 4.2, two deductions were made. The first

deduction was that at a given instant, hydrostatic pressure on the blades is confined to

the geodetically lower parts that are in touch with water. This was expected since the

trough is partially filled. The second deduction was that pressure on each blade

increases radially outwards to a maximum magnitude of 1447 Pa at the tip of the blade.

This can be explained by the fact that hydrostatic pressure increases with depth. The

result agrees with the work of Maulana et al. (2018) in which they simulated flow

through the AST using CFD and obtained pressure contour as the output. The pressure-

contour output covered the entire diameter of the screw, but still showered that pressure

increases radially to a maximum at the blade tip. The difference (pressure contour covering the entire AST diameter) can be explained by the assumptions of single face flow and stationary screw that they made in their model.

Other results obtained from the analysis such as free surface, overflow and gap leakage were shown in Figure 4.3.
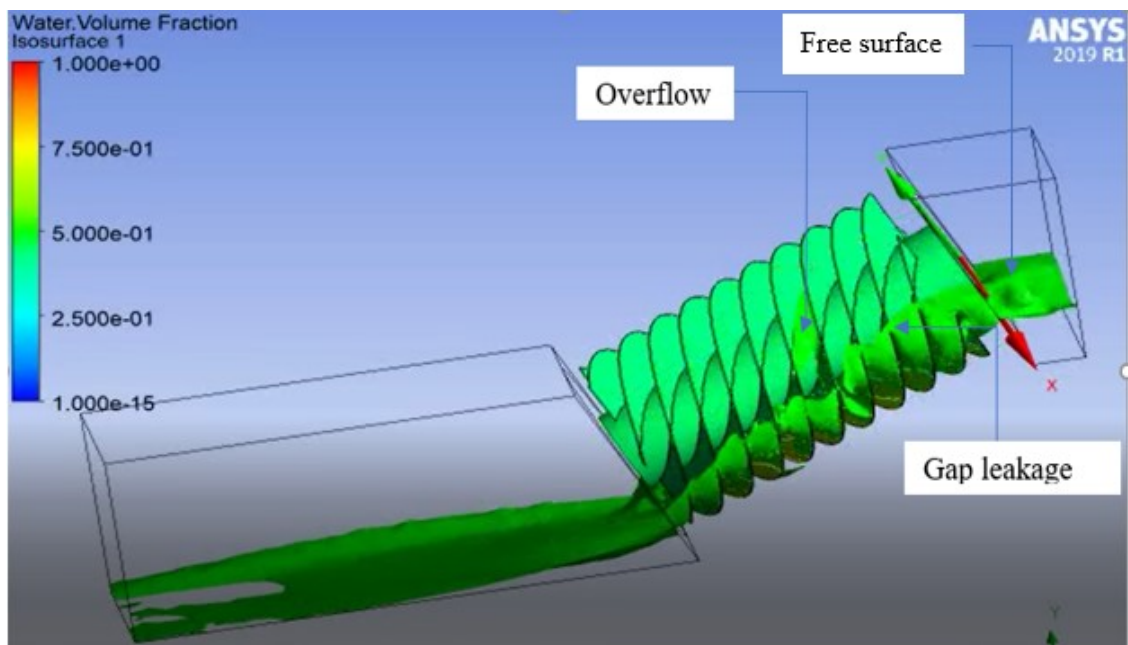
Figure 4. 3: Image showing Free Surface, Overflow and Gap Leakage

Overflow, as shown in Figure 4.3, is water that flows over the shaft and hence does not take part in generating hydrostatic force on the blades; Thus, it is energy lost. Gap leakage also results in energy loss. It refers to water seeping through the clearance gap between the tip of the blade and the trough that hosts the screw. The presence of the losses lowers the efficiency of the AST. Lyons (2014), while commenting on energy loss occasioned by the size of the gap width indicated that the small size of lab screws exaggerates the effect of the gap leakage on the mechanical efficiency which then appear lower than would be expected of a full-size AST. Gap leakage is minimized by reducing the gap width, but within the constraint of sagging of the screw shaft (Kotronis, 2016), while overflow is

minimized by operating the AST at a fill factor not exceeding 1 or at a speed that is sub-optimal for the design flow rate (Dellinger et al., 2016).

Further, results of the simulation showed that the generated torque had two characteristics. These were:

(i)   At equilibrium, the generated torque fluctuated about a mean value of 3.97 Nm. Initially the torque rose from zero to a higher magnitude at which it started exhibited an equilibrium condition in which the torque oscillated sinusoidally for the rest of the timesteps. Figure 4.4. shows average and peak torque levels for the reference screw when rotating at 40 rpm.
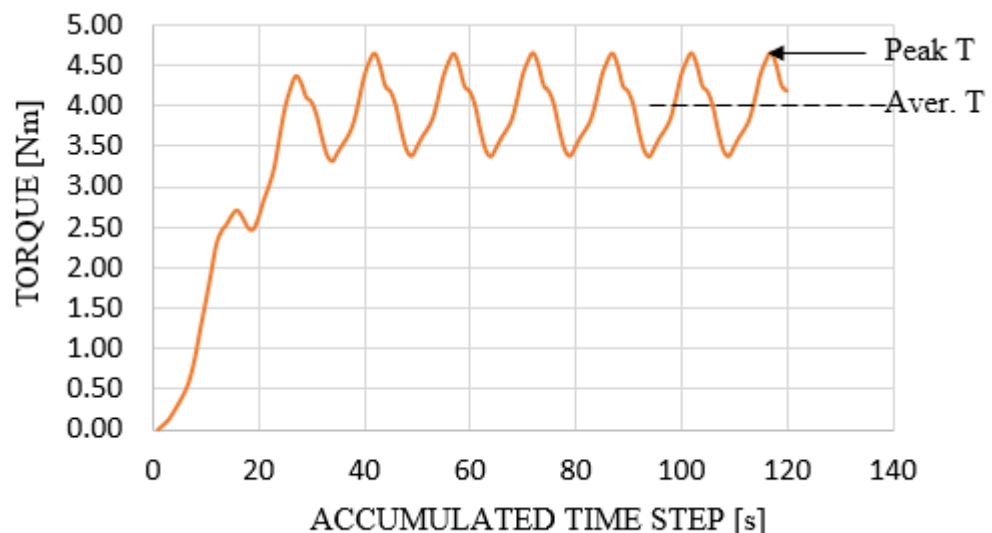
Figure 4. 4: Torque Curve for Reference Screw Rotating at 40 rpm

The initial rise in in torque from zero to a maximum level can be attributed to the gradual filling of the turbine, starting from fill level at the instance when flow rate was zero and reaching a fill level of 1 at the instance when water is flowing steadily at the

outlet. Thus, the section is not relevant when determining average value of the generated torque.

After the initial rise, torque started fluctuating/oscillating about a mean value. This is the section of the graph from which both average and peak values of torque are determined. The arithmetic difference between the peak and the average torque values is referred to as the amplitude of fluctuation. The fluctuations in torque can be attributed differences in the pressure exerted on the blades at different instances as was occasioned by varying circumferential positions of the blades. The result agrees with that of Dellinger et al. (2016), who in their numerical analysis of the AST found out that an AST having 3 number of blades produced 3 maxima on the torque-curve in one rotation of the screw.

(ii)   The amplitude of torque-fluctuation decreased with decreasing rotational speed. The reference screw was initially rotated at 40 rpm and it generated torque with large fluctuations (amplitude = 0.9 Nm) as shown in Figure 4.4. The same screw was rotated at 20 rpm and it generated torque with very little fluctuations (amplitude = 0.2 Nm) as shown in Figure 4.5.
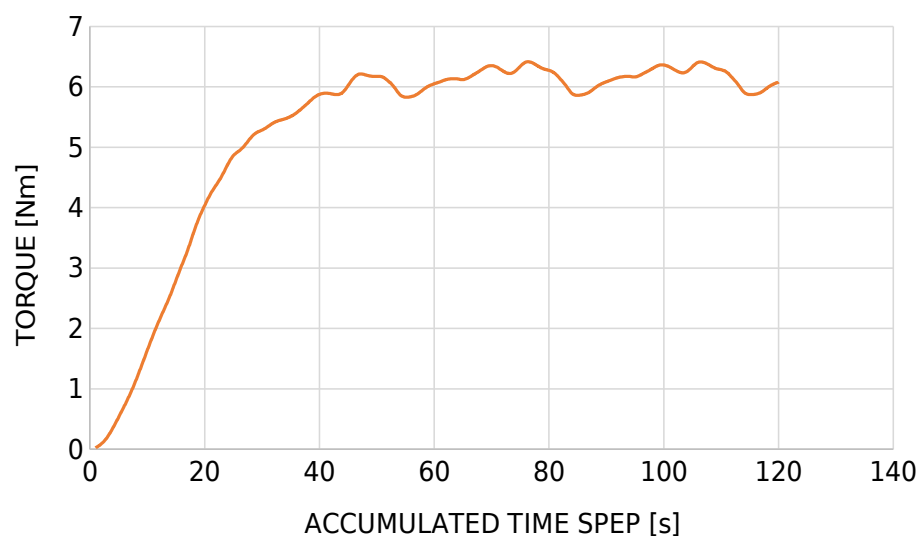
Figure 4. 5: Torque Curve for Reference Screw Rotating at 20 rpm

At high rotational speeds the rate of translating water downstream increases hence underfilling which in turn increases the magnitudes of the differences in pressure on the blades. Slow speed ensures higher fill levels of the buckets thus reducing pressure differences that are occasioned by circumferential positions of the blades. The result supports the need to operate ASTs at low speed values in order to reduce fluctuations in generated torque and mechanical power.

4.1.1 Grid Independence Study

The reference screw, flow rate of 10 kg/s, rotational speed of 30 rpm and element sizes ranging from 6 mm to 20 mm were used in the grid independent study. Results of the study were presented in both Table 4.1 and Figure 4.6.

Table 4. 1: Effect of Element Size on Torque

Run	Element Size (mm)	Mean Torque (Nm)
1	6	5.0062
2	7	5.0076
3	8	5.0082
4	9	5.5224
5	10	6.0384
6	15	8.6734
7	20	10.4762
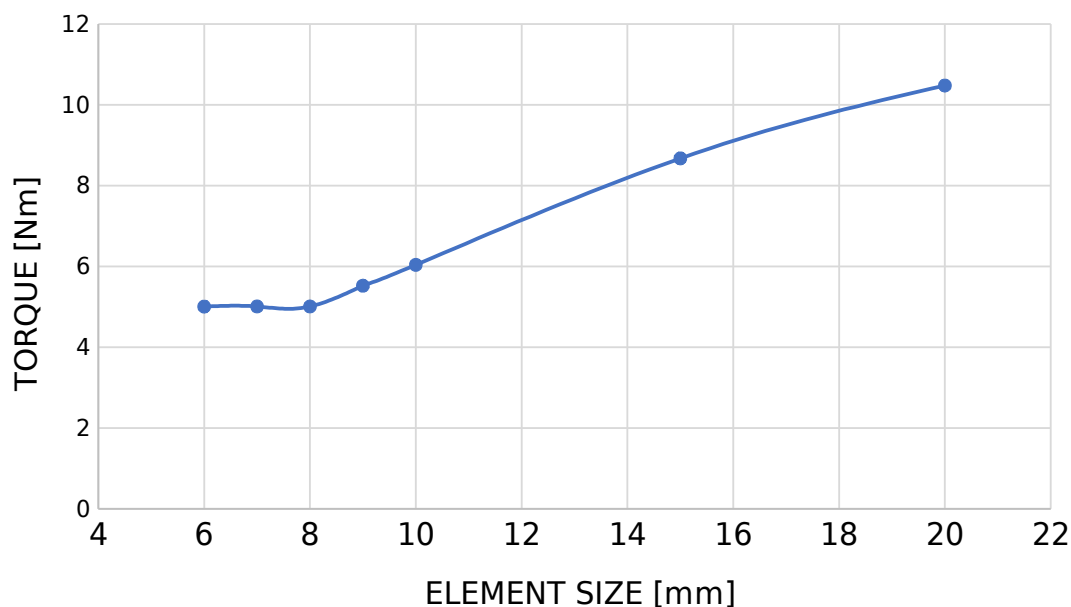
Figure 4. 6: Grid Independence Study graph

From the results presented in Figure 4.6, torque value remained constant at a magnitude of 5.0 Nm (to 1 decimal place) for element sizes between 6 mm and 8 mm. Thereafter, torque appreciably increased from 5.5 Nm at the element size of 9 mm to 10.5 Nm at the element size of 20 mm. Consequently, 8 mm was chosen as the appropriate element size for this study. A smaller element size would be computationally expensive in terms of storage space and computational time, while a larger element size would give inaccurate outputs. A researcher, Salam et al. (2018), also conducted a steady analysis of an AST model and used an optimal element size of 7.5 mm. The difference in the two values (8 mm and 7.5 mm) is understandable since the screws were not identical.

4.2 Combined Effects of Related Parameters on Torque, Mechanical Power and Efficiency of AST

4.2.1 Combined Effect of Inclination Angle (β) and Screw Length (L)

Figure 4.7 shows images of the five screw geometries (S1, S2, S3, S4 and S5) that were created and used to determine the combined effects of inclination angle (β) and length (L) on torque. Based on the images, it is clear that screw length decreases with increase in inclination angle.
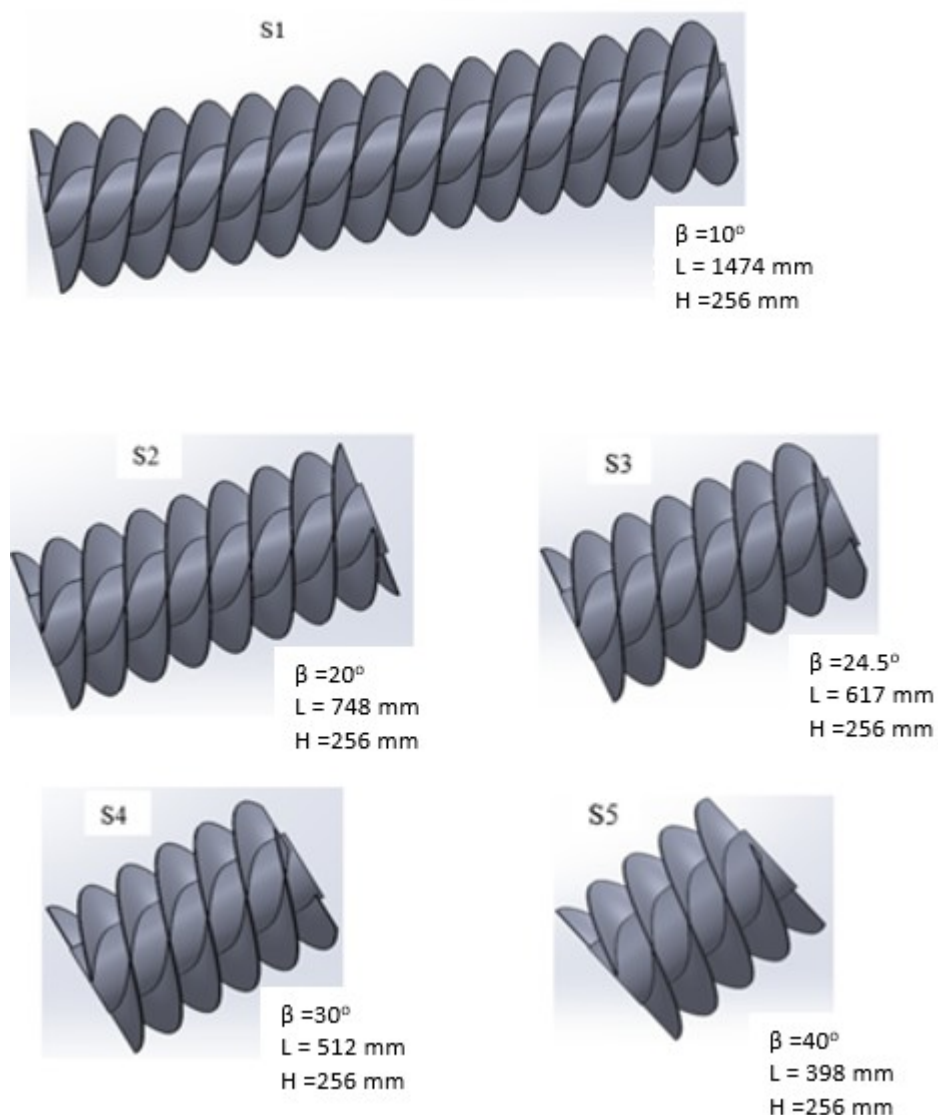
Figure 4. 7: Geometries for Screws with Different Values of β and L

For each of the five screw geometries shown in Figure 4.7, flow simulations were run at seven different rotational speeds of the screw: 20 rpm, 30 rpm, 40 rpm, 50 rpm, 60 rpm, 70 rpm and 80 rpm. Torque generated at each of the speeds was recorded and the average torque versus the rotational speed were plotted for each inclination angle as shown in Figure 4.8.
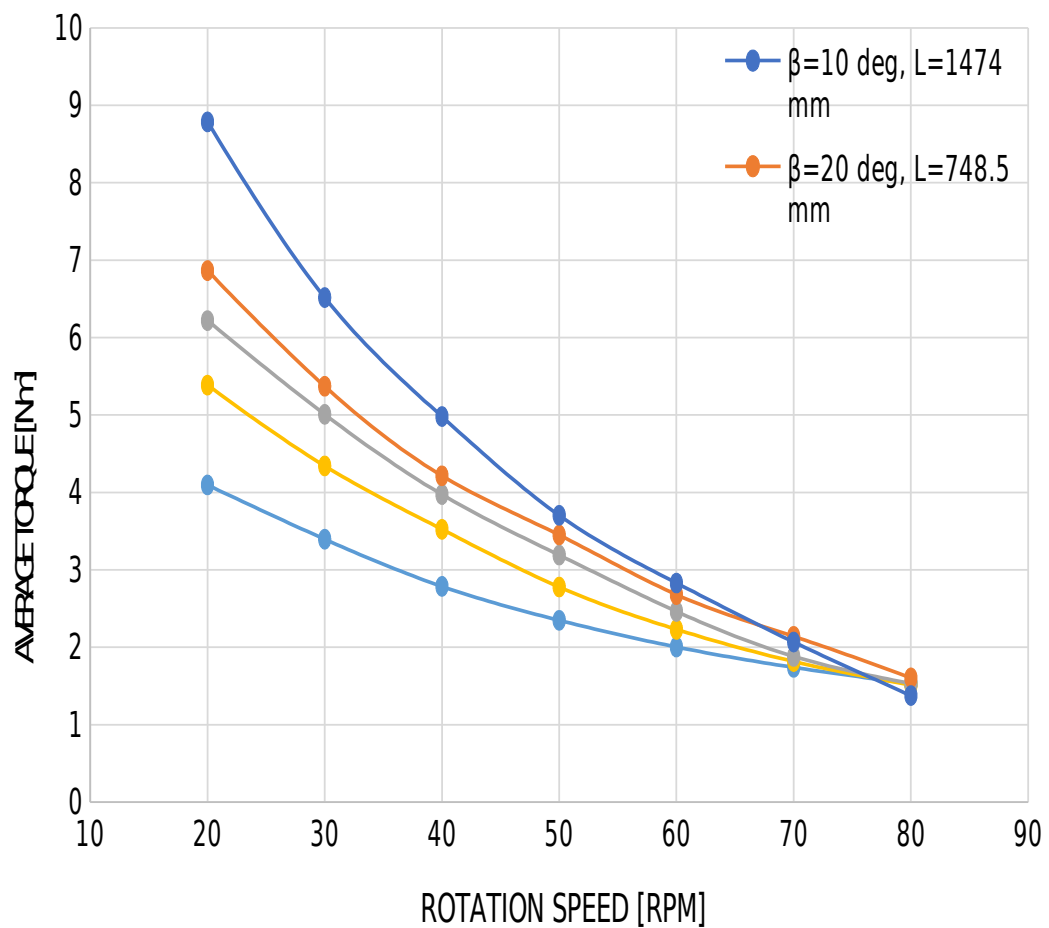
Figure 4. 8: Combined Effect of β and L on Average Torque

As can be seen from Figure 4.8, torque generally decreased with increase in rotational speed. This can be explained by the fact that a slower rotational speed provides more time for filling of buckets since linear velocity of water through the turbine is slower. This leads to higher fill factor for the buckets and hence greater hydrostatic force. In

contrast, faster rotational rate implies faster linear velocity of water through the turbine hence lower fill factor and less hydrostatic force. This characteristic curve for torque versus rotational speed was also realized by Lyons (2014) who further noted that the steepness of the curve varies greatly between different geometries.

It can also be observed (from Figure 4.8) that, the average torque increased with decrease in inclination angle (β) and corresponding increase in length for rotation speed range of 20 rpm to 65 rpm. This can be explained by the fact that decrease in inclination angle hence increase in screw length lead to increase in the number of buckets for torque generation.

For rotational speed above 65 rpm, torque values for screws with large inclination angles seemed to surpass those for screws with smaller inclination angles. This observation shows that screws with smaller inclination angles experienced faster reduction in torque as rotational speed increased. It is important to note that bucket fill factor is affected by both the number of buckets and rotational speed. Consequently, a combination of high speed and many buckets automatically produces huge reduction in fill factor hence a point can be reached beyond which the gains from additional number of buckets are outweighed by the losses that are associated with reduced fill factor.

Results for peak torques, at different magnitudes of inclination angle, were presented in Figure 4.9. It was evident that the curves for peak torque followed the same trend as those of average torque. However, as was expected, each peak torque had a greater magnitude than its corresponding average torque.
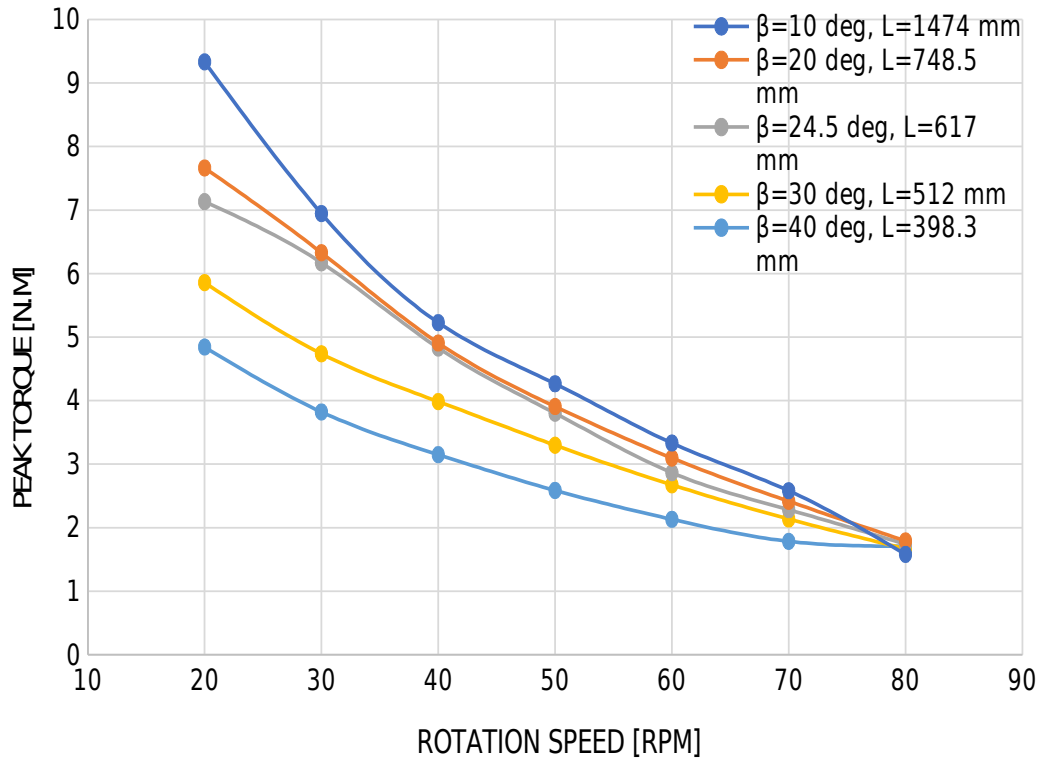
Figure 4. 9: Combined Effect of β and L on Peak Torque

The screw that was inclined at an inclination angle of 10°, and which had the longest length of 1474 mm, generated the highest peak torque in the tested range. Peak torque progressively increased with decrease in inclination angle (and increase in screw length) within the rotational speed range of 20 rpm to 70 rpm. The trend was attributed to the fact that, since the hydraulic head was maintained at a constant size, a smaller inclination angle corresponded to a greater screw length and hence increase in number of buckets.

Figure 4.10 is a graphical representation of results of the combined effect of β and L on average power from which several observations can be made.
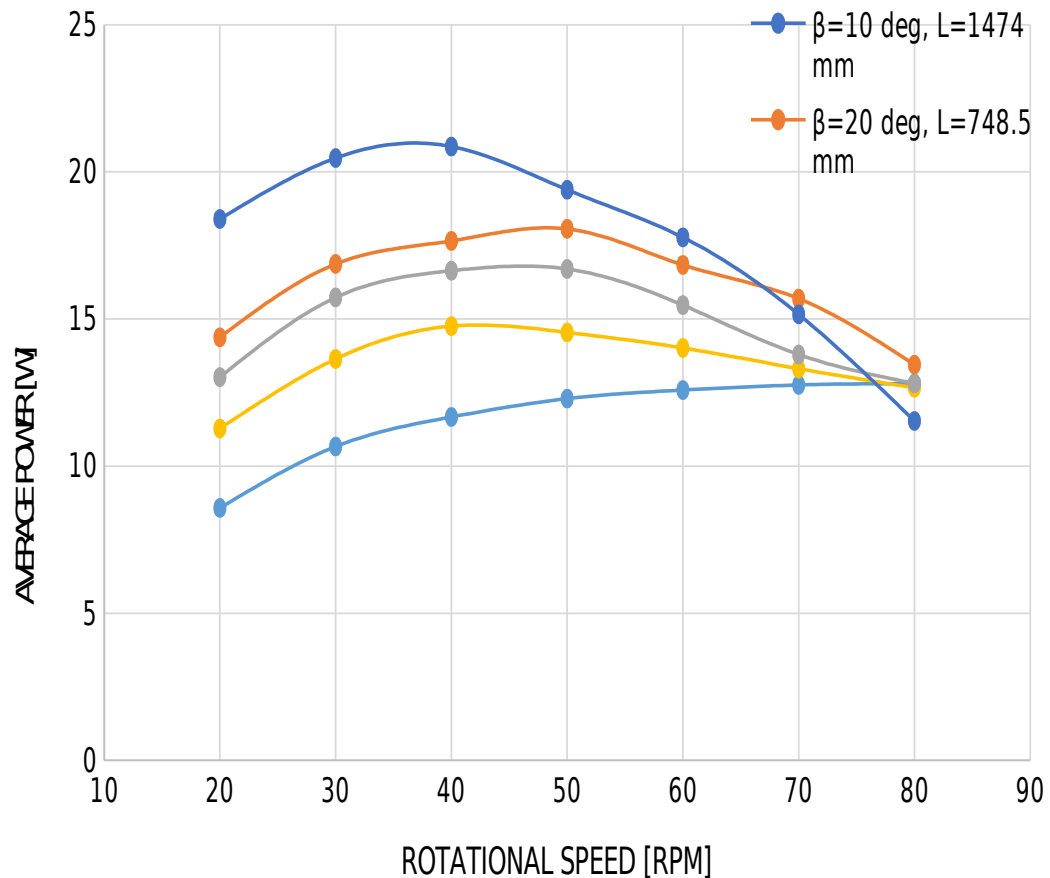
Figure 4. 10: Combined Effect of β and L on Average Mechanical Power

Firstly, for rotational speed values from 20 rpm to 65 rpm, the smaller the inclination angle and the longer the screw the higher the generated average power. This is consistent with the results on average torque as presented in Figure 4.8. It is also clear from the graphs that for every combination of β and L, average power increases with increase in rotational speed from 20 rpm up to a maximum value at a critical speed (for example, maximum average power of 20.9 W at 40 rpm for screw inclined at 10°) beyond which the graph begins to drop. This result is consistent with that of Songin (2017) and Lyons (2014) in terms of power characteristic curve for AST, even though they used steady state analysis of AST instead of transient.

The existence of critical rotational speed can be explained using the concept of fill factor (f) of buckets. At speeds lower than the critical speed, the buckets are over-filled (f > 1), which implies overflow losses and hence less power. At speeds above the critical speed the buckets are under-filled (f < 1) hence less hydrostatic pressure is generated per bucket. Low hydrostatic pressure corresponds to low magnitudes of both torque and power. Lastly, the graphs in Figure 4.10 show that the screw having the smallest inclination angle of 10° produced the highest average mechanical power of 20.86 W which occurs at a rotational speed of 40 rpm.

Average and peak power exhibited the same characteristic curves. From Figure 4.11, it can be seen that for rotational speed range of 20 rpm to 70 rpm, decrease in inclination angle led to increase in peak mechanical power. Like in the case of average mechanical power, the smaller the inclination angle the higher the peak mechanical power.
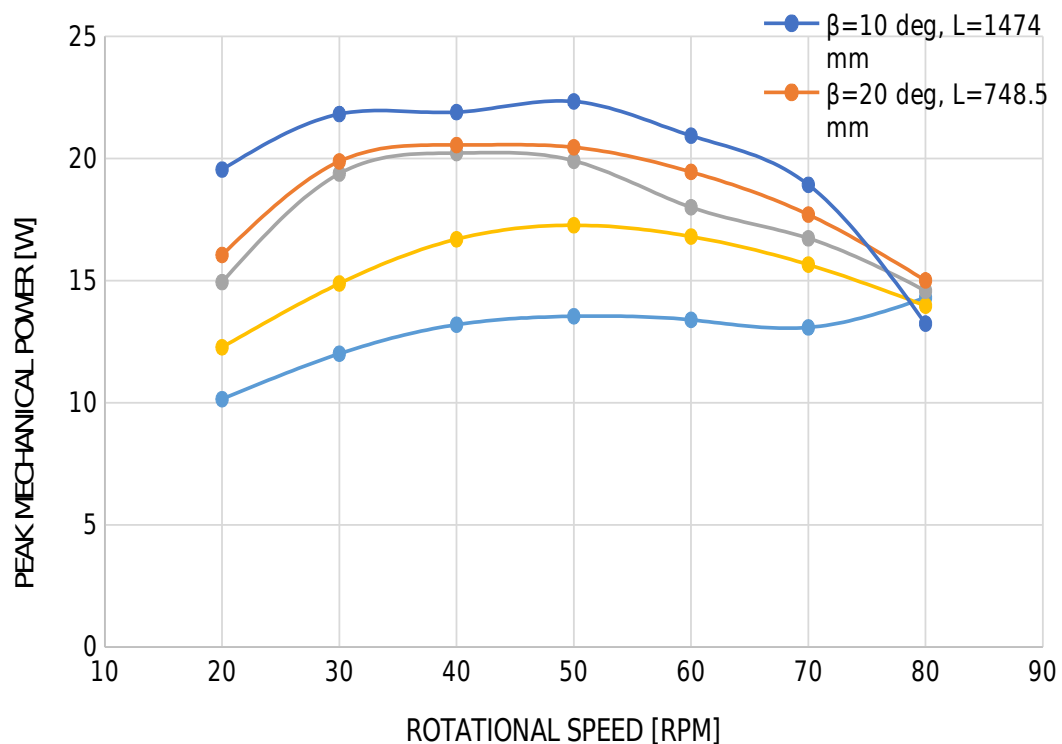
Figure 4. 11: Combined Effect of β and L on Peak Mechanical Power

For each curve in Figure 4.11, peak mechanical power increased with increase in rotational speed up to a critical speed beyond which further increase in speed caused decrease in the power. The trend can be explained using the interdependency between fill factor, rotational speed and mechanical power. At speed values below critical speed, over-filling of buckets occurred hence overflow losses were experienced. At the critical speed, the buckets were optimally filled hence maximum power was generated. Lastly, at speed values above the critical speed the buckets were under-filled hence lower magnitudes of both hydrostatic pressure and mechanical power. Highest peak power of 22.34 W was generated by the longest screw that was inclined at 10° and rotating at a speed of 50 rpm.

Mechanical efficiency was another important output that was considered in this study. It was calculated as the ratio of mechanical power to available power, expressed as a percentage. Figure 4.12 shows graphs for average mechanical efficiency versus rotational speed.
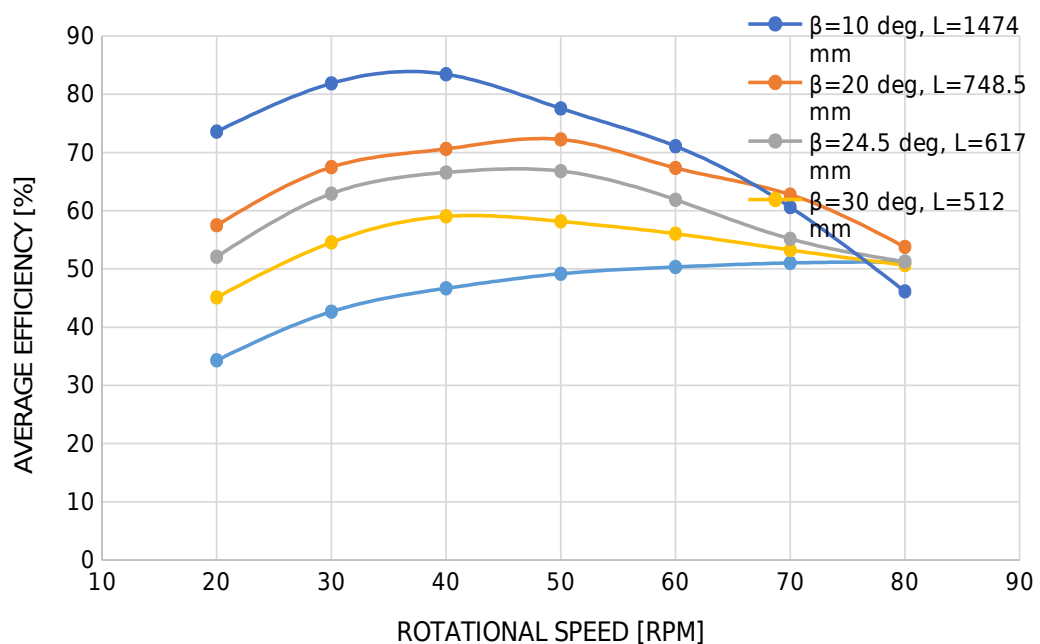
Figure 4. 12: Combined Effect of β and L on Average Efficiency

For rotational speed between 20 rpm and 65 rpm, it is clear that as the angle of inclination was decreased the average mechanical efficiency increased. This was expected since average efficiency is directly proportional to average power. It is also clear from the graphs that average mechanical efficiency for each screw increased with increase in rotational speed up to a maximum value and thereafter it progressively decreases with further increase in the speed. The same pattern was observed with average torque (Figure 4.8), hence the explanation based on fill factor of buckets holds for this case too. The screw geometry that had inclination angle of 10^0 and corresponding screw length of 1474 mm gave highest average mechanical efficiency values for all speeds in the range of 20 rpm to 65 rpm. Maximum average mechanical efficiency of 83.4% occurred at a rotational speed of 40 rpm, but efficiency range was limited to 1.5 % in the speed range of 30 rpm to 40 rpm.

The results shown in Figure 4.12 were also presented using a 3D surface chart as shown on Figure 4.13. The chart shows that the average mechanical efficiency was high in the speed range of 30 rpm to 40 rpm.
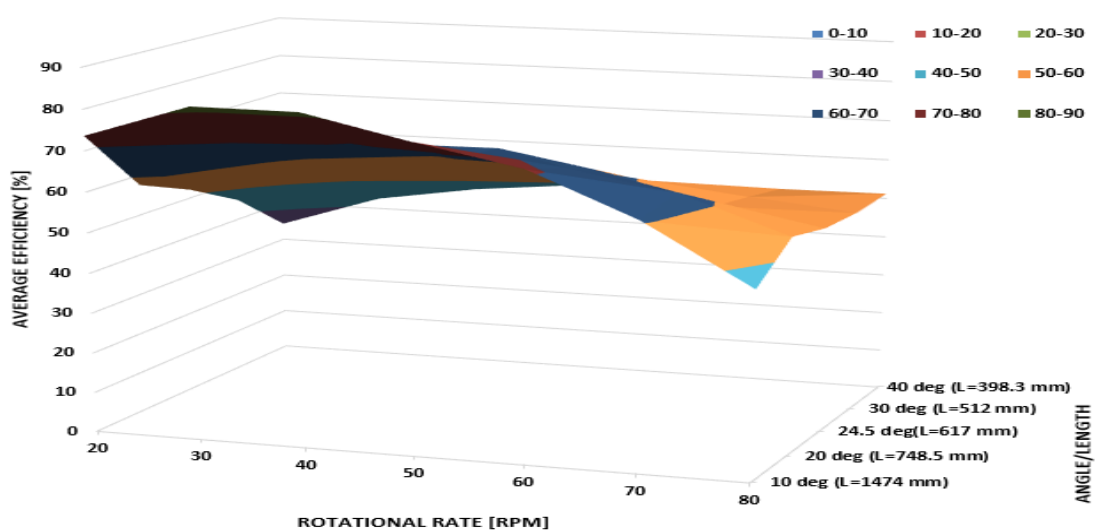
Figure 4. 13: Surface Chart for the Combined Effect of β and L on Average Efficiency of an AST

Graphs for peak mechanical efficiency mirrored those of peak mechanical power. Figure 4.14 shows graphs for peak mechanical efficiency versus rotational speed for five screw geometries inclined at 10º, 20º, 24.5º, 30º and 40º respectively.
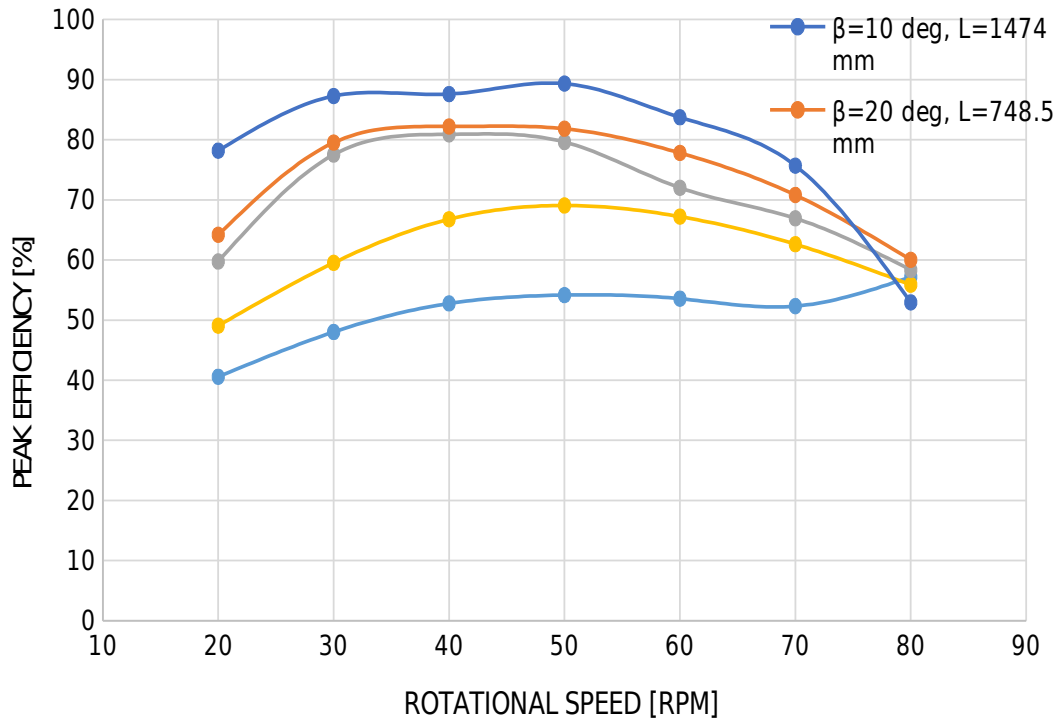
Figure 4. 14: Combined Effect of β and L on Peak Mechanical Efficiency

From the graphical representation of peak efficiency in Figure 4.14, within the speed range of 20 rpm to 70 rpm, it can be seen that reduction in inclination angle resulted in increase in peak mechanical efficiency. This was expected since a smaller inclination angle has a corresponding longer length hence higher number of buckets. The maximum peak mechanical efficiency obtained was 89.4%, given by the screw having the smallest inclination angle of 10^0 and a rotational speed of 50 rpm. Figure 4.15 shows the same results in 3D using a surface chart.
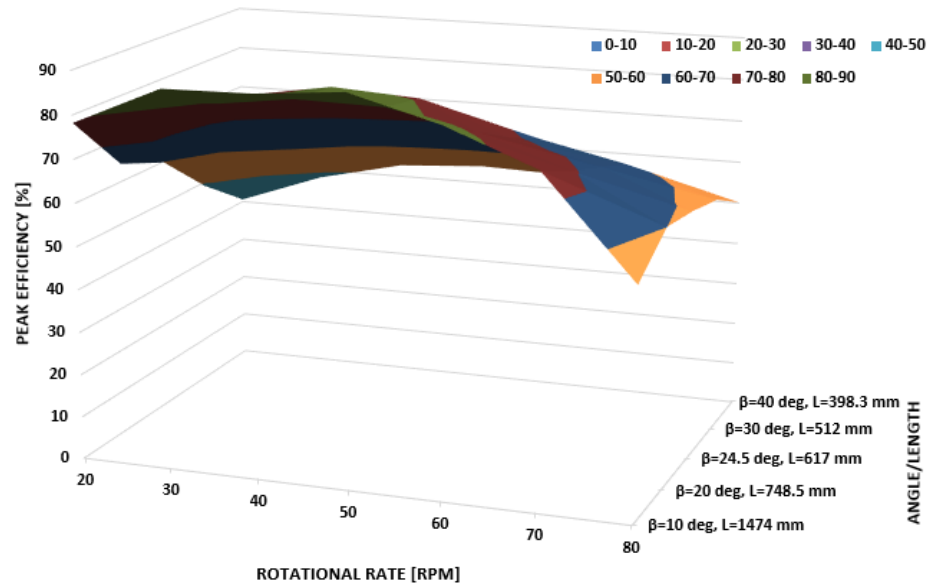
Figure 4. 15: Surface Chart for the Combined Effect of β and L on Peak Efficiency of an AST

4.2.2 Combined Effect of Number of Blades (N) and Pitch (S)

In this section transient simulations were run on different geometries in order to determine the combined effect number of blades (N) and pitch (S) on torque, mechanical power and efficiency of ASTs. Initially, simulations were run at a constant bucket width (W_b) of 95.25 mm for five screw geometries having 2 blades, 3 blades, 4 blades, 5 blades and 6 blades respectively. The geometry that produced the highest mechanical efficiency was further tested, with W_b as the sole variable, in order to find the optimal W_b size.

Images of the initial five screw geometries that were used in the tests are shown in Figure 4.16.
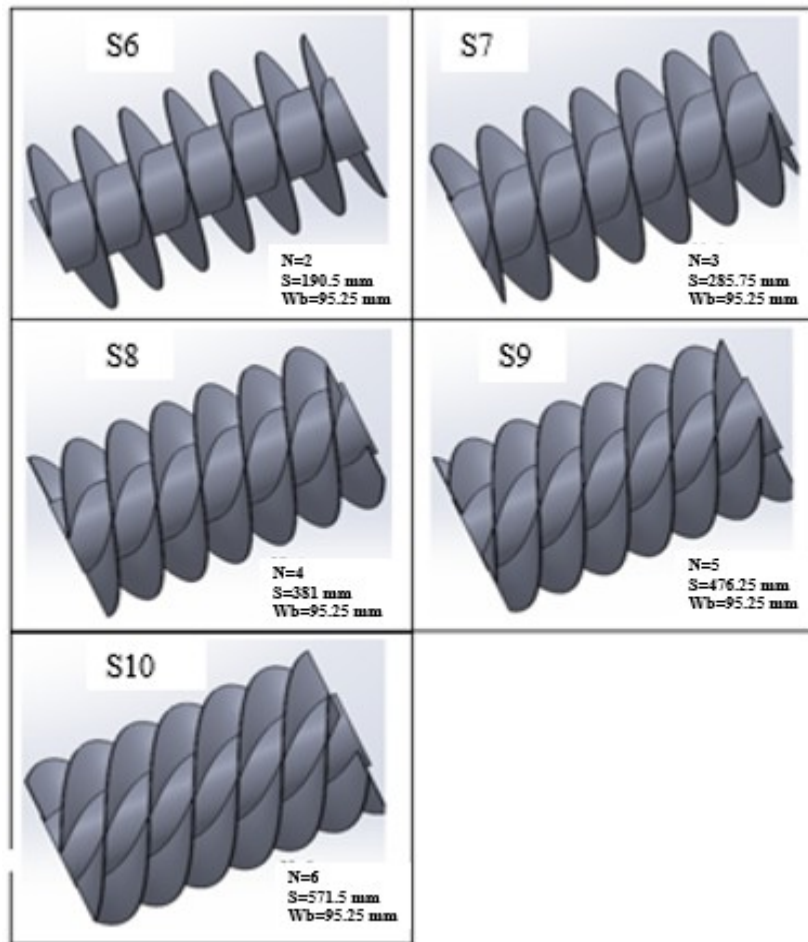
Figure 4. 16: Geometries for Screws with Different Values of N and S

Figure 4.17 shows results of average torque outputs for the five geometries. The results show there was no single geometry which consistently generated higher average torque values than the rest in the tested range of speeds. However, for design considerations, it was noted that a higher rotational speed required a screw with lesser number of blades.
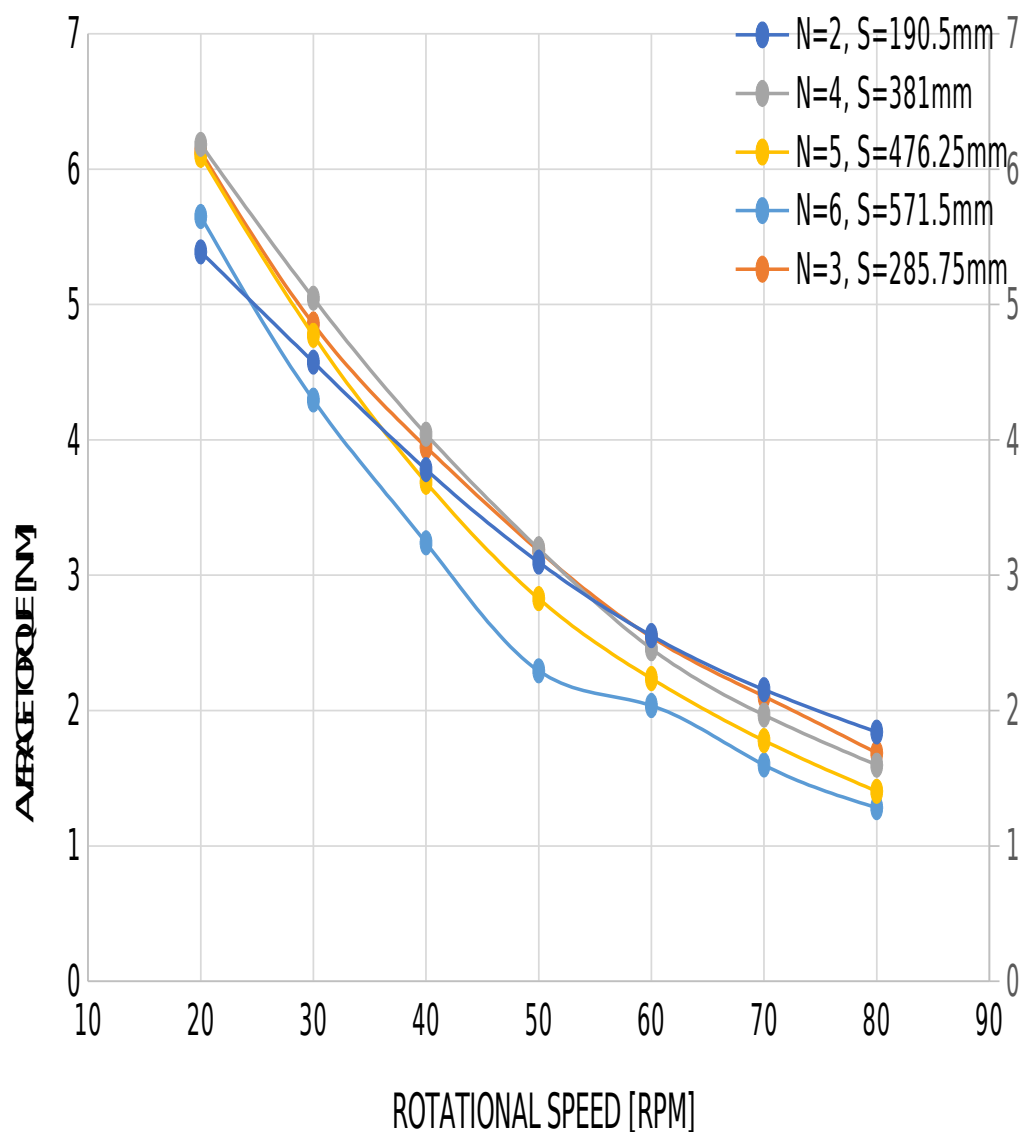
Figure 4. 17: Combine Effect of N and S on Average Torque

The screw geometry having 4 blades generated higher values of average torque than the other screws for all design points in the speed range starting from 20 rpm up to 50 rpm. Similarly, screws having 3 blades and 2 blades performed better than the other screws in the speed ranges of 50 rpm to 60 rpm and 60 rpm to 80 rpm respectively.

Figure 4.17 shows that for rotational speeds above 70 rpm, increase in the number of blades resulted in decrease in the average torque. This observation can be explained using the effect of blade-frequency at the interface between the inlet section (weir) and

the screw section, on bucket filling. For both rotational speed values above 70 rpm and high number of blades, the blade frequency at the interface was very high hence little time was available for filling of the buckets through the gaps between the blades. This led to low fill factor. Thus, a screw having few blades tend to generate more torque at high rotational speed values than a screw having more blades.

Figure 4.18 shows results for performance of the screws in terms of generated peak torque.
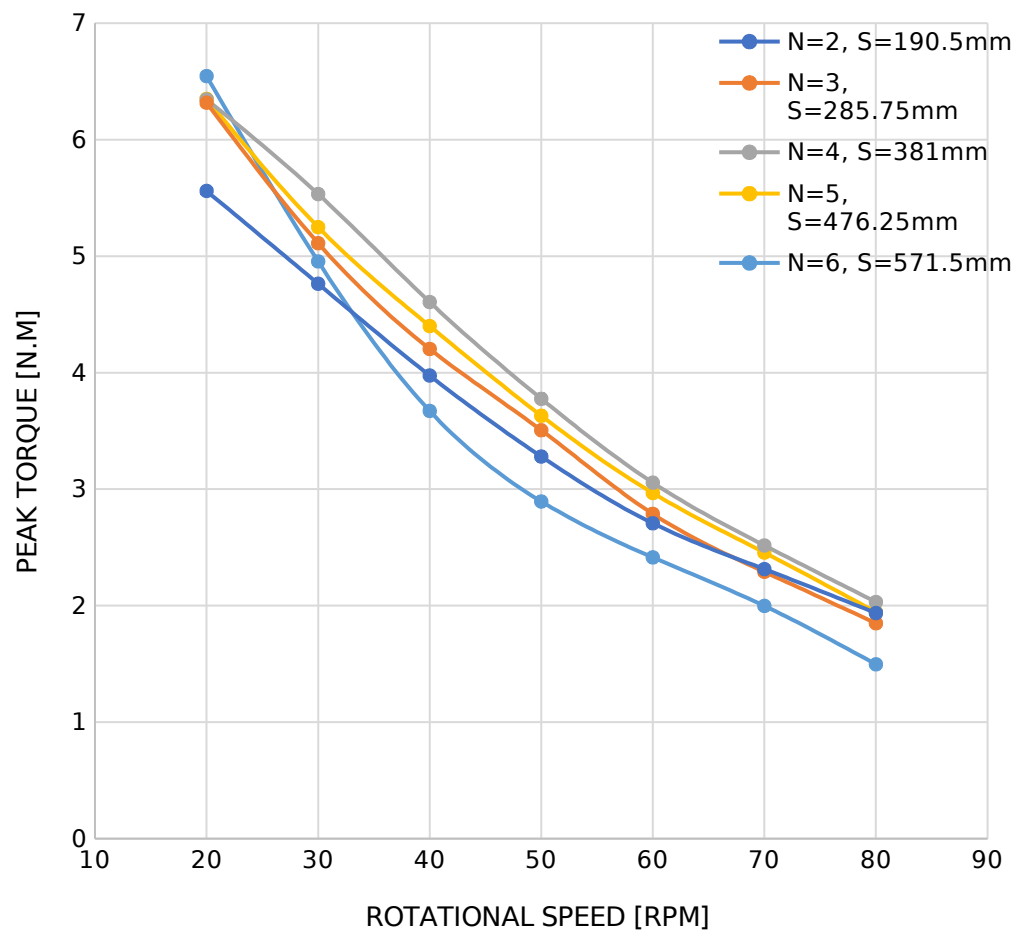
Figure 4. 18: Combined Effect of N and S on Peak Torque

Based on Figure 4.18, the screw having 4 blades generated higher peak torque than the other four screws for almost the entire speed range. Its performance was followed closely by that of the screw having 5 blades. The screw having 6 blades produced the best performance at a speed of 20 rpm, but performed very poorly as the speed increased such that it generated lower torque values than the other four screws for all speed values between 35 rpm and 80 rpm. The good performance at 20 rpm, by the screw, can be attributed to low blade-frequency at low rotational speed values. However, as the speed increased beyond 35 rpm, the high number of blades became a disadvantage since it led to high blade frequency hence lower fill factor.

Performance of the screw geometries was also analyzed based on mechanical power as shown in Figure 4.19. Like it was in the case of torque, the generated mechanical power was constrained to application of a constant bucket width (W_b) of 95.25m
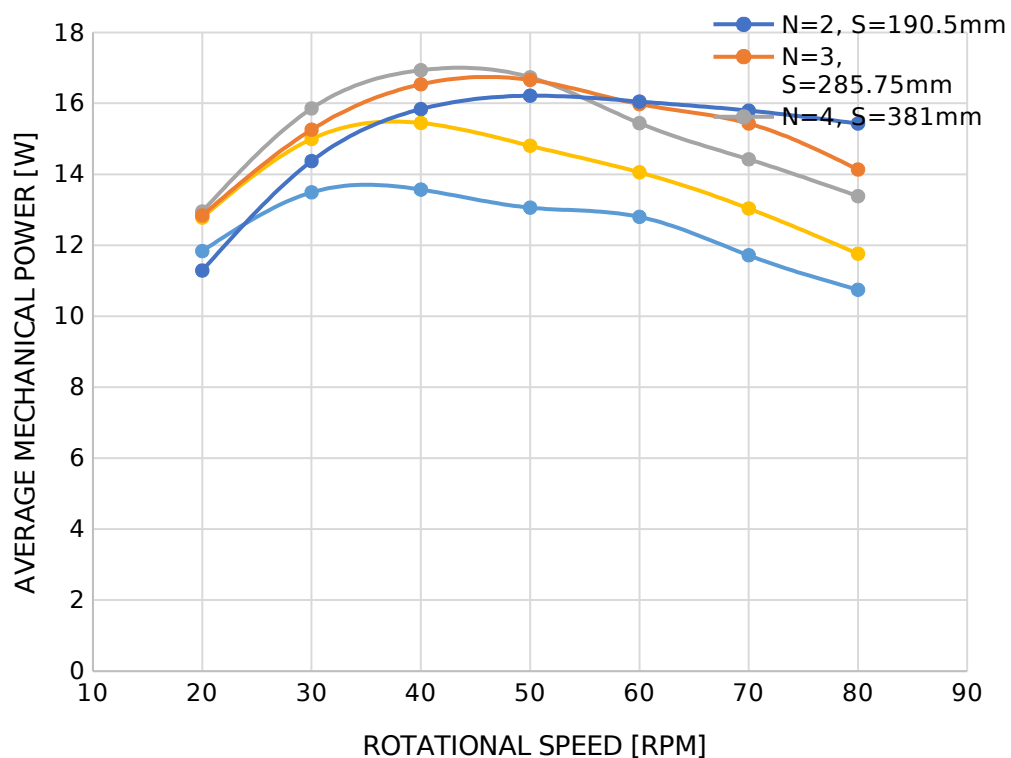
Figure 4. 19: Combined effect of N and S on Average Mechanical Power

For each geometry, as presented in Figure 4.19, the average mechanical power increased with increase in rotational speed up to a maximum value at a critical rotational speed beyond which further increase in speed produced diminished values of the output. Taking the case of the screw geometry having four blades and a pitch of 381 mm, the average mechanical power increased from 12.78 W at a rotational speed of 20 rpm to a maximum of 16.93 W at 40 rpm followed by a decline to 13.38 W at 80 rpm. This behavior is characteristic of ATS's power versus rotational speed (Lyons, 2014) and can be explained using overflow losses at speeds lower than the critical speed and underfilling at speeds above the critical angle, hence reduced hydrostatic pressure. The decrease in the output values was augmented by increase in frictional losses at higher rotational speeds. Further, within the tested range of speed, no single screw geometry consistently generated higher values of average mechanical power than the rest of the screws. This is consistent with the results of average torque shown in Figure 4.17. The highest average power of 16.9 W was generated by the screw having 4 blades when rotating at a speed of 40 rpm.

Results for peak mechanical power were presented in Figure 4.20.
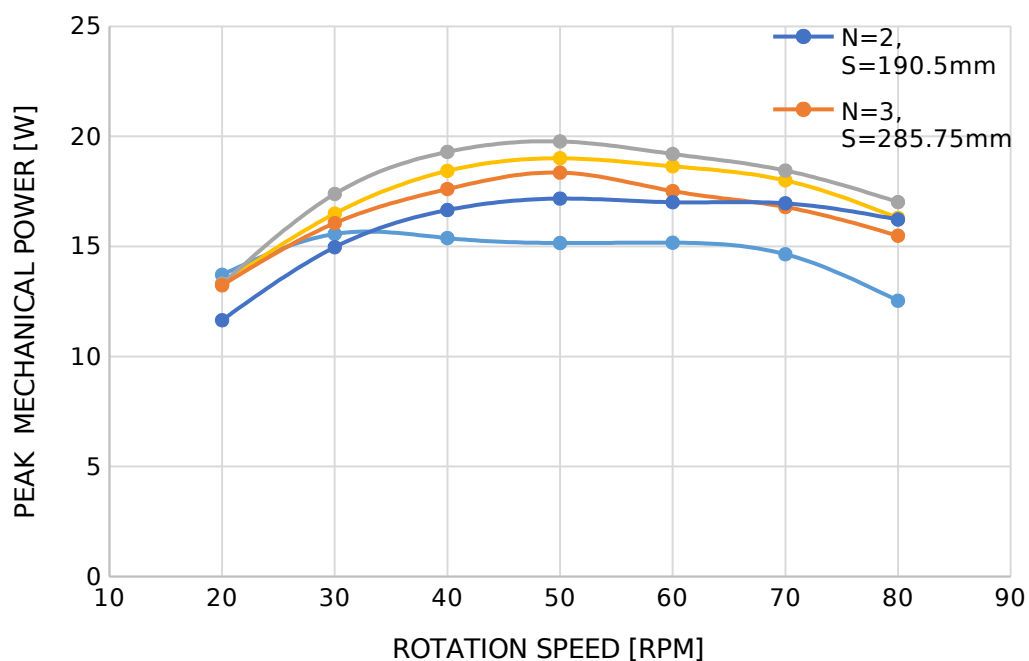
Figure 4. 20: Combined Effect of N and S on Peak Mechanical power

As shown in Figure 4.20, the screw having 4 blades generated the highest peak power across the entire range. This can be attributed a better balance between number of buckets and fill factor. The highest peak power of 19.8 W occurred at a rotation speed of 50 rpm.

As was expected, the pattern for both average and peak efficiencies reflected those of average and peak powers respectively. Figure 4.21 shows curves for average mechanical efficiency versus rotational speed for the five screw geometries. The average mechanical efficiency increased with increase in rotational speed up to a maximum then reduced progressively with further increase in the speed.
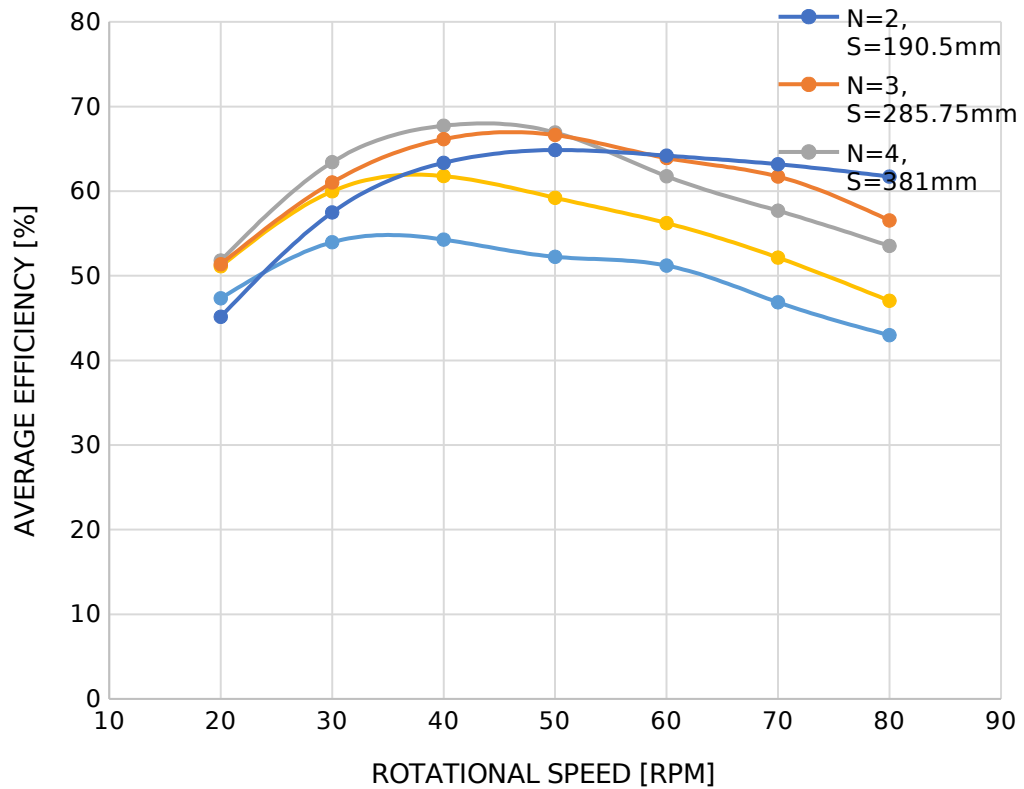
Figure 4. 21: Combined Effect of N and S on Average Mechanical Efficiency

The screw that produced higher values of the average efficiency than the rest for rotational speed ranges of 20 rpm to 50 rpm, 50 rpm to 60 rpm and 60 rpm to 80 rpm were screws having N = 4, N =3 and N = 2 respectively. The screw having 4 blades produced the highest average mechanical efficiency of 67.7%, which was achieved at a speed of 40 rpm. Figure 4.22 shows 3D surface chart for the data on Figure 4.21.

+
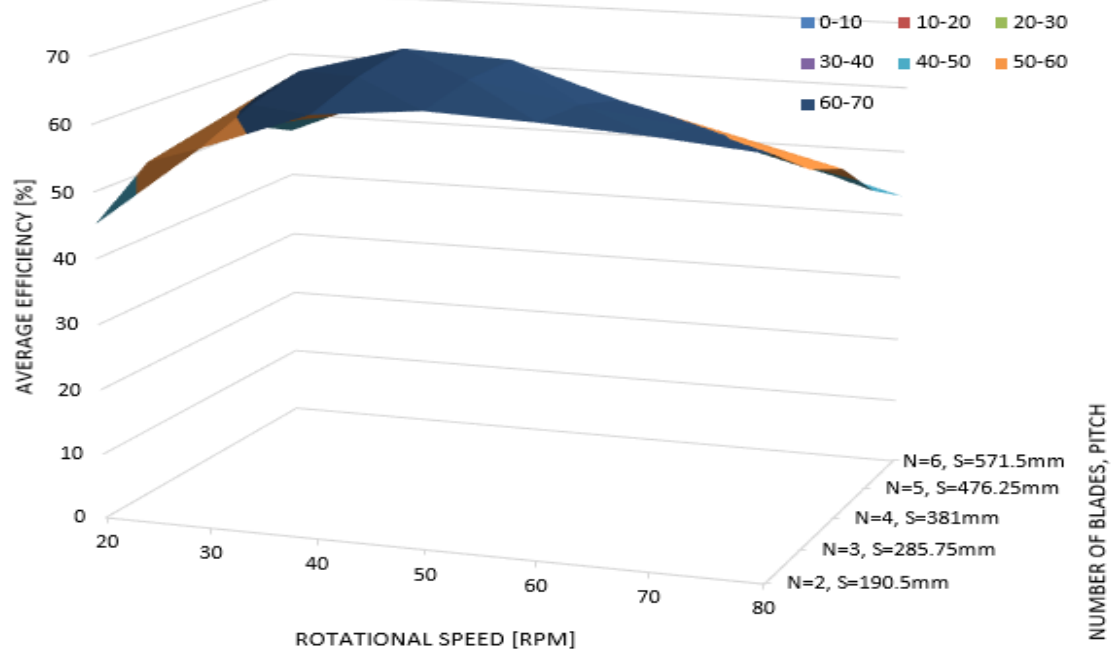
Figure 4. 22: Surface Chart for the Combined Effect of N and S on Average

   Efficiency of an AST

Peak mechanical efficiency graphs exhibited trends similar to those of average

mechanical efficiency. Figure 4.23 shows results for the combined effect of N and S on

peak mechanical efficiency.
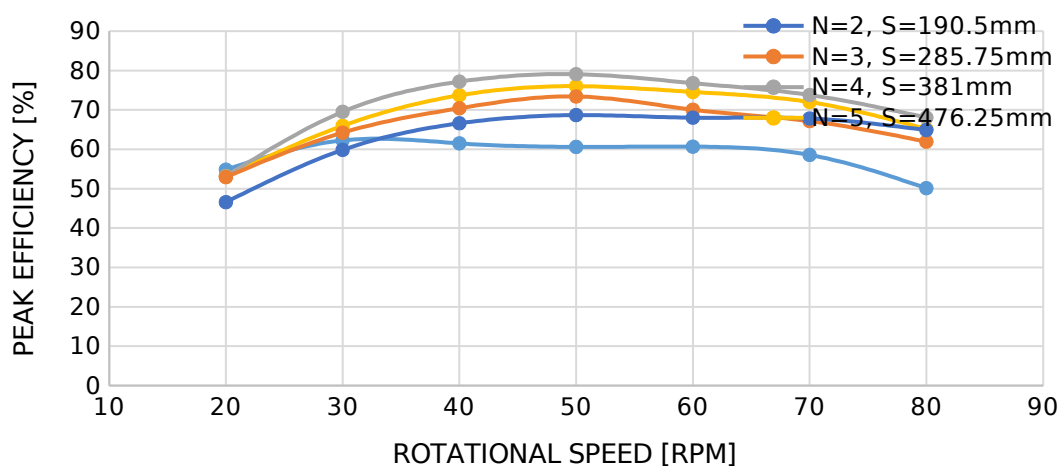
Figure 4. 23: Combined Effect of N and S on Peak Mechanical Efficiency

The screw with 4 blades gave the highest peak mechanical efficiency of 79.0 %. This was expected because the same screw generated the highest mechanical peak power in the same rotational range of 20 rpm to 60 rpm. Figure 4.24 shows a 3D visualization of the data in Figure 4.23.
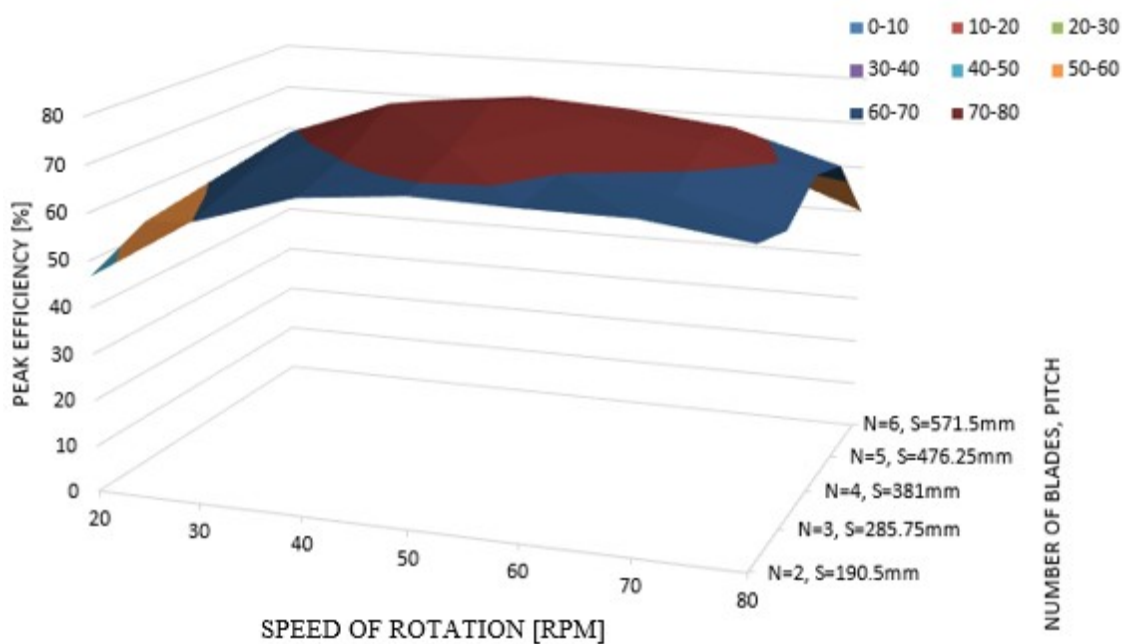
Figure 4. 24: Surface Chart for the Combined Effect of N and S on Peak

Efficiency of an AST

In general, the screw having 4 blades performed better than the other four screws in terms of highest values of both average and peak efficiencies at a bucket with (Wb) of 95.25. The results presented here disagrees with the outcomes of previous studies such as Rosly et al. (2016) who concluded that number of blades have no appreciable effect on AST's efficiency and Waters (2015) who concluded that increase in number of blades leads to reduction in AST's efficiency. The results could have been confounded by methodological and assumption of steady state flow analysis.

Finally, keeping all the other parameters constant, bucket width (W_b) for the 4-blade screw (S8) was varied in order to determine the optimal value of the parameter (W_b). Constant parameters were: N = 4, D_i = 168 mm, D_o = 381 mm, L = 617 mm, Q = 10 l/s, β = 24.5 and rotational speed of 40 rpm. Bucket width (W_b) was then varied taking values between 30 mm and 127 mm as shown in Table 4.2. Thus, a total of nine screw geometries were used in the test.

Table 4. 2: Variable Parameters for Testing Effect of Bucket Width (W_b)

Screw	Bucket width (W_b) in mm	Bucket width ratio (W_{br}); $W_{br} = W_b/D_o$	Pitch (S) in mm	Pitch ratio (S_r); $S_r = S/D_o$
S11	30	0.0787	120	0.31
S12	40	0.1050	160	0.42
S13	50	0.1312	200	0.52
S14	65	0.1706	260	0.68
S15	71.5	0.1877	286	0.75
S16	80	0.2100	320	0.84
S17	95	0.25	380	1.00
S18	110	0.2887	440	1.15
S19	127	0.3333	508	1.33

Images of the nine screw geometries are shown in Figure 4.25.
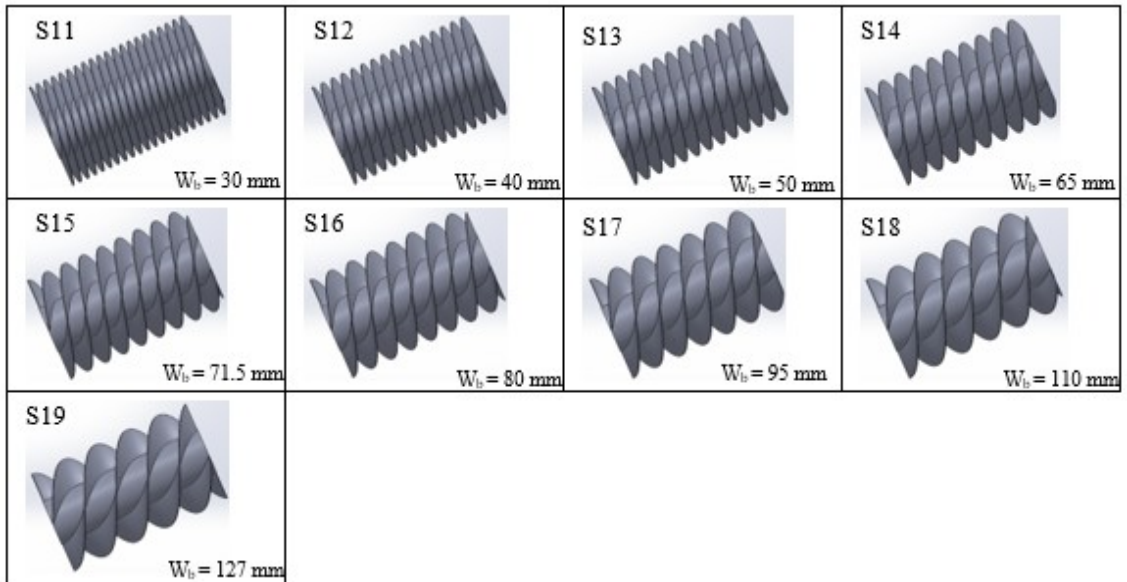
Figure 4. 25: Images of Screw Models having 4 Blades, but Different Sizes of

Bucket Width (W$_b$)

Transient simulations, for the nine geometries, were run and results presented on Figure
4.26 and Figure 4.27.
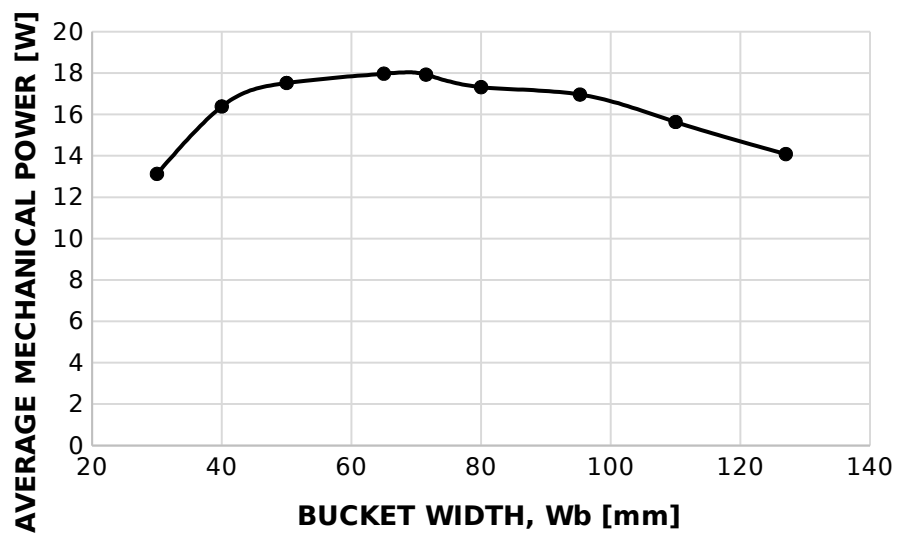
Figure 4. 26: Effect of Bucket Width (W$_b$) on Average Mechanical Power

Based on the results shown in Figure 4.26 it can be seen that the average mechanical
power increased with increase in bucket width (W$_b$) up to a maximum level, beyond

which the output gradually diminishes with further increase in W_b. The highest average mechanical power of 17.97 W was produced at a bucket width (W_b) of 65 mm. This corresponded to a bucket width ratio (W_{br}) of 0.17, pitch (S) of 260 mm and pitch ratio (S_r) of 0.68 as shown in Table 4.2 above.

Figure 4.27 shows the effect of bucket width ratio (W_{br}) on average mechanical efficiency. W_{br} is a non-dimensional parameter defined $W_{b_r} = \dfrac{W_b}{D_0}$.
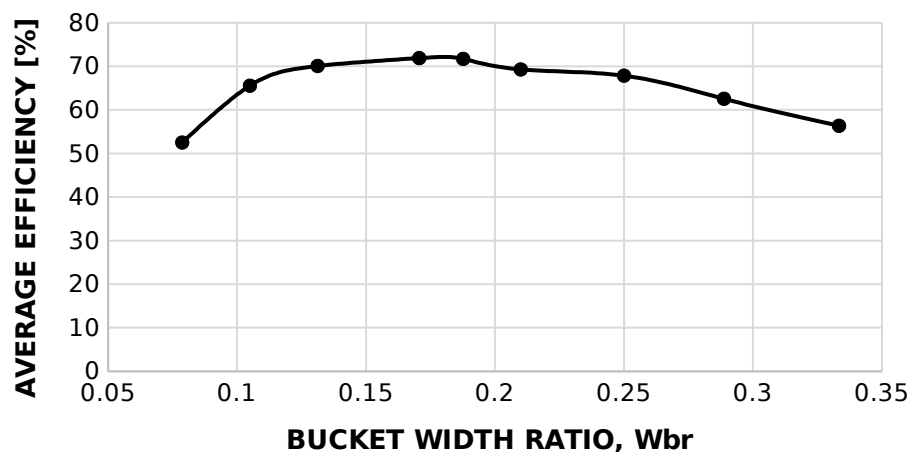
Figure 4. 27: Effect of Bucket Width Ratio (W_{br}) on Average Mechanical Efficiency

From Figure 4.27, the highest average mechanical efficiency of 71.9 % was produced at a bucket width ratio (W_{br}) of 0.17 and pitch ratio (S_r) of 0.68.

4.2.3 Effects of Independent Parameters on outputs of an AST

Knowledge of the effects of individual parameters such as β and N played a great role as prerequisite information upon which realistic interpretation of the combined effects of related parameters such as β/L and N/S were made.

4.2.3.1 Effect of Inclination Angle (β)

The reference screw model was used to test the individual effect of inclination angle(β) on torque, mechanical power and efficiency of AST. Average and peak values of torque, mechanical power and efficiency were determined at three different sizes of inclination angles: 24.5º, 20º and 10º. Images of the three geometries (S20, S21 and S22) are shown in Figure 4.28.
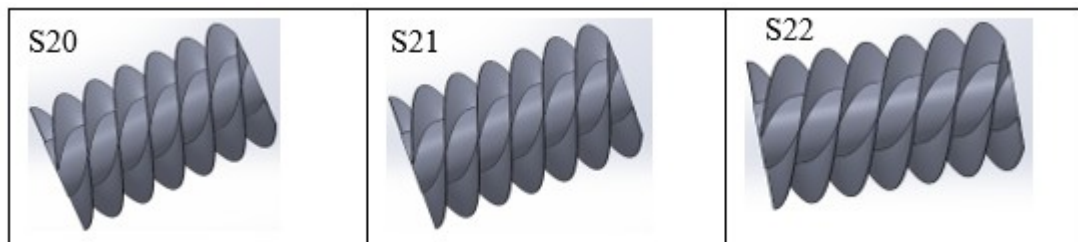
Figure 4. 28: Geometries showing Variation of Inclination Angle at Constant Screw Length

Simulations were conducted at flow rate of 10 kg/s and rotational speeds in the range of 20 rpm and 80 rpm. Results were used as baseline information for interpreting the results on the combined effects of β and L on AST's outputs.

Figure 4.29 shows results of the effect of inclination angle (β) on average torque.
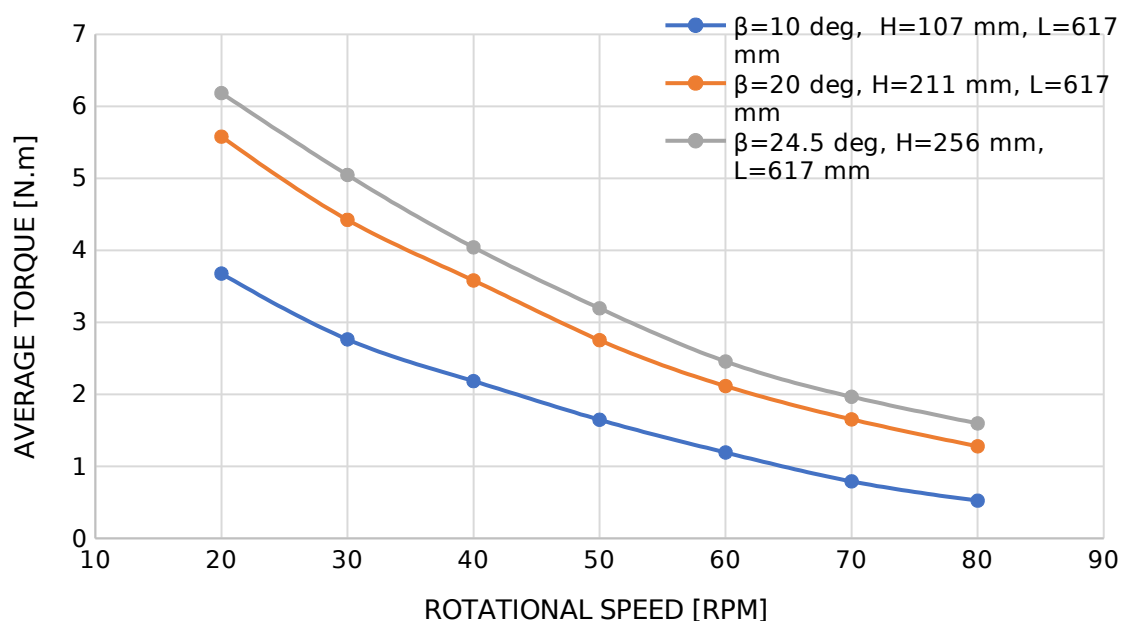
Figure 4. 29: Effect of β on Average Torque

It can be seen that the greater the inclination angle the higher the generated average torque. The trends can be explained by the fact that, for an AST with constant length, increase in angle leads to increased head, hence increase in input power. A point to note, however, is that the trend is restricted to the inclination angle range that was tested. A change of screw length may widen the range and probably generate a trend with a critical value of inclination angle.

Graphs for peak torque, as presented in Figure 4.30, exhibited the same trends as graphs for average torque.
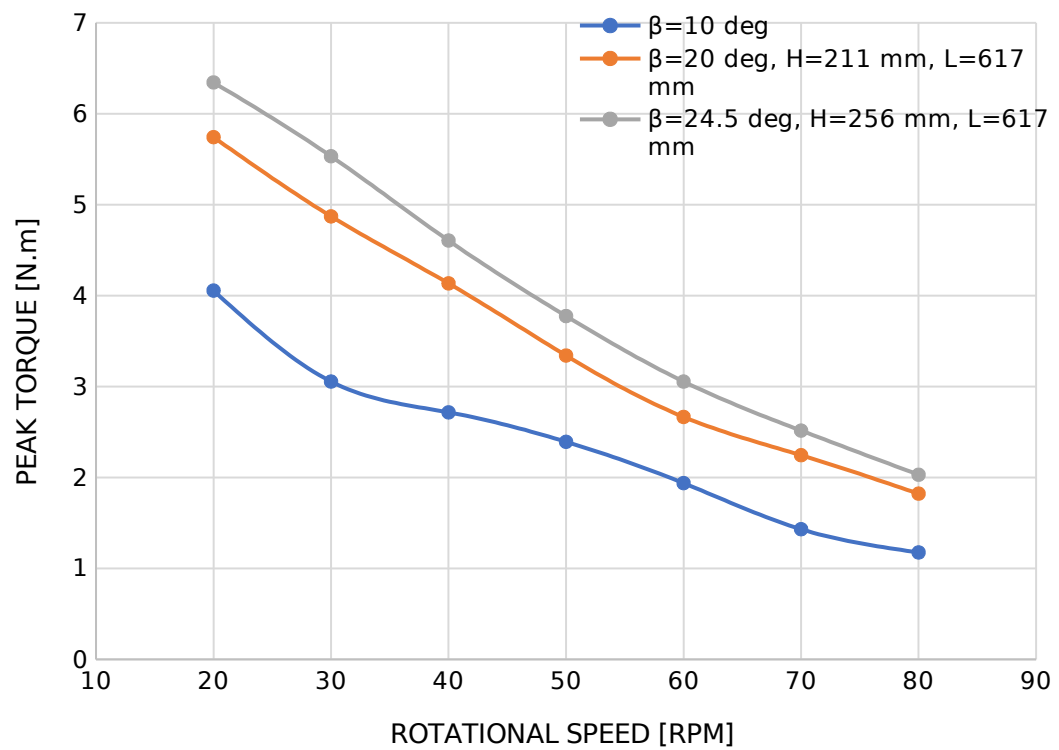
Figure 4. 30: Effect of β on Peak Torque

Based on the results, peak torque increased with increase in inclination angle. This can be explained by the fact that each time the inclination angle was reduced, the head also decreased. This led to lower input power and hence smaller peak torque values.

Mechanical power was also plotted against rotational speed for the three sizes of inclination angle (β). Figure 4.31 shows the results for average mechanical power.
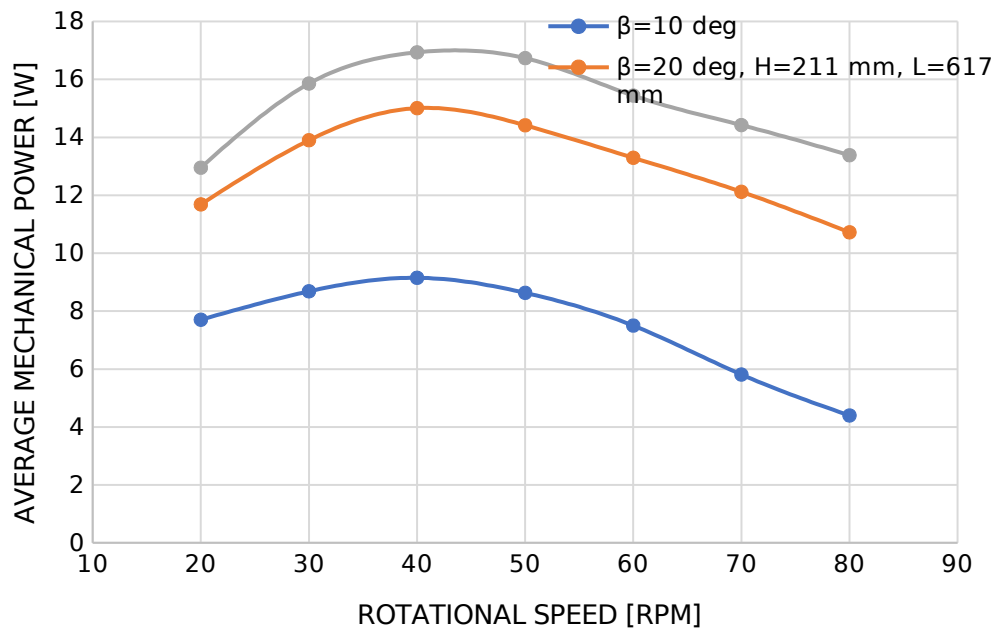
Figure 4. 31: Effect of β on Average Mechanical Power

Mechanical power increased with increase in rotational speed up to a critical speed beyond which diminishing returns were observed. The highest average power of 16.9 W occurred at an angle on 24.5^0 and at a rotational speed of 40 rpm. Further, reduction in inclination angle (β) led to decrease in average mechanical power. This trend is in sharp contrast with that of the combined effect of β and L (Figure 4.10). Further still,

tests based on the individual effect of β produced lower outputs than tests based on the combined effect of β and L. While tests based on β produced highest average torque of 16.9 W, tests that were based on simultaneous variation of β and L produced highest average power of 20.9 W (Figure 4.10). It is therefore apparent that treating inclination angle (β) and screw length (L) as related parameters improved the magnitude of average mechanical power produced by the AST.

Based on the results presented on Figure 4.32, peak mechanical power followed the same trend as that of average mechanical power. The highest peak power of 19.8 W occurred at an angle of 24.5^0 and at a rotational speed of 50 rpm. Comparatively, this was lower than the highest peak power of 22.3 W that was produced from combined effect of β and L (Figure 4.11).
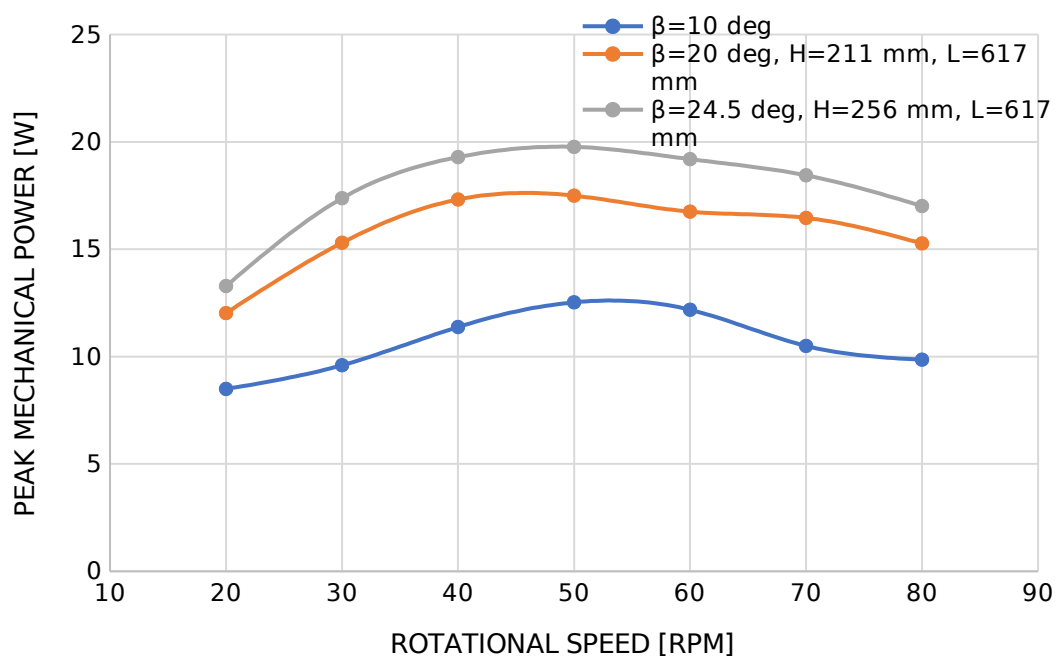
Figure 4. 32: Effect of β on Peak Mechanical Power

Results of average mechanical efficiency were presented in Figure 4.33.
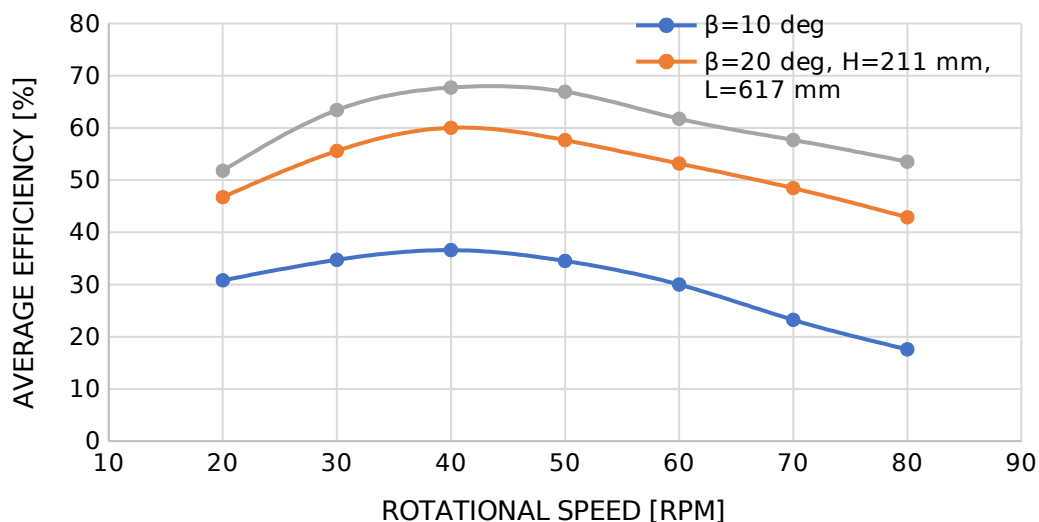
Figure 4. 33: Effect of β on Average Mechanical Efficiency

From Figure 4.33, the greater the inclination angle the higher the average mechanical efficiency. This trend was expected because increasing the inclination angle (β) at constant screw length, led to increase in head and hence increase in input power. Lyons (2014) conducted an experimental study of the AST for inclination angle range from 17.2^o to 34.7^o; he found out that increasing the angle lead to increase in hydraulic head, mechanical power and efficiency of the machine.

The highest average mechanical efficiency of 67.7 % occurred at the maximum inclination angle of 24.5^0, maximum head of 0.256 m and a rotational speed of 40 rpm. Conversely, for the same maximum head of 256 mm, the highest average mechanical efficiency from the graphs of combined effect of β and L was 83.4 W (Figure 4.12). Again, the results from tests on combined effects produced better output. The explanation for the difference in the maximum values of the two categories of tests is that, for the combined effect of β and L the reduction in angle was accompanied by increase in number of buckets and a constant head drop across the ends of the screw

while for the second case a reduction in angle was accompanied by loss of head drop across the ends of the screw and no increase in number of buckets.

The results for peak mechanical efficiency mirrored the trends of peak mechanical power. The highest peak efficiency of 79.1% occurred at an angle of 24.5^0 and at a rotation speed of 50 rpm as shown in Figure 4.34.
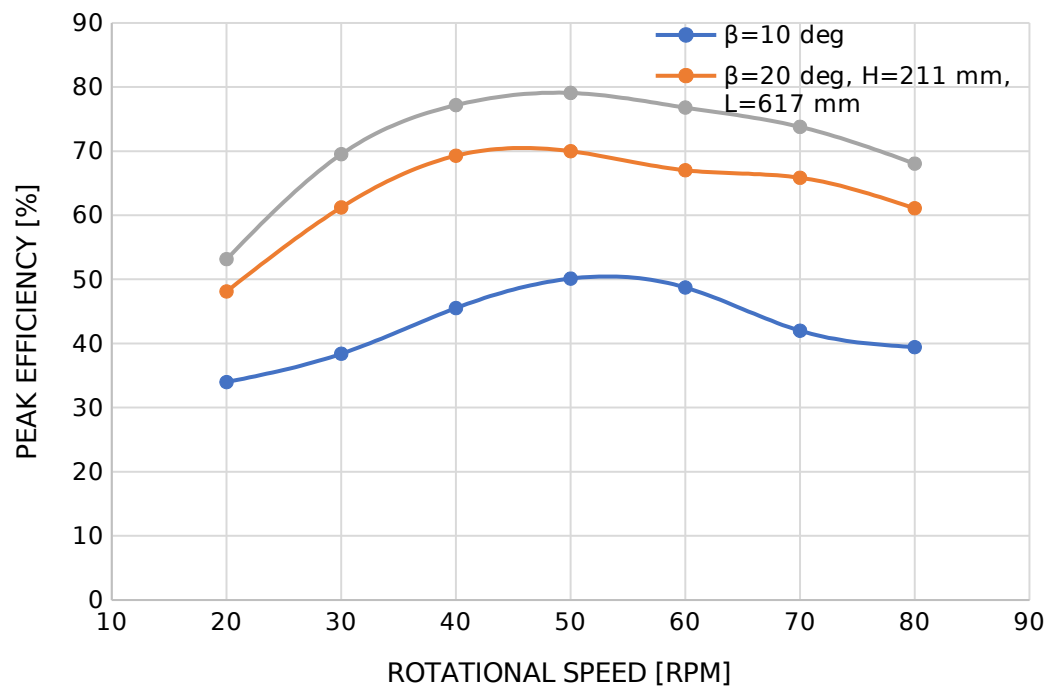
Figure 4. 34: Effect of β on Peak Mechanical Efficiency

In contrast to the results in Figure 4.34, the results for the tests on the combined effect of β and L produced a higher value of peak mechanical efficiency of 89.4 W (Figure 4.14).

In general, the designs that were based on the combined effects of β and L produced higher output values than those which were based on individual effect of β.

4.2.3.2 Effect of Number of Blades (N)

In order to test the effect of number of blades (N) on AST's output, the magnitude of pitch (S) and other parameters were maintained at constant values except for the number of blades. Consequently, five screw models (S23, S24, S25, S26 and S27) were created having five different number of blades ranging from N = 2 to N = 6. Parameters whose sizes were maintained constant included $\beta = 24.5°$, L = 617 mm, D_o = 381 mm, D_i = 168 mm, S = 381 mm and Q = 10 kg/s. Figure 4.35 shows the images of the five geometries.
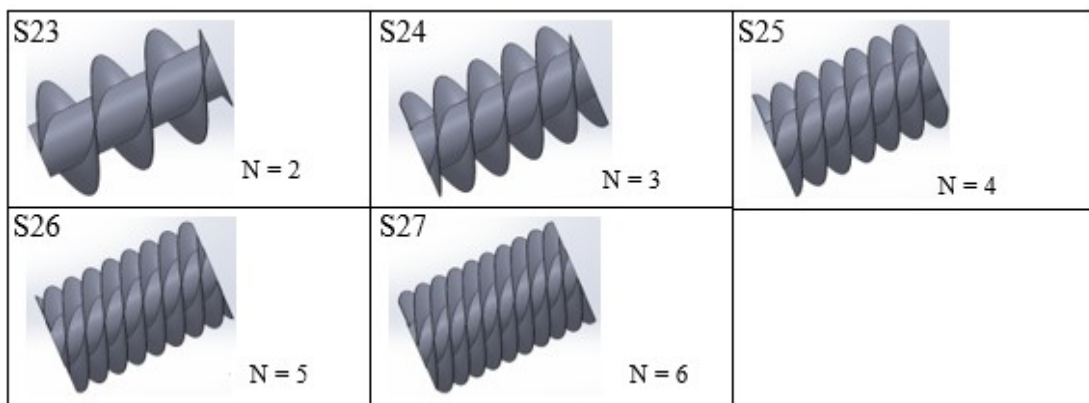
Figure 4. 35: AST Models having Different Number of Blades

For each of the five geometries, simulation runs were conducted at rotational speeds ranging from 20 rpm to 80 rpm. Figure 4.36 shows graphs for the average torque versus rotational speed for the geometries.
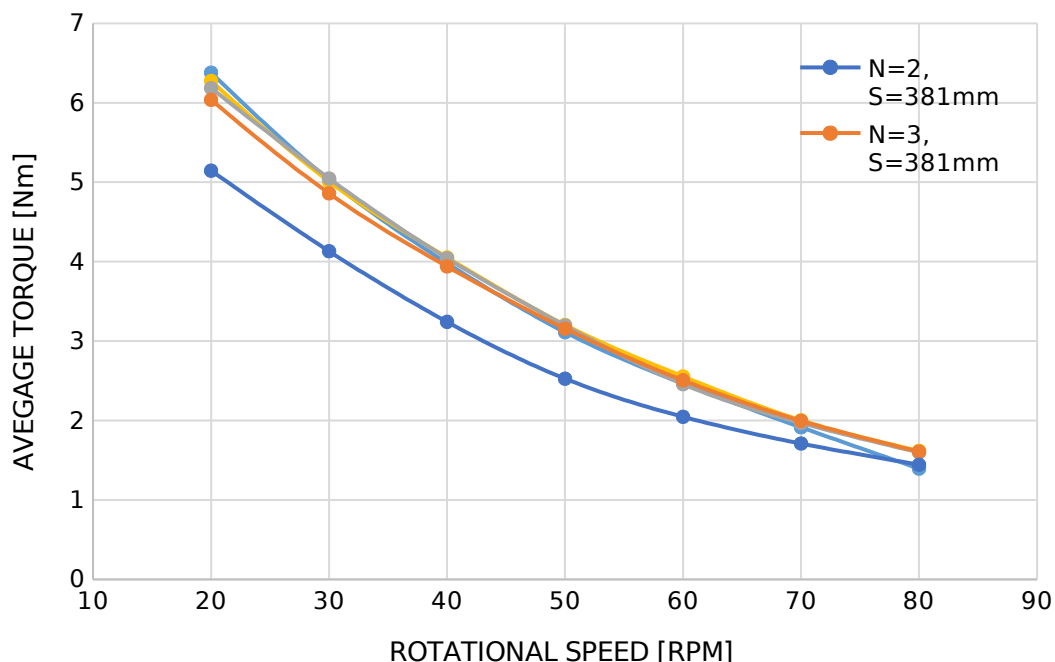
Figure 4. 36: Effect of N on Average Torque

It was expected that a higher number of blades would give higher torque due to increased number of buckets. However, from the results in Figure 4.36 such a trend was not exhibited. Instead, four screws having N = 3, N = 4, N = 5 and N = 6 respectively generated almost the same magnitudes of average torque within the speed-range of 20 rpm to 70 rpm. In order to explain the results in Figure 4.36, it is important to note that increase in number of blades led to increase in number of buckets hence more hydrostatic pressure. However, it also led to increase in frictional losses. When the number of blades (N) were increased from 2 to 3, the gains due to increased number of buckets outweighed frictional losses. However, when the number of buckets were increased from 3 to 4 and above, the gains brought about by increased number of buckets were offset by high frictional losses.

The graphs for peak torque exhibited the same trend as those of average torque. Figure 4.37 shows results for peak torque.
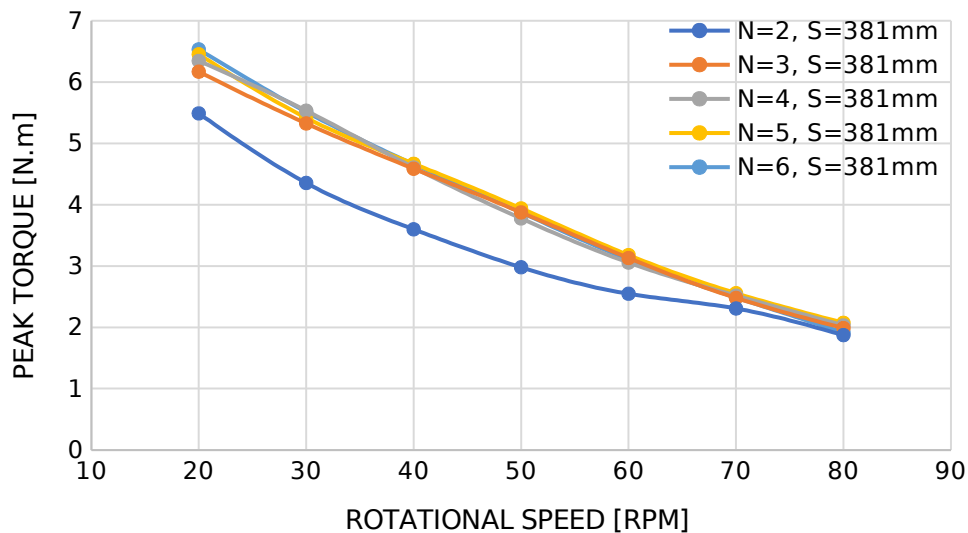
Figure 4. 37: Effect of N on Peak Torque

As displayed in Figure 4.37, four screw geometries having N= 3, N = 4, N =5 and N = 6 blades respectively had almost equal magnitudes of peak torque values in the entire range of rotational speeds. Conversely, the geometry having 2 blades had a distinctively lower magnitudes of peak torque. As was the case with average torque, the explanation for the trends was anchored on the interplay between the gains due to additional buckets and losses due to friction.

Figure 4.38, Figure 4.39, Figure 4.40 and Figure 4.41, show that the magnitudes of both average and peak mechanical power and efficiency increased with increase in rotational speed up to a critical speed beyond which the magnitudes of the outputs decreased with further increase in speed. Figure 4.38 shows curves for average mechanical power against speed.
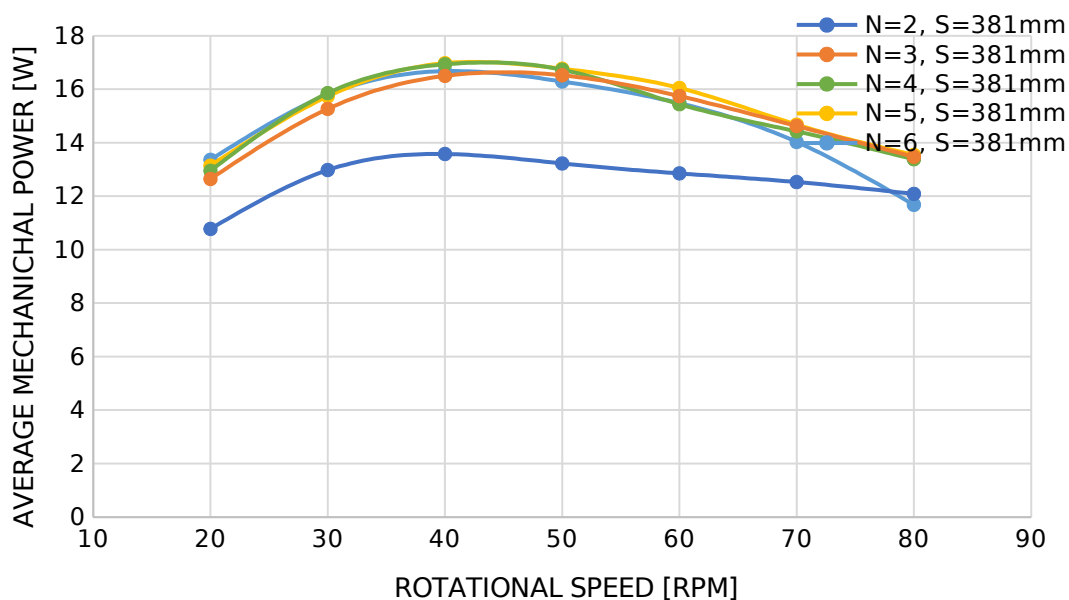
Figure 4. 38: Effect of N on Average Mechanical Power

The screws having N = 3, N = 4, N = 5 and N = 6 blades generated high values of both average and peak mechanical power, but the one having 2 blades did very poorly. As previously explained for torque, increase in number of blades (N) corresponded to increase in number of buckets and higher frictional losses too. The highest average mechanical power of 16.97 W was generated by the screw having 5 blades and rotating at 40 rpm. This performance is lower than the highest average mechanical power of 17. 97 W that was achieved by varying both N and S at the optimal W_{br} of 0.17 (Figure 4.27).

The performance curves showing peak mechanical power, as presented in Figure 4.39, exhibited similar trends as those of average mechanical power.
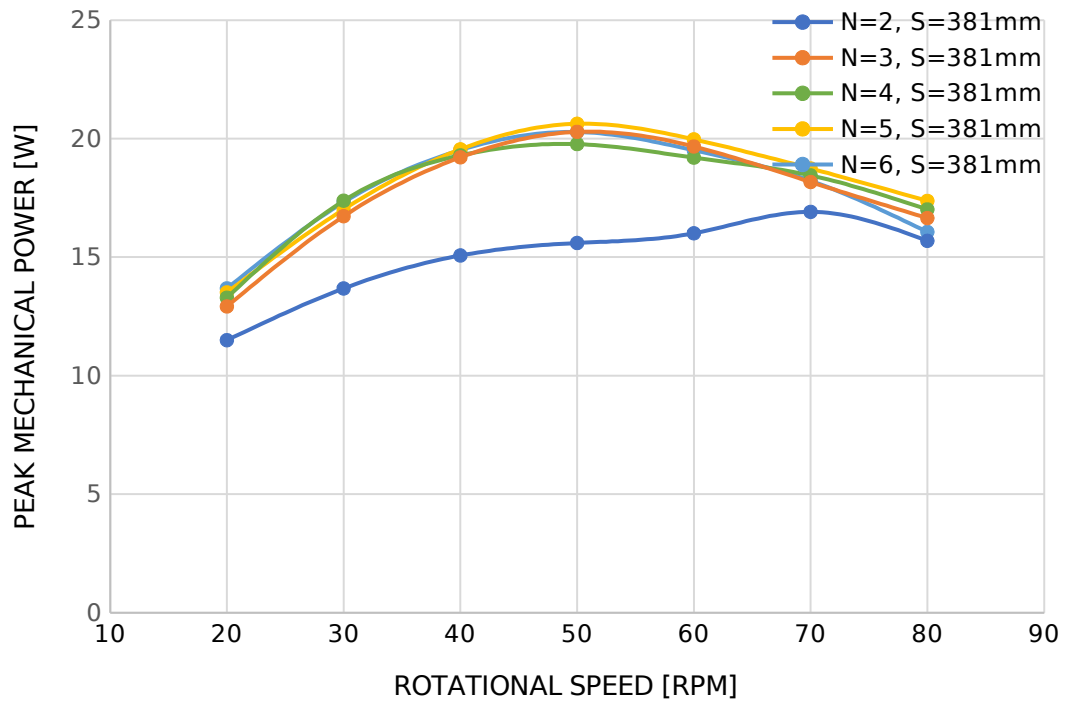
Figure 4. 39: Effect of N on Peak Mechanical Power

Average mechanical efficiency is directly proportional to average power; hence its output exhibited the same pattern as that of average mechanical power. Figure 4.40 shows graphs for average mechanical efficiency versus rotation speed for the five screws having different number of blades, but same pitch.
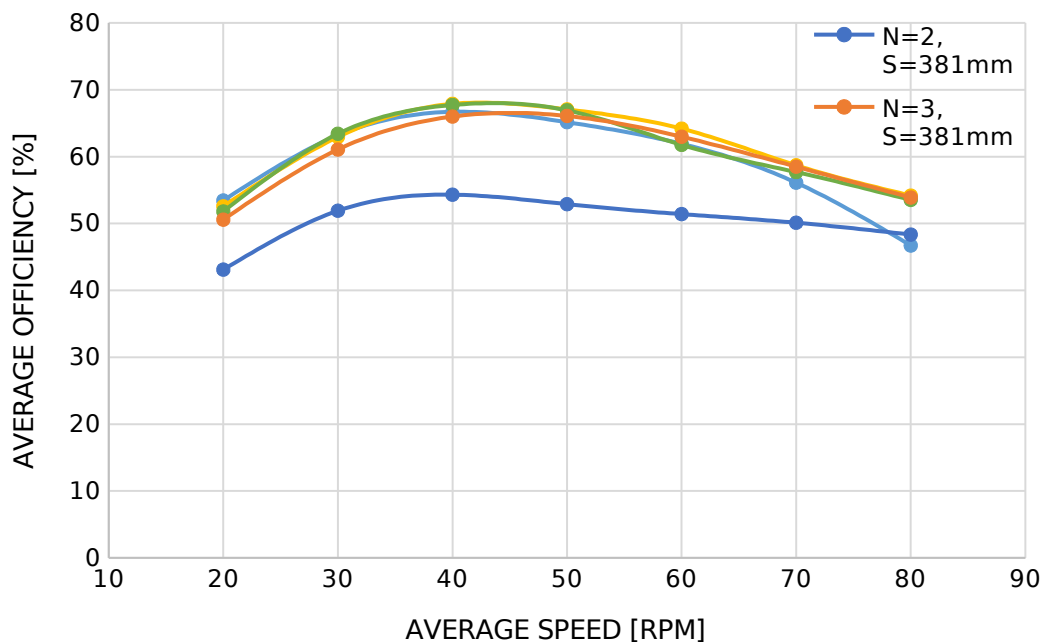
Figure 4. 40: Effect of N on Average Efficiency

Examining the curves on Figure 4.40, the highest average mechanical efficiency of 67.9 % was produced by the screw having 5 blades and rotating at 40 rpm. However, the performance is lower than the corresponding highest average mechanical efficiency of 71.9 % (Figure 4.27) that was produced by the combined effect of related parameters, N and S, at the optimal bucket width ratio (W_{br}) of 0.17. This is a further indicator that designs based on combined effects of related parameters produces higher performance than those based on independent effects of parameters.

Further, at the same rotational speed of 40 rpm, the screws having N = 3, N = 4, and N = 6 blades also registered high average mechanical efficiency values of 66.0 %, 67.7 % and 66.7 % respectively. In contrast, the screw having 2 blades performed dismally at 54.3 %. Therefore, it is clear that increasing the number of blades from 2 to 3 had a greater effect on average mechanical efficiency than the subsequent increments. This was attributed to huge gains due to additional number of buckets

and less losses due to friction. In the subsequent increases in number of blades, frictional losses increased thereby reducing the overall gain. Beyond 5 blades, greater losses reduced the average mechanical efficiency from 67.9 % for the screw having 5 blades to 66.7% for the screw having 6 blades. This could be attributed to losses having overtaken gains.

In the same manner, based on Figure 4.41, screws having N = 3, N = 4, N = 5 and N = 6 blades have close magnitudes of peak mechanical efficiency in the tested range of rotational speed.
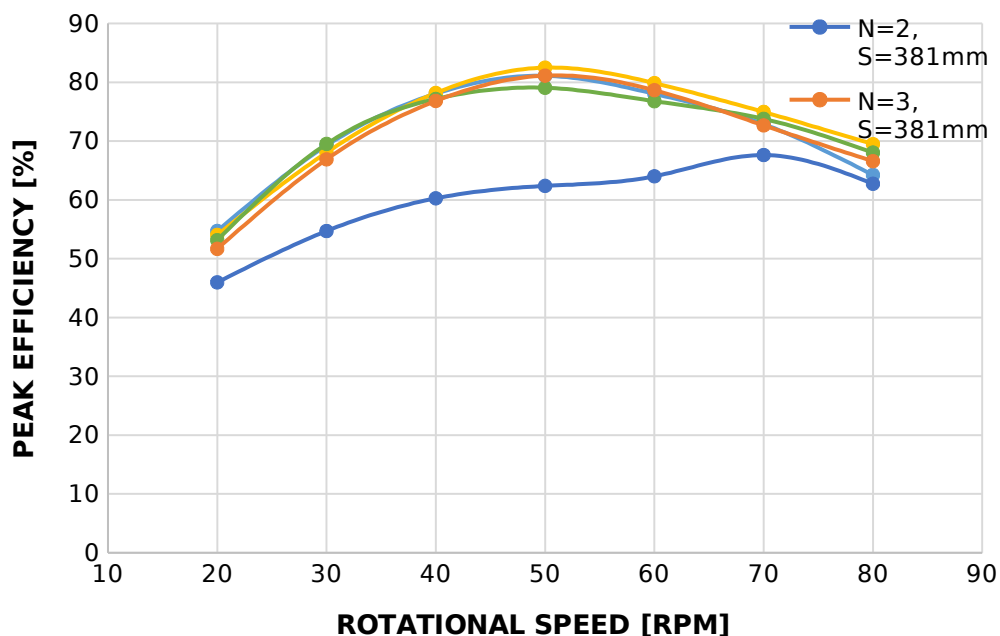
Figure 4. 41: Effect of N on Peak Mechanical Efficiency

From Figure 4.41, the highest peak efficiency of 82.5% was produced by the screw having 5 screws and rotating at 50 rpm. The screw having two blades, as was the case with the results of average mechanical power, had lower values of average efficiency.

4.3 Optimal Value for Related Parameters

Since the study was entirely based on fluid flow analysis, parameter values that corresponded to highest values of mechanical efficiency were taken to be optimal.

4.3.1 Optimal Value of Inclination Angle/ Screw Length (B/L)

Based on the results shown in both Figure 4.12 and Figure 4.14, it was clearly evident that a decrease in inclination angle and corresponding increase in screw length resulted in an increase in the magnitudes of both average and peak efficiencies. Hence, for the tested range of inclination angles (10° to 40°), the smallest angle of 10° and the corresponding screw length of 1474 mm produced the highest values of average and peak efficiencies of 83.4 % and 89.4 % respectively. Thus, 10° was taken to be the optimal inclination angle for the tested range.

4.3.2 Optimal Value of Number of Blades/Pitch (N/S)

Figure 4.27, showed that the highest average mechanical efficiency of 71.9 % corresponded to a pitch ratio of 0.68, bucket width ratio (W_{br}) of 0.17 and N = 4. Thus, optimal screw parameters were: N = 4 blades, W_{br} = 0.17 and S_r = 0.68.

4.4 Validation of Results

Results from the numerical study were validated using data from an experimental study of AST by Simmons et al. (2019). In the experimental study, a laboratory-size AST having the following parameters was used: N = 4, β = 24.5^{o}, L = 617 mm, S = 381 mm, D_o = 381 mm and D_i = 168 mm. Similarly, a screw model having the same magnitudes of parameters as the laboratory-size screw was used in the numerical work. Peak mechanical efficiency for both the experimental and numerical studies were plotted on the same axes as shown in Figure 4.42.
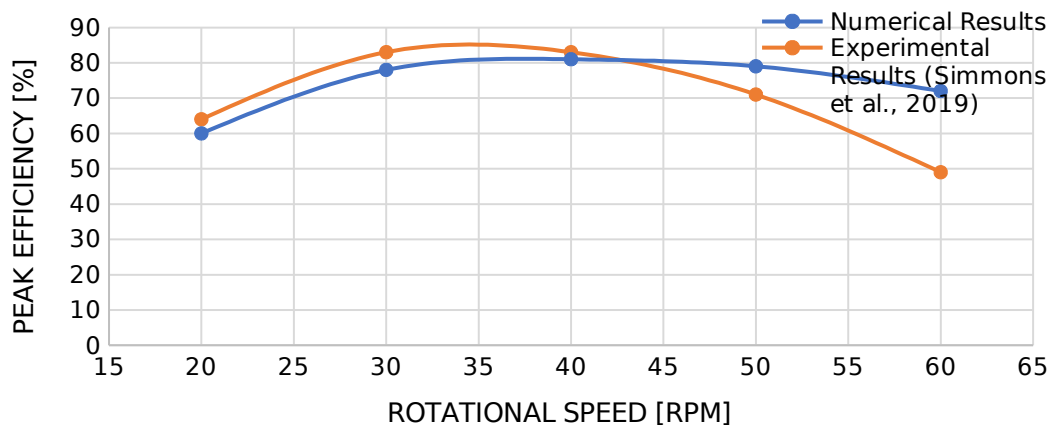
Figure 4. 42: Numerical and Experimental Graphs for Peak Efficiency for the 4N

AST, Inclined at 24.5º

Comparing the two graphs in Figure 4.4, it can be seen that numerical and experimental data show the same trend. Further, it can be seen that at low values of rotational speed, results from numerical analysis closely estimated the peak mechanical efficiency obtained from the experimental study. However, beyond 45 rpm the numerical model overestimated the peak mechanical efficiency. This could be due to the numerical model not being able to accurately predict turbulence at rotational speed values greater than 45 rpm.

CHAPTER FIVE: CONCLUSION AND RECOMMENDATIONS

5.1 Conclusion

This study was aimed at numerically solving fluid flow around Archimedes Screw turbine (AST) in order to study parametric performance of AST with respect to combined effects of related parameters such as angle of inclination/screw length (β/L) and number of blades/pitch (N/S). Tests on effects of individual parameters such as β and N were also conducted to act as baseline information upon which results on effects of related parameters could be interpreted. The aim of the study was achieved with results showing that designs that are based on related parameters (β/L and N/S) improve both the mechanical power and efficiency of the AST. The results are summarized in table 5.1.

Table 5.1 Performance of AST Based on Individual and Related Parameters

Output	β [º]	β/L [º / m]	Increase in efficiency [%]	N	N/S	Increase in efficiency [%]
Highest Average Mechanical Efficiency [%]	67.7	83.4	15.7	66.7	71.9 (at Wbr = 0.17)	5.2
Highest Peak Mechanical Efficiency [%]	79.1	89.4	10.3	81.1		

From the table, the magnitude of the highest average mechanical efficiency was 67.7 % and 83.4 % for tests on β and β/L respectively. This represents an improvement of 15.7 %. This result validates the argument fronted by both Waters (2015) and Lyons (2014) that AST designs that are based on smaller inclination angles and greater screw lengths may exhibit higher mechanical efficiency values than those that are based on larger inclination angles and constant screw lengths.

The first specific objective was to develop a 3D CAD model of an AST using typical parameters and dimensions and hence simulate flow through the machine. The CAD model was successfully developed in Solidworks software and flow analysis through it conducted in Ansys-CFX software. The analysis showed that pressure on each blade increased radially to a maximum value at the tip of the blade. Consequently, it was concluded that the blade-tip is a critical design point when designing against blade failure. The second observation from the results was that the amplitude of torque fluctuation decreased with reduction in the rotational speed of the screw. Thus, it was concluded that, in order to optimize speed of rotation, a trade in between torque output and the amplitude of torque fluctuation is necessary.

The second specific objective was to determine the combined effects of related parameters (β/L and N/S) on the torque, mechanical power and mechanical efficiency of an AST. The first set of related parameters to be investigated was inclination angle/screw length (β/L). For each magnitude of inclination angle, the corresponding magnitude of screw length was calculated using the equation **sin β = Head ÷ Length.** Thus, 5 different screw geometries were developed while maintaining a constant hydraulic head of 256 mm. The sizes of β/L for the shortest screw were 40°/398 mm while that of the longest screw were 10°/1474 mm. From the results obtained, it was evident that both the mechanical power and mechanical efficiency of the AST increases with decrease in inclination angle and corresponding increase in screw length. Consequently, the screw having β/L = 10°/1474 produce the highest peak mechanical efficiency of 89.4 %. Thus, it is apparent that the angle of inclination should be designed to be as small as practically possible bearing in mind that the greatest length that can be accommodated in design of an AST is affected by other engineering concepts such as torsional yielding and sagging of the AST's shaft which are beyond

the scope of this work. Further, the study involved another set of related parameters: number of blades/ pitch (N/S). Results of the study showed that the variation of N/S affect efficiency, but the relationship lacks a clear trend. Further still, it was evident from the tests that the bucket width (W_b) is critical in the design of an AST. The screw geometry having 4 blades produced the highest average mechanical efficiency of 71.9 % at a bucket width ratio (Wbr) of 0.17.

The third specific objective was to establish optimal values of the parameters based on the results from the second specific objective. It was concluded from the results that the optimal parameters for the AST are: $N/S_r = 4/0.68$, $W_{br} = 0.17$ and the smallest possible size of β for which the screw shaft (which also increases with decrease in inclination angle) does not fail under torsion or sagging.

5.2 Recommendations

The tests on the combined effects of related parameters (β/L, N/S) on the mechanical power and efficiency of the AST were conducted at a constant diameter ratio (D_r) of 0.44. For further research studies, the diameter ratio (D_r) need to be varied in order to ascertain the range of values for the parameter for which designs based on related parameters produce higher magnitudes of mechanical efficiency than those based on individual parameters.

The result on the effect of related parameters β/L showed that the smaller the angle and the longer the corresponding length, the higher the mechanical efficiency of an AST. However, since the greatest length that can be accommodated in the design of an AST is affected by other factors such as torsional yielding and sagging of the AST's shaft, further studies on AST should involve the effect of torsional yielding and sagging of the screw shaft on maximum screw length for different screw geometries.

Further still, since scaling for AST has not been established, this study recommends further tests on the related parameters using full-size prototype ASTs.

REFERENCES

Ansys Inc. (2013). CFX solver modelling guide, release 15.0. ANSYS CFX-Solver Modeling Guide, 15317(November), 724-46.

Ansys, I. (2013). ANSYS meshing user's guide. vol, 15317, 724-746

ANSYS. (2004). ANSYS Modeling and Meshing Guide. Release 9.0.

ANSYS. (2011). ANSYS CFX: Solver Theory Guide: 14.0.

ANSYS. (2012). Lecture 09: Domains, Boundary Conditions and Sources.

Breeze, P. (2018). Hydropower. Academic Press.

Çelikdemir, S., YILDIRIM, B., & ÖZDEMİR, M. T. (2017). Cost analysis of mini hydro power plant using bacterial swarm optimization. International Journal of Energy and Smart Grid, 2(2), 64-81.

Dellinger, G., Garambois, P. A., Dufresne, M., Terfous, A., Vazquez, J., & Ghenaim, A. (2016, November). Numerical and experimental study of an Archimedean Screw Generator. In IOP Conference Series: Earth and Environmental Science (Vol. 49, No. 10, p. 102002). IOP Publishing.

Doven, J., Hanania, J., & Stenhouse, K. (2020). Crossflow Turbine. https://energyeducation.ca/encyclopedia/Crossflow_turbine

El Najjar, R. E. B. (2017). *Collaborative methods and tools to remotely develop multi-sites engineering standards: the case of GE renewable energy-hydro* (Doctoral dissertation, Université Grenoble Alpes).

Elbatran, A. H., Yaakob, O. B., Ahmed, Y. M., & Shabara, H. M. (2015). Operation, performance and economic analysis of low head micro-hydropower turbines for rural and remote areas: A review. Renewable and Sustainable Energy Reviews, 43, 40-50.

Espinosa Vila, F. X. (2019). CFD simulations of an Archimedes screw (Bachelor's thesis, Universitat Politècnica de Catalunya).

Fluent, A. N. S. Y. S. (2009). ANSYS Fluent 12.0 user's guide. Ansys Inc, 15317, 1-2498.

Fulford, D. J., Mosley, P., & Gill, A. (2000). Recommendations on the use of micro-hydro power in rural development. Journal of international Development, 12(7), 975.

Hatata, A. Y., El-Saadawi, M. M., & Saad, S. (2019). A feasibility study of small hydro power for selected locations in Egypt. Energy Strategy Reviews, 24, 300-313.

Hidayat, M. N., Ronilaya, F., Eryk, I. H., & Joelianto, G. (2020). Design and analysis of a portable spiral vortex hydro turbine for a Pico Hydro Power Plant. In IOP Conference Series: Materials Science and Engineering (Vol. 732, No. 1, p. 012051). IOP Publishing.

Kaunda, C. S., Kimambo, C. Z., & Nielsen, T. K. (2012). Potential of small-scale hydropower for electricity generation in Sub-Saharan Africa. *International Scholarly Research Notices*, *2012*.

Kiplagat, J. K., Wang, R. Z., & Li, T. X. (2011). Renewable energy in Kenya: Resource potential and status of exploitation. Renewable and Sustainable Energy Reviews, 15(6), 2960-2973.

Kothandaraman, C. P. (2007). Fluid mechanics and machinery. New Age International.

Kotronis, I. K. (2016). *Low Head Hydropower: A Performance Improvement Study for Archimedes Screw Turbines Using Mathematical Modelling* (Doctoral dissertation, Lancaster University (United Kingdom)).

Kozyn, A. (2016). Power loss model for Archimedes screw turbines (Doctoral dissertation).

Laghari, J. A., Mokhlis, H., Bakar, A. H. A., & Mohammad, H. (2013). A comprehensive overview of new designs in the hydraulic, electrical equipments and controllers of mini hydro power plants making it cost effective technology. Renewable and sustainable Energy reviews, 20, 279-293.

Lashofer, A., Hawle, W., & Pelikan, B. (2012). State of technology and design guidelines for the Archimedes screw turbine. Proceedings of the Hydro.

Lyons, M. (2014). *Lab testing and modeling of Archimedes screw turbines* (Doctoral dissertation, University of Guelph).

Lyons, M., & Lubitz, W. D. (2013, July). Archimedes screws for microhydro power generation. In *Energy Sustainability* (Vol. 55515, p. V001T15A003). American Society of Mechanical Engineers.

Maulana, M. I., Syuhada, A., & Almas, F. (2018). Computational fluid dynamic predictions on effects of screw number on performance of single blade Archimedes screw turbine. In E3S Web of Conferences (Vol. 67, p. 04027). EDP Sciences.

Mechanicaljungle. (n.d). Reaction Turbine. Retrieved on 16 January, 2022 from https:// mechanicaljungle.com/reaction-turbine/

Mechstuff. (2021). Amazing Archimedean Screw. Retrieved on 10 August, 2021 from https://mechstuff.com/amazing-archimedean-screw/

Mrope, H. A., Chande Jande, Y. A., & Kivevele, T. T. (2021). A review on computational fluid dynamics applications in the design and optimization of crossflow hydro turbines. Journal of Renewable Energy, 2021, 1-13.

Müller, G., & Senior, J. (2009). Simplified theory of Archimedean screws. *Journal of Hydraulic Research*, *47*(5), 666-669.

Nuramal, A., Bismantolo, P., Date, A., Akbarzadeh, A., Mainil, A. K., & Suryono, A. F. (2017). Experimental study of screw turbine performance based on different angle of inclination. *Energy Procedia, 110,* 8-13.

Okot, D. K. (2013). Review of small hydropower technology. Renewable and Sustainable Energy Reviews, 26, 515-520.

Paish, O. (2002). Micro-hydropower: status and prospects. Proceedings of the Institution of Mechanical Engineers, Part A: Journal of Power and Energy, 216(1), 31-40.

Potter, M. C., Wiggert, D. C., & Ramadan, B. H. (2016). *Mechanics of fluids*. Cengage Learning.

Rorres, C. (2000). The turn of the screw: Optimal design of an Archimedes screw. *Journal of hydraulic engineering*, *126*(1), 72-80.

Rosly, C. Z., Jamaludin, U. K., Azahari, N. S., Mu'tasim, M. A. N., Oumer, A. N., & Rao, N. T. (2016). Parametric study on efficiency of Archimedes screw turbine. *ARPN Journal of Engineering and Applied Sciences*, *11*(18), 10904-10908.

Roy, D. N. (1988). Applied fluid mechanics. Ellis Horwood.

Salam, A. C. A., Issac, J. M., & Markose, B. (2018). Numerical study of Archimedean screw turbine. International Research Journal of Engineering and Technology (IRJET), 5, 2401.

Sangal, S., Garg, A., & Kumar, D. (2013). Review of optimal selection of turbines for hydroelectric projects. International Journal of Emerging Technology and Advance Engineering, 3(3), 424-430.

Schleicher, W.C. (2012). Numerical Investigation and Performance Characteristic Mapping of an Archimedes Screw Hydroturbine.

Shedage, S. Numerical investigation of micro scale flows in narrow gaps (Doctoral dissertation, PhD thesis, NITIE-National Institute of Industrial Engineering, 12 2014).

Simmons, S., Dellinger, G., Lyons, M., Terfous, A., Ghenaim, A., & Lubitz, W. D. (2021). Effects of inclination angle on Archimedes screw generator power production with constant head. Journal of Hydraulic Engineering, 147(3), 04021001.

SIMSCALE. (January 21, 2022). CFD Numerics: Non-Orthogonal Correctors. https://www.simscale.com/docs/simulation-setup/numerics/non-orthogonal-correctors/

Songin, K. (2017). Experimental analysis of Archimedes screw turbines (Doctoral dissertation, University of Guelph).

Tu, J., Yeoh, G. H., & Liu, C. (2018). Computational fluid dynamics: a practical approach. Butterworth-Heinemann.

Versteeg, H. K., & Malalasekera, W. (2007). An introduction to computational fluid dynamics: the finite volume method. Pearson education.

Warjito, W., Adanta, D., & Syafei, M. G. (2017, September). Development of Archimedes Turbine Research. In Seminar Nasional Tahunan Teknik Mesin XVI-2017.

Waters, S. R. (2015). *Analysing the performance of the Archimedes Screw Turbine within tidal range technologies* (Doctoral dissertation, Lancaster University (United Kingdom)).

Woodbury, A. C., Shepherd, J. F., Staten, M. L., & Benzley, S. E. (2008). Localized coarsening of conforming all-hexahedral meshes. In Proceedings of the 17th International Meshing Roundtable (pp. 603-619). Springer, Berlin, Heidelberg.

Yi, S.S., Htoo, A.M., & Sein, M.M. (2018). Design of Crossflow Turbine (Runner and Shaft). *International Journal of Science, Engineering and Technology Research* (IJSETR)Volume 7, Issue 10, October 2018, ISSN: 2278 -7798.

YoosefDoost, A., & Lubitz, W. D. (2020). Archimedes screw turbines: A sustainable development solution for green and renewable energy generation—A review of potential and design procedures. Sustainability, 12(18), 7352.

Yulianto, Bambang. P., Fathoni & Hari, S. (2019). Design and Testing of Screw Turbines for Flat Flow with Uneven Blade Distance. American Journal of Engineering and Applied Sciences 2019, 12 (1): 10.19 DOI: 10.3844/ajeassp.2019.10.19.

APPENDICES

APPENDIX I: LICENSE FOR ANSYS 19 R1 SOFTWARE

Copies for both the notification for renewal of the license and the license are attached.

NOTIFICATION FOR ANSYS LICENCE RENEWAL

QFINSOFT

Quotation number:	**MOI-270120**
Date:	27 January 2020

To:
Prof. Makokha
Moi University

Annual Payment Notification for ANSYS TECS (Technical Enhancements and Customer Support)

This letter is to inform you that your ANSYS Technical Enhancements and Customer Support (TECS) or LEASE will be expiring soon. Please use this payment notification to initiate payment into our account to prevent your TECS contract from expiring. As soon as payment is received, we will issue an invoice and renew your contract with ANSYS. Alternatively, you can use this document as a quotation and raise a purchase order. Once we receive the purchase order, we would then issue an invoice to initiate payment. Please find our banking details below.

Document Control

COPYRIGHT

Any questions regarding this document should be directed to:
Danie de Kock
E-mail: danie@qfinsoft.co.za
Tel: 012 345 1917
Mobile: 083 777 0935

DOCUMENT HISTORY			
VERSION NO	DATE	PAGES	EDITED BY
MOI-270120	27 January 2020	All	Danie de Kock

DOCUMENT DISTRIBUTION			
CONTACT	COMPANY	DATE	COMMENT
Prof. Makokha	Moi University	27 January 2020	Quote request
Danie de Kock	Qfinsoft	27 January 2020	

INTRODUCTION

Qfinsoft (PTY) Ltd is delighted at this opportunity to provide you with a proposal for ANSYS/Rocky DEM licenses. We have spent the past 20 years establishing relationships with our suppliers to bring you the best of computer aided engineering solutions available today. Should you require any more information on these products, visit our website or contact us. Our engineers will gladly assist with consulting for those once-off scenarios where the application does not justify the cost of the software. We have a team of engineers performing these projects and this enables us to provide outstanding technical support.
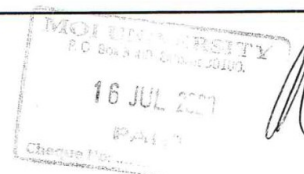
LICENSE:

SERVER user-PC DISK_SERIAL_NUM=be8582a0 1055

VENDOR ansyslmd

USE_SERVER

 # Products licensed in this file:

 # 1. ANSYS Academic Research CFD (5 tasks): 1 task(s) Permanent with TECS expiring 31-Jan-2021 Customer # 1074555

INCREMENT aa_mcad ansyslmd 2021.0131 permanent 5 8886B3BBDBDB \
    VENDOR_STRING=customer:01074555 SUPERSEDE ISSUER=SIEBEL \
    "ISSUED=28-aug-2020 START=01-feb-2019 SIGN2=""009D A2C8 1031 \"
    "BD69 6CB4 1273 B1A2 9200 5F15 CAF5 E5F3 EFC1 4E15 BED1 BD37"""

INCREMENT aa_r_cfd ansyslmd 2021.0131 permanent 5 DE0151639C14 \
    VENDOR_STRING=customer:01074555 SUPERSEDE ISSUER=SIEBEL \
    "ISSUED=28-aug-2020 START=01-feb-2019 SIGN2=""00CB 436B 8060 \"
    "59E9 80E1 8BA8 FE5F D100 8421 4860 B561 5F01 4802 9E6E 4D36"""

INCREMENT acfd_vki ansyslmd 2021.0131 permanent 5 2C0C2EBCAD08 \
    VENDOR_STRING=customer:01074555 SUPERSEDE ISSUER=SIEBEL \
    "ISSUED=28-aug-2020 START=01-feb-2019 SIGN2=""0037 A4F8 96D7 \"
    "FFF3 06B2 A334 F044 4D00 5B8A C1BF 9E61 5A93 D7A2 8757 657D"""

INCREMENT afsp_gui ansyslmd 2021.0131 permanent 5 53383A23F088 \
    VENDOR_STRING=customer:01074555 SUPERSEDE ISSUER=SIEBEL \
    "ISSUED=28-aug-2020 START=01-feb-2019 SIGN2=""0027 5005 7BE2 \"
    "1FC1 D3F5 9372 97DA E900 02DA E4F7 0CC4 63F7 6B31 FEF6 6A55"""

INCREMENT afsp_optigrid ansyslmd 2021.0131 permanent 5 800948FF5F11 \
    VENDOR_STRING=customer:01074555 SUPERSEDE ISSUER=SIEBEL \
    "ISSUED=28-aug-2020 START=01-feb-2019 SIGN2=""0065 8A51 622F \"
    "6C15 CFF7 7185 8064 A200 3305 5EB5 D0A3 B7E8 8275 E756 2D59"""

INCREMENT afsp_viewmerical ansyslmd 2021.0131 permanent 5 \
    0D1DB777D318 VENDOR_STRING=customer:01074555 SUPERSEDE \
    "ISSUER=SIEBEL ISSUED=28-aug-2020 START=01-feb-2019
SIGN2=""0074 \"
    93D1 422F CA7C 75F8 ABFF E32B 8C00 8B87 3D9C 4D39 E1C0 DE68 \

    "C77A 43DC"""

INCREMENT aim_mp1 ansyslmd 2021.0131 permanent 5 177FF5F21DC9 \
        VENDOR_STRING=customer:01074555 SUPERSEDE ISSUER=SIEBEL \
        "ISSUED=28-aug-2020 START=01-feb-2019 SIGN2=""0009 BDA8 8243 \"
        "2C0B BC5B 7A1B 5A44 6100 AE05 A46E 3E7F 0BE0 5180 8FC7 947F"""

INCREMENT ensight_enterprise ansyslmd 2021.0131 permanent 5 \
        784D3D244BCB VENDOR_STRING=customer:01074555 SUPERSEDE \
        "ISSUER=SIEBEL ISSUED=28-aug-2020 START=01-feb-2019
SIGN2=""000E \"
        6E4C 45D5 5671 02C3 C9CA DECC 4100 A70A 5675 2977 0A02 EDD6 \
        "4DFD 8379"""

INCREMENT envision_pro ansyslmd 2021.0131 permanent 5 7460AA1F2E2D \
        VENDOR_STRING=customer:01074555 SUPERSEDE ISSUER=SIEBEL \
        "ISSUED=28-aug-2020 START=01-feb-2019 SIGN2=""00D5 EB38 3266 \"
        "2905 BABB E31C EEF1 6400 14E5 39BE 56F2 50F6 0786 6BC9 FE49"""

APPENDIX II: EXTRACTS FROM SIMMONS ET AL., (2019)

EFFECTS OF VARYING INCLINATION ANGLE ON ARCHIMEDES SCREW GENERATOR POWER PRODUCTION WITH CONSTANT HEAD

Scott Simmons[1], Murray Lyons, and William Lubitz
School of Engineering
University of Guelph
Guelph, Canada
[1] ssimmons@uoguelph.ca

Guilhem Dellinger
ICube Laboratory
ENGEES, INSA Strasbourg
Strasbourg, France
guilhem.dellinger@engees.unistra.fr

Abstract—Archimedes screw generators are small-scale hydropower devices that are usually installed as diversion systems at sites with low head and moderate flow rates. Screw generators are usually designed empirically – they have been in use as pumps for millennia, and the same practical design principles are commonly implemented on generator schemes. For example, most Archimedes screws are installed at inclination angles at or about 25° - however, there is a lack of evidence to prove that this is best practice. This experiment tested three different screws, identical in all parameters except overall length so that the inclination angle could be varied while maintaining a constant head difference across the screw. Each of the screws were set in a test rig to measure power production. Since the head across the screws was the same, the screws were installed at varying inclination angles to meet this constraint. It was found that the longest screw (with the smallest inclination angle of 15°) performed the best, followed closely by the screw set at the common inclination angle of 25°. The shortest screw (at the steepest inclination angle of 33.8°) performed the poorest. Some suggestions are made with regards to the performance of the screws, and how to improve future power prediction models for Archimedes screw generators.

II. EXPERIMENTAL METHODS

There is a set of three screws in the University of Guelph's Archimedes Screw laboratory that have identical parameters except their flighted length – allowing them to be set at varying inclination angles that correspond to the same flow and head conditions at the screw's inlet and outlet. For the purposes of this paper, the three screws will be called the "short screw", "medium screw", and "long screw". They are shown drawn to scale in Fig. 3.
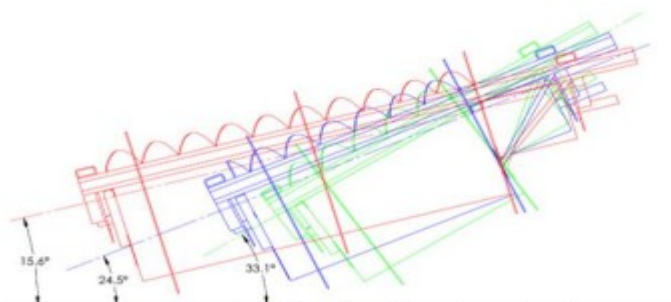

Figure 3. Angles of three screws with constant head. The short screw (green) has the steepest inclination angle, the long screw (red) has the shallowest inclination angle, and the medium screw (blue) has been set at an inclination angle of $\beta = 24.5°$ to match with previously collected data and the most common inclination angles of real-world ASG installations.

The dimensions of the three lab-screws are shown in Table 1. The inclination angle is found with respect to the flighted length of the screw and the constant head difference between the set of screws. The tests were started with the medium screw, since it was the closest representation to a typical "real-world" installation's inclination angle. The screw was installed in the Archimedes screw test rig at the University of Guelph shown in Fig. 5.

Table 1.   Experimental screw dimensions with corresponding inclination angles.

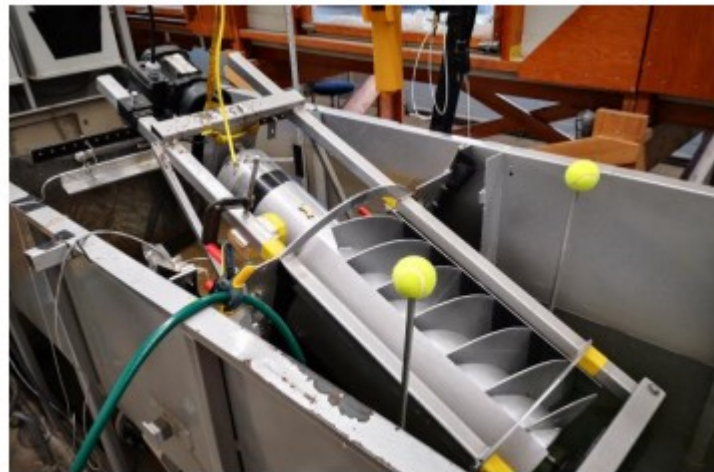|	Symbol	Short Screw	Medium Screw	Long Screw
Number of Blades	N	4	4	4
Inner Diameter (mm)	D_i	168	168	168
Outer Diameter (mm)	D_o	381	381	381
Pitch (mm)	S	381	381	381
Flighted Length (mm)	L	478	617	952
Inclination Angle (deg)	β	33.8	24.5	15.6

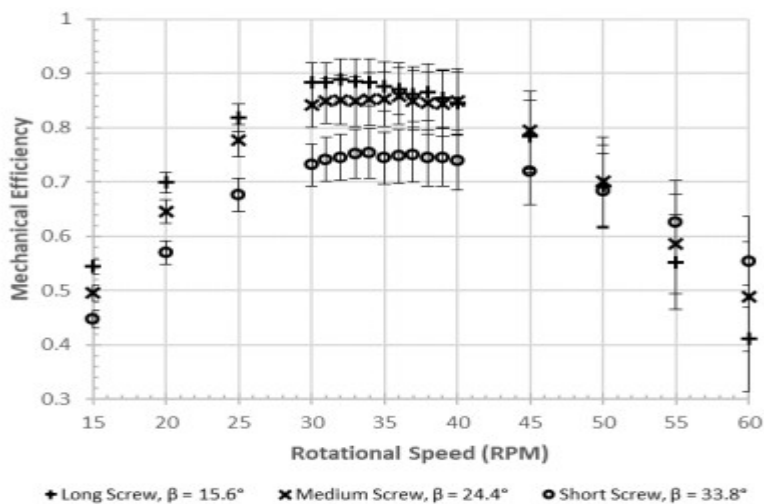Figure 5.   Laboratory test setup.

III. RESULTS

Figure 7. Mechanical efficiency of screw 14, 15, and 16 for varying rotational speeds.

The short and long screws were then run at 10 L/s for the same range of rotational speeds, the results of these tests are shown in Fig. 7. As the figure shows, the long screw (with the smallest inclination angle) proved to be the best performing screw – it generated the most power and was thusly the most efficient of the three inclination angles. The medium screw had similarly high efficiencies and the two trends seemed to converge as the rotational speed increased. The short screw (i.e. the steepest inclination angle) was the least efficient option but performed better at higher rotational speeds as it has less drop off near the end of the curve.

IV. CONCLUSIONS

The experiment presented in this paper provides valuable insight into the effect of inclination angle on the performance of Archimedes screw generators. Experience has suggested that ASGs operate best at inclination angles around 25°, but the laboratory-scale data shows that this may not be true for all sizes of screws. Indeed, at this system scale the best performing screw had an inclination angle of β=15.6°.

APPENDIX III: SOLIDWORKS LICENCE
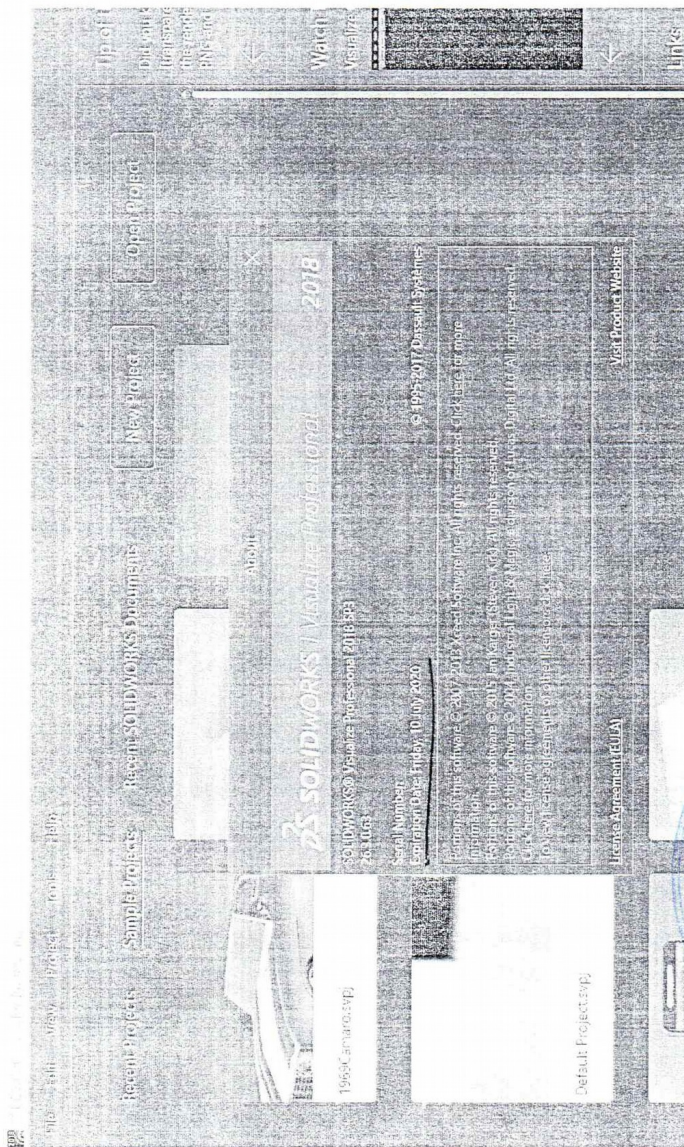
APPENDIX IV: PLAGIARISM CHECK

(Turnitin plagiarism checker was applied)

PARAMETRIC ANALYSIS OF ARCHIMEDES SCREW TURBINE FOR MICRO

HYDROPOWER GENERATION USING CFD

Submission date: 21-Nov-2022 08:42AM (UTC-0500)

Submission ID: 1960299088

File name: II_PROJECT-PHAREZ_CHIDA.docx (5.57M)

Word count: 19230

Character count: 96680

CHIDA

ORIGINALITY REPORT

11%	8%	5%	4%
SIMILARITY INDEX	INTERNET SOURCES	PUBLICATIONS	STUDENT PAPERS

PRIMARY SOURCES